UNVEILING THE ULTRAVIOLET PROPERTIES OF TYPE IA SUPERNOVAE

A Dissertation

by

YASWANT DEVARAKONDA

Submitted to the Graduate and Professional School of
Texas A&M University
in partial fulfillment of the requirements for the degree of

DOCTOR OF PHILOSOPHY

Chair of Committee,	Nicholas Suntzeff
Co-Chair of Committee,	Peter Brown
Committee Members,	Anirban Bhattacharya
	Justin Spilker
Head of Department,	Grigory Rogachev

May 2023

Major Subject: Astronomy

ABSTRACT

Type Ia supernovae are some of the most luminous transient events in our universe, but their ultraviolet (UV) properties remain relatively unexplored when compared to the optical and infrared properties. In this dissertation I introduce various techniques that take advantage of the Neil Gehrels Swift Observatory Ultra-Violet/Optical Telescope's (UVOT) multi-wavelength coverage in order to connect the well known optical properties of Type Ia supernovae with the lesser-known UV properties. First, I statistically compare the light curves of 97 nearby supernovae, showing for the first time that the UV and optical light curve properties of Type Ia supernovae are strongly correlated and have similar variability The light curves were modeled with templates, which were created by a technique called functional principal component analysis. This modeling technique allows for almost any light curve to be described as a linear combination of various weighted templates. Next I measure the intrinsic brightness, dust extinction, and k-corrections for a sample of 40 supernovae. With this I characterise the intrinsic variability of supernovae in the UV and optical, which when combined with the light curve correlations will pave the way for future cosmology studies that utilize the rest-frame UV emission. I accomplish this by creating multi-color models of the supernova's spectral energy density with a range of artificial template spectra. Finally I demonstrate a light curve modeling technique that is capable of estimating the peak magnitudes of a supernova with as little as three epochs of observation. All of these modeling techniques and statistical analyses will be highly useful when the next generation of high redshift transient surveys, such as the Rubin Observatory and the Roman Space Telescope, come online and observe the rest-frame UV light of supernovae.

DEDICATION

To my family, who have loved and supported me through my entire life. To Lulu, my precious companion. To my fellow graduate students, who are the greatest community that anyone could ask for. To Peter and Nick, who took a chance on me and helped me grow as a scientist.

ACKNOWLEDGMENTS

A PhD dissertation, like a child, takes an entire village to raise. I'm immensely grateful that I was able to write this dissertation with the love and support of so many wonderful people.

First I'd like to thank Peter Brown, who took a chance on me when I was ready to quit and gave me the time and space to grow as a scientist. He helped me start over from scratch and guided me through an entirely new field of research, with the kindness and patience that I desperately needed at the time.

My thanks to Nicholas Suntzeff, who during one of my lowest moments told me that I was the brightest student that he had seen in the program. I don't know where I would have been without his kind words and steadfast support over the years.

To my committee members, Justin Spilker and Anirban Bhattacharya, thank you for agreeing to advise me on a topic that was out of your comfort zone, and in turn reminding me to broaden my thinking. To Rob Kennicutt, Casey Papovich, Louis Strigari, and Jonelle Walsh, thank you for giving me such an amazing faculty support network. There were countless cases where I knocked on one of your doors looking for help, and y'all never hesitated to answer the call. I loved that our conversations could flow naturally from science to sports in a matter of seconds, and that there was always a feeling of mutual respect between us.

I'd like to thank the many postdocs who have supported me. Jon Cohn is one of my first friends at Texas A&M, and helped me grow into a better person, a better scientist, and a better game master. Jasleen Matharu guided me through some of the most difficult moments of my PhD, and I will always treasure the bond we forged. Jack Birkin, Kate Pitchford, and Shuvo Uddin were amazing postdoc mentors and always made time for me, even if it was just to chat about nothing at all. Grace Olivier and Paul Zvick were wonderful friends and mentors. There aren't many people who would be able to discuss the nuances of research proposals over a game of Dungeons and Dragons, the fact that two such people existed in my life is a blessing.

I'd like to thank the staff of the TAMU Department of Physics & Astronomy, who do the hard

work of making sure this department runs, and made sure I was able to graduate in time despite my best efforts, I would especially like to thank Amanda Barreiro, Sherree Kessler, Brendan Martin, Veronica Rodriguez, RaéChel Superville, Heather Walker, and the amazing custodial staff for everything they've done for me and the department.

The graduate students here at Texas A&M are truly the greatest community that one could ever ask for. My cohort, Lauren Aldoroty and Claire Qi, have been with me since day one, and I am proud to be walking out hand-in-hand with them. Lauren has stepped up to be my best friend here, my neighbor, and my closest research collaborator. Their love and support means the world to me. To my fellow Type Ia researchers, Gesa Chen and Jiawen Yang, thank you so much for your help through these years.

I want to thank Tarini Konchady, the star queen who helped me reconnect with my culture and who was always willing to stop by for a bottle or two of wine. I thank Sarah Cantu and Taylor Hutchison, who were the best academic big sisters that I could ask for, and for whom I owe many shots. My thanks to Leo Alcorn, Peter Ferguson, and Vince Estrada-Carpenter for being such an eclectic group of role models for me just as I was getting started as a scientist. I thank Alex Riley and Jessica O'Brian, who were amazing neighbors that were the core of my community in the heart of the pandemic. I will always cherish going to your apartment to discuss musicals, politics, and min-maxing, and I am truly honored to have been the officiant to your wedding.

I'd like to thank the current graduate community at A&M. Jacqueline Antwi-Danso is a treasured friend and mentor, and I am proud to call her my academic auntie. Silvana Delgado Andrade, Addy Evans, and Micalyn Rowe are all amazing scientists and humans, and I'm proud to have seen them grow within the department. Justin Cole and Kaitlin Webber arrived in the midst of the pandemic, and despite that became central figures within our department. Nikko Cleri and Maeve Curliss are some of the smartest and most hard-working graduate students that I've seen, and I'm honored to have been a part of their lives. Refa Al-Amri, Vinny Donofrio, Divya Mishra, and Franklin Wang may be the newest additions to our department, but they impress me everyday with the knowledge and dedication, and they push me to be a better researcher and mentor. To my

friends in the Texas A&M LGBTQ community, particularly Sophia Ahmed, thank you so much for getting me out of my apartment giving me a chance to explore different aspects of myself in a safe environment, and trusting me to help lead the way for future queer Aggies. To my friends in GPSG, especially Amon Cox, Nick Farmer, Caitlin Madison, Robert McCaffery, Nirmitee Mulgaonkar, Rohan Singh Wilko, Jake Stukenberg, Megan Svajda-Hardy, and Natalie Vest, thank you so much for being by my side as I try to negotiate university politics as well as finish my PhD. I am so grateful to have been a part of this movement with y'all.

I thank my dearest friends and longhorns, Jacqueline Feuge, Anna McGilvray, Melissa Morris, Liz Nguyen, Richard Seifert, and Christian Tatum. Y'all some of my oldest and dearest friends, and I am immensely thankful to have each of you in my life. I want to thank Channel Hicks, Jon Hicks, and Cousin Liza for immediately becoming the closest family I have, and for nourishing my physically and emotionally when I needed it the most.

Finally I want to thank my family, Chalapathy, Rajasree, and Apurva Devarakonda. You three have been by my side since birth, and have supported me through every step and miss-step that I made. I'm proud to be a part of the family, and I hope to make you all proud.

To everyone who has helped me make it this far, I love you.

CONTRIBUTORS AND FUNDING SOURCES

Contributors

This work was supported by a dissertation committee consisting of Professors Peter Brown (co-advisor) and Nicholas Suntzeff (co-advisor) and Justin Spilker of the Department of [Physics & Astronomy] and Professor Anirban Bhattacharya of the Department of Statistics.

UV photometry came from the Swift Optical/Ultraviolet Supernova Archive (SOUSA), which is supported by NASA's Astrophysics Data Analysis Program through grant NNX13AF35G. This work made use of public data in the Swift data archive and the NASA/IPAC Extragalactic Database (NED), which is operated by the Jet Propulsion Laboratory, California Institute of Technology, under contract with NASA. UV spectra came from observations with the NASA/ESA Hubble Space Telescope obtained at the Space Telescope Science Institute, which is operated by the Association of Universities for Research in Astronomy, Incorporated, under NASA contract NAS5-26555.

This work used arXiv.org and NASA's Astrophysics Data System for bibliographic information.

The data used in Chapter 2 & 3 was provided by Dr. Peter Brown. Light curve modeling with SNooPy in Chapter 3 was provided by Lauren Aldoroty. All other work conducted for the dissertation was completed by the student independently.

Funding Sources

This work was supported by NASA grant 80NSSC20K0456, "SOUSA's Sequel: Improving Standard Candles by Improving UV Calibration". Support for Program numbers 16221 and 16190 was provided through a grant from the STScI under NASA contract NAS5-26555. This work was also supported by NASA ADAP grant 80NSSC20K0456 and Swift GI Programs 80NSSC20K0951 and 80NSSC19K0316. Graduate study was supported by funding from the George P. and Cynthia Woods Mitchell Institute for Physics and Astronomy.

NOMENCLATURE

$\Delta m_{15}(B)$	15 day decline rate in the B filter
ATLAS	Asteroid Terrestrial-impact Last Alert System
ASAS-SN	All-Sky Automated Survey for Supernovae
BAYESN	A Hierarchical Bayesian SED Model for Type Ia Supernovae in the Optical to Near-Infrared
CMAGIC	Color-Magnitude InterCept
CO	Carbon-Oxygen
CSM	CircumStellar Medium
FPCA	Functional Principal Componant Analysis
FUV	Far UltraViolet
HST	Hubble Space Telescope
Ia	Type Ia
IaX	Type IaX
IME	Intermediate Mass Elements
IR	InfraRed
JWST	James Webb Space Telescope
Mag	Magnitudes
MLCS	Multi-Light Curve Stretch
NIR	Near InfraRed
NUV	Near UltraViolet
P99	Phillips et al. 1999
PC	Principal Componant

PHANGS	Physics at High Angular resolution in Nearby GalaxieS
SALT	Spectral Adaptive Light-curve Template
SED	Spectral Energy Density
SIRAH	Supernovae in the InfraRed Avec Hubble
SN	Supernova
SNe	Supernovae
SNooPy	Supernova light curve fitting, Python based
SOUSA	Swift's Optical/Ultraviolet Supernova Archive
Sub-C	Sub-Chandrasekhar mass
Super-C	Super-Chandrasekhar mass
UV	UltraViolet
UVOT	UltraViolet/Optical Telescope
WFC3	Wide-Field Camera 3
ZTF	Zwicky Transient Facility

TABLE OF CONTENTS

Page

LIST OF FIGURES

FIGURE Page

LIST OF TABLES

TABLE Page

1. INTRODUCTION AND LITERATURE REVIEW

Type Ia supernovae (SNe Ia) are some of the most luminous transient events in the universe, often exceeding the brightness of their host galaxy. Unlike core-collapse supernovae, which are caused by high mass stars at the end of their life spans, SNe Ia are thermonuclear explosions of white dwarf stars. These white dwarfs are thought to accrete matter from a binary companion until they reach a critical mass, at which point carbon fusion ignites within the core [Mazzali et al., 2007]. The white dwarf is unable to effectively cool through expansion, and thus unbinds as a supernova. The critical mass at which a carbon-oxygen (CO) white dwarf unbinds is more commonly called the Chandrasekhar Mass, and is around 1.4 $M_{\odot}$ [Hillebrandt and Niemeyer, 2000]. The Chandrasekhar Mass is often confused with the Chandrasekhar Limit, which is the maximum mass that a white dwarf can grow to while being sustained by electron degeneracy pressure [Chandrasekhar, 1931]. If white dwarf could reach this limit without undergoing carbon fusion, then it would likely collapse into a neutron star [Maeda, 2022].

1.1 Type Ia Progenitors

Current models point to two main pathways for a Type Ia, the single-degenerate and double-degenerate model [Maeda and Terada, 2016]. Here, degenerate refers to objects held up by degeneracy pressure, such as white dwarfs. A single degenerate system contains an accreting white dwarf and a non-degenerate donor companion, such as a main sequence star or a red giant. A double-degenerate system would contain two white dwarfs, either in an accreter-donor pair similar to the single degenerate case or in a merging/colliding pair.

Both pathways start with a pair of main sequence stars. If the two are close enough when the primary evolves into a red giant, then the resulting common envelope phase will lead the objects to in-spiral until the envelope is expelled, at which point it becomes a close binary pair containing a CO white dwarf and a main sequence star. When the secondary expands, it may transfer mass onto the primary. If the primary gains enough mass to trigger carbon fusion, then this process

will result in a single-degenerate Type Ia supernova. This was once thought to be the dominant pathway for SNe Ia [Whelan and Iben, 1973, Claeys et al., 2014]. However the single-degenerate channel would result in a number of observable signatures that have not been reported in large number. For instance the companion star is expected to survive the explosion and would be ejected from the system at a high velocity, but surveys of SNe Ia remnants have mostly been unable to find any hyper-velocity companions [Li et al., 2019]. In addition, the shock of the supernova ejecta colliding with the surface of the companion is expected to result in excess flux during the earliest phases of the supernova. [Kasen, 2010, Piro and Nakar, 2014]. Surveys in the optical and IR claim to have found evidence for shock interaction consistent with the single-degenerate channel [Burke et al., 2022]. Models also suggest that the shock signal should be brightest in the UV, but very few SNe Ia have been found with early UV excess [Brown et al., 2012b, Scalzo et al., 2014, Hosseinzadeh et al., 2022]. This would either suggest that the shock interaction models are incorrect or that the single-degenerate channel is not as common as once believed.

If the primary does not explode during the previous phase, then the result is a close binary of two CO white dwarfs (the double-degenerate channel). Gravitational wave decay causes the objects to further in-spiral until they are close enough to interact [Maeda and Terada, 2016]. From here the white dwarfs may merge or collide, forming either a single high-mass white dwarf or a Type Ia supernova if carbon fusion is triggered [Cheng et al., 2020]. If the secondary companion maintains a He shell after evolving, the primary may accrete the He in a similar manner to the single-degenerate channel [Roy et al., 2022]. Thanks to the stronger constraints on the binary fraction of white dwarfs in galaxies, the double-degenerate channel is now believed to be the dominant channel for SNe Ia, [Maoz and Hallakoun, 2017].

Peculiar events have led to further sub-types of progenitor models. "Super-C" explosions have been seen with initial mass estimates of up to 2 $M_{\odot}$, far greater than the Chandrasekhar limit [Howell et al., 2006, Hsiao et al., 2020]. These are thought to be caused by the high rotational velocities of some white dwarfs, which allow them to maintain electron degeneracy pressure at high masses [Kilic et al., 2021]. Meanwhile "Sub-C" events are thought to be caused by an external

explosion, such as helium fusion in the accretion stream, which then triggers carbon fusion in the core and unbinds the white dwarf before it reaches the Chandrasekhar Mass [Roy et al., 2022]. Extremely sub-luminous SNe Ia, known as "IaX", are another outlier. These may be the result of a partial disruption of a white dwarf, and the progenitor may survive the explosion in a diminished state [Foley et al., 2015, Camacho-Neves et al., 2023].

1.2 Light Curve Evolution

The luminosity of SNe Ia changes over time as the ejecta expands and evolves into different phases. The amount of flux at any given time is roughly determined by two factors, the stages of nucleosynthesis and the photospheric properties. Nuclear burning in the high density core results in a large mass of ^{56}Ni, the decay of which into ^{56}Co dominates the flux output near peak brightness [Mazzali et al., 2007]. The amount of ^{56}Ni generated greatly effects the shape of the light curve; larger amounts of ^{56}Ni results in broader and brighter light curves, while fast-declining SNe Ia tend to have lower amounts of ^{56}Ni [Kasen and Woosley, 2007]. At very late times ($\geq$ 200 days post-explosion) the light curve is powered by the decay of ^{56}Co into ^{56}Fe [Graur et al., 2018], and as such SNe Ia are thought to be the dominant source of Fe in the universe [Arcones and Thielemann, 2023].

Intermediate mass elements (IME), such as iron, form in the lower density outer ejecta [Mazzali et al., 2007]. At early phases these IME dominate the absorption features of the SNe Ia, particularly in the UV [DerKacy et al., 2020]. As a result the early UV light curves show substantial diversity when compared to the optical light curves [Milne et al., 2010, Devarakonda and Brown, 2022]. The photospheric velocity, often characterized by the $SiII\lambda6355$ line, can affect the mean free path of photons and thus the light curve behavior. Some studies suggest that high velocity SNe Ia tend to be redder than normal, perhaps due to increased line-blanketing from the ejects [Foley and Kasen, 2011] or from circum-stellar medium (CSM) stripped from a SD accretion stream [Wang et al., 2019]. However other studies have not found that correlation in the optical colors [Dettman et al., 2021]. The UV colors do seem the be highly correlated with the $SiII$ velocity at peak brightness, perhaps due to their increased susceptibility to photospheric properties at that epoch relative to the

optical colors [Brown et al., 2018].

1.3 Cosmology

Because the peak luminosity of SNe Ia is determined by the amount of ^{56}Ni decay, SNe Ia are useful as cosmological distance indicators [Pskovskii, 1977, Phillips, 1993, Riess et al., 1996, Phillips et al., 1999]. This is normally done by correlating the intrinsic brightness to the Δm_{15} (the decline rate for the first 15 days after peak) [Phillips, 1993, Garnavich et al., 2004], or by fitting a stretch to a light curve/color curve template [Goldhaber et al., 2001, Riess et al., 1996, Jha et al., 2007]. Through studies of high redshift Sne Ia, it was discovered that supernovae that were further away were fainter than expected from a steady expansion, resulting in the first direct evidence for dark energy [Riess et al., 1998, Perlmutter et al., 1999]. However these estimates for the expansion of the universe differed significantly from results of Cosmic Microwave Background (CMB) studies [Planck Collaboration et al., 2018, Freedman et al., 2019].

Efforts to resolve the so-called "Hubble Tension" has lead to a deeper search into the systematic uncertainties in SNe Ia measurements, revealing a great deal about the inherent diversity in these objects. For instance, many sub-types of SNe Ia deviate significantly from the known width-luminosity relations, such as IaXs which tend to be under-luminous and Super-C objects which are overly luminous [Stahl et al., 2019]. In addition SNe Ia in high mass galaxies ($\geq 10^{10} M_{\odot}$) tend to be brighter than expected, suggesting different progenitor channels for SNe Ia in different galaxies [Uddin et al., 2020].

1.4 Beyond Optical

The near-infrared (NIR) light curves of SNe Ia have been found to significantly reduce the scatter in Hubble residuals [Dhawan et al., 2018, Avelino et al., 2019]. This due to less dust extinction and lower intrinsic scatter in the width-luminosity relation in the NIR [Krisciunas et al., 2000, Wood-Vasey et al., 2008, Mandel et al., 2011, Kattner et al., 2012]. With the upcoming Nancy J. Roman Space Telescope, combined optical-NIR studies may be able statistically constrain cosmological parameters out to $z \sim 0.4$ [Pierel et al., 2022]. NIR observations of nebular

phase emission ($\geq$ 200 days past peak) offer promising insight into the physics of SNe Ia as well. Evidence of elements with large half-lives and/or low masses can be more easily observed at these phases [Graham et al., 2022, Tucker et al., 2022], as can CSM interaction and light echos [Elias-Rosa et al., 2021, Drozdov et al., 2015, Wang et al., 2019]. Each of these can provide a clearer picture of the progenitor that is not visible at the near-peak phases.

With the launch of JWST [Rigby et al., 2022], detailed observations into the mid-infrared (MIR) properties of SNe Ia become possible. At the time of writing only one such object has been observed, SN2021aefx, which was observed at $\sim$ 255 days after peak as part of the PHANGS-JWST Treasury survey [Lee et al., 2022]. Analysis of the nebular line profiles and the presence of stable Ni would suggest that SN2021aefx was caused by a delayed-detonation explosion, where the initial nuclear burning in the core of a near-Chandrasekhar Mass white dwarf creates a sub-sonic flame (deflagration) that propogates through the core, eventually leading to a detonation [Chen et al., 2023, DerKacy et al., 2023, Kwok et al., 2023]. Those studies were even able to estimate a $\sim 30^o$ viewing angle for the deflagration-detonation transition, highlighting the potential for JWST in SNe Ia astrophysics.

Meanwhile, studies in the ultraviolet (UV) suggest that the light curves and spectra are much more diverse than the optical or NIR light curves [Jha et al., 2006, Kessler et al., 2009, Brown et al., 2010, Milne et al., 2010], and perhaps exists in at least two distinct UV populations (UV-blue and UV-red) [Brown et al., 2017]. Much of this diversity is due to the the increased absorption and scattering of UV photons by metals in the ejecta and/or dust in the surrounding environment [Brown et al., 2015, Brown et al., 2017]. The differences in UV flux may arise from the initial star formation conditions of the SNe progenitor, in which case there would be a correlation between the host galaxy metallicity and the SNe UV flux level. However photometric [Brown and Crumpler, 2020] and spectroscopic [Pan et al., 2020] studies conflict on the existence of such a correlation.

The UV shows promise in identifying other important characteristics of SNe Ia, such with classifying non-standard SNe. Super-C SNe, for instance, have been found to have unusually bright UV fluxes [Brown et al., 2014b] and reach their peak UV flux much earlier than in the

optical [Devarakonda and Brown, 2022]. Shock interaction with the companion at early phases [Kasen, 2010, Brown et al., 2012b] or the circumstellar medium at late phases [Graham et al., 2019] should be UV bright, however the lack of substantial detections seems to imply that these events are rare or that the source of the excess is due to other physical processes [Scalzo et al., 2014, Burke et al., 2021].

Facilities such as the Neil Gehrels Swift Observatory's Ultra-Violet Optical Telescope (UVOT) [Gehrels, 1997, Roming et al., 2005] have built up a large archive of SNe Ia observations that is prime for exploration [Brown et al., 2014a]. The upcoming Vera C. Rubin Observatory will detect thousands of high redshift SNe Ia in the rest-frame UV, increasing the amount of available data considerably. In order to take advantage of this treasure trove of data, new tools for analyzing SNe Ia will need to be developed.

1.5 Light Curve Modeling

In the optical and NIR, there are a number of common light curve fitting techniques. MLCS (Multi-color Light Curve Shape) [Riess et al., 1996, Jha et al., 2007] directly models the light curve data using vectorized templates over a hypothesized grid. It primarily relies on a Δ factor, which denotes the difference in luminosity of an object against empirical relations, such as the width-luminosity relation. As such the fit parameters have some physical motivation, although the technique is sensitive to the luminosity and extinction estimates in the training set. Similarly, SNooPy [Burns et al., 2011] applies a simple stretch term to a library of template light curves in order to fit observations. It differs from MLCS primarily through it's compatibility with different data sets. CMAGIC [Wang et al., 2003, Aldoroty et al., 2022], or the Color-MAGnitude Intercept Calibration method, examines the light curves of a SNe Ia as a function of color rather than of time. As a SNe Ia evolves into it's nebular phase, the color dramatically shifts blue-ward. The nature of this transition is correlated with the width-luminosity relation, and fitting this transition in color-magnitude space is as simple as drawing two lines. As a result, CMAGIC can be used to estimate light curve properties without the use of light curve templates, avoiding potential bias in training sets. However it requires observations over a longer phase space to accurately fit the

transition in color, and it has only been shown to be accurate for "normal" type SNe Ia

SALT3 [Kenworthy et al., 2021] is the latest generation of the Spectral Adaptive Light-curve Template (SALT) programs. It uses a library of SNe Ia spectra to generate spectral energy density templates (SEDs), which can then be used to fit light curves from a variety of instruments. This method allows it to fit more nuanced variations in SNe Ia, such as metallicity effects or dust. BayeSN is is another SED based light curve fitter [Mandel et al., 2022]; it takes a hierarchical Bayesian approach to modeling time and wavelength dependent uncertainties simultaneously. This approach results in a reduced uncertainty in distance when compared to other techniques, and it's probabilistic approach allows it to better separate effects due to intrinsic variability and extinction. However both methods lack adequate training sets in the UV to create robust models, limiting use to the optical and IR.

While all of these methods have extensive use in the optical and NIR, few methods exist to model UV light curves due to the lack of training data. We attempt to address this shortcoming by investigating a series of light curve fitting methods, starting with the FPCA template method [He et al., 2018]. Functional Principal Component Analysis (FPCA) is a statistical technique that attempts to describe the behavior of a data set (in this case SNe Ia light curves) as a linear combination of a mean function and a few principal component functions. These principal component function explain the statistical behavior of the light curves, not the physical properties. A "band-vague" version of the template, trained on optical and NIR observations, was created to fit the light curve of a SNe Ia regardless of the rest-frame emission. This could be useful during Rubin observations if accurate host galaxy information is not available. Despite the lack of UV training data, this template was able to model the UV and optical light curves of SNe Ia simultaneously and demonstrate the statistical similarity between the UV and optical light curves near peak luminosity [Devarakonda and Brown, 2022].

1.6 Dissertation Outline

In Chapter 2, I present my analysis of 97 nearby SNe Ia in the UV and optical using the FPCA template. In Chapter 3 I detail a new color-based SED modeling program that can estimate the

dust extinction and $K(z)$ correction values for SNe Ia in the UV and optical. I then examine the scatter in the absolute magnitudes and correction factors for a sample of 44 SNe Ia. At the end of the chapter, I introduce the SIRAH project, which will combine space and ground based UV/optical/NIR data of SNe Ia into the Hubble Flow. As part of that project, I describe a simple stretch-based fitting technique to estimate the peak luminosity of SNe Ia in the UV and optical with a sparse amount of observations. Finally I summarize my research and remark on future studies.

2. COMPARISONS OF TYPE IA SUPERNOVA LIGHT CURVES IN THE UV AND OPTICAL WITH THE SWIFT ULTRA-VIOLET/OPTICAL TELESCOPE *

We examine the light curve parameters of 97 nearby Type Ia supernovae in the ultraviolet and optical using observations from the Swift Ultra-Violet/Optical Telescope. Our light curve models used a linear combinations of templates, which were based on Functional Principal Component Analysis of the optical photometry of SNIa. The weights for each principal component used in the fit capture certain aspects of the light curve properties. We find that there is little difference in the overall variability of principal component scores across filters. We also find correlations between certain filters and PC components, indicating that the UV and optical properties seem to be tied together. This is a promising step in UV SNIa analysis, and suggests that UV light curves may be used to infer optical properties, paving the way for future cosmological studies.

2.1 Introduction

Type Ia Supernovae (SNIa) are useful as cosmological tools due to their highly uniform optical luminosity, which correlates strongly with their optical light curve profile and color [Pskovskii, 1977, Phillips, 1993, Riess et al., 1996, Phillips et al., 1999]. This has led to their use in studies for distance measurements and constraints on cosmological parameters [Riess et al., 1998, Perlmutter et al., 1999].

In optical wavelengths, SNIa have a strong relationship between their peak luminosity and luminosity-decline rate, leading to their widespread usage as standardizable candles [Branch, 1998, Leibundgut, 2001]. This process is generally done by calibrating the peak luminosity with distance-independent metrics such as the light curve shape. This can be done by measuring the decline rate for the first 15 days after maximum brightness (Δm_{15}), often in the B band [Phillips, 1993, Phillips et al., 1999, Garnavich et al., 2004]. Another common method is measuring the

stretch of a light curve when fitting to a template [Goldhaber et al., 2001].

The luminosity-width relation shows that more luminous SNIa have broader light curves. The cause of this relation is believed to be the production of ^{56}Ni during the SNIa explosion, and the change in the temperature and ionization evolution as a result [Nugent et al., 1995, Höflich et al., 1996, Mazzali et al., 2001, Kasen and Woosley, 2007]. ^{56}Ni drives much of the SNIa luminosity, and the light curve shape is greatly affected by opacity effects from^{56}Ni and Fe-group elements [Mazzali et al., 2007].

Subsequent studies have looked beyond the optical to see if these strong correlations still hold true at other wavelengths. For example, the near-infrared (NIR) luminosity has been shown to be less susceptible to the effects of interstellar extinction while also having a diminished dependence on the shape of the light curve [Krisciunas et al., 2000, Wood-Vasey et al., 2008, Mandel et al., 2011, Kattner et al., 2012]. Meanwhile, studies in the near-ultraviolet have shown that the correlations have much larger scatter [Jha et al., 2006, Kessler et al., 2009, Brown et al., 2010, Milne et al., 2010, Brown et al., 2017]. Understanding the scatter at shorter wavelengths will be an important task, as it enables us to better predict SNIa properties at larger distances where their rest-frame UV emission will be redshifted into the optical.

One issue with analyzing the UV light curves of SNIa is the lack of empirical templates at those wavelengths. In the optical, the most common optical fitting techniques are MLCS [Riess et al., 1996, Jha et al., 2007] and SALT3 [Kenworthy et al., 2021]. MLCS directly models the light curve data using vectorized templates over a hypothesized grid, whereas SALT3 uses spectral energy distributions to model light curves. Here, we use templates based on functional principal component analysis (FPCA) of optical SNIa light curves [He et al., 2018]. We apply these templates to UV and optical observations of 97 SNIa to examine how well this technique can characterize light curves in a regime that it wasn't trained in, and if the fitted parameters can shed new light into the diversity of SNIa in the UV.

In Section 2.2 we describe our observations and methodology for template fitting. Then in Section 2.3 we apply statistical tests to compare the diversity and correlation of our fitted param-

eters in the UV and optical regimes. Finally, in Section 2.4 we examine our results in detail and summarize our work in Section 2.5.

2.2 Methods

2.2.1 Observations

Observations were done with the Ultra-Violet Optical Telescope (UVOT; [Roming et al., 2005])on the Neil Gehrels Swift Observatory [Gehrels et al., 2004]. Observations were usually performed in all six medium-band UVOT filters: $UVW2$, $UVM2$, $UVW1$, U, B, and V. See [Poole et al., 2008] for calibration and filter curve details, and [Brown et al., 2010] for the effective throughput for a SN Ia. In total, 219 SNIa were observed by Swift UVOT between March 2005 and October 2016 (SNIa 2005am through 2016gxp, inclusive) with photometry available through the Swift Optical Ultra-Violet Supernova Archive (SOUSA; [Brown et al., 2014b]). A 3" or 5" aperture was used to maximise the signal-to-noise and zeropoints were based on the updated calibration of [Breeveld et al., 2011] and the time-sensitivity correction from July 2015.

Upon manual inspection of the galaxy-subtracted UVOT light curves, we selected 110 SNIa which had at least four data points in the $UVW1$ filter covering the peak and early decline. Due to the faintness of SNIa in the mid-UV, some did not have adequate light curves in $UVW2$ and $UVM2$, and some were saturated in the U, B, and V filters at peak. The light curves were initially fit following the procedure in [Brown et al., 2017]. Template light curves were fit to our data, using the peak magnitude, time of maximum, and stretch (linear scaling in the time axis) as free parameters. We used the B and V template curves from MLCS2k2 [Jha et al., 2007] and the $UVW2$, $UVM2$, and $UVW1$ light curves of SN 2011fe [Brown et al., 2012a]. The $UVW1$ light curve of SN 2011fe was also used to fit the U band light curves due to the similarity of the mean light curves of U and $UVW1$ bands found by [Milne et al., 2010] and the saturation of the Swift U band light curve of SN 2011fe near peak.

2.2.2 FPCA Model

To model our sample, we used templates constructed from functional principal component analysis (FPCA, [He et al., 2018]), a statistical method that uses a linear combination of a mean function and a few principal component (PC) functions to represent the light curve. The coefficients associated with these functions are called PC scores. The mean light curve function and PC functions were trained using a data set of light curve photometry for 111 SNIa in the $BVRI$ bands. A four PC template was created for each band, as well as a generic (band-vague) template that combined the training data across bands that can be used to model light curves in any filter.

To retrain the FPCA model to include UV photometry would require more quality observations and an amount of work beyond the scope of this paper. Rather, we take the simpler step of using the band-vague template to fit the UV and optical light curves simultaneously. While the inclusion of the R and I band in the training set leads to an over-prediction of flux at later phases, we find (2.2.4) that the quality of the fit is comparable between the UV and optical bands in the regions near peak flux. Using the same template to fit across all bands has the added benefit of each PC controlling the same aspects of each light curve, allowing for direct comparisons. In Section 2.4 we examine possible future work with UV trained modeling.

Per [He et al., 2018], the first PC reflects the decline rate after the peak, and the second PC reflects the light curve width around the peak. The third PC adjusts the pre-peak rise as well as a bump 20 days after peak that is commonly seen in the near-IR bands, while the fourth PC accounts for more complex fluctuations. While the first three components are tied to certain light curve properties, they also describe a wider range of parameters. This means that while the first PC is related to the decline rate, it is not a perfect one-to-one correlation. In the original data set that this template was tested on the first PC score explained 92$\%$ of variability, the first two explained 96$\%$, and all four explained 99$\%$ of variability. In Figure 2.1 we replicate the effects of a typical range of PC weights for visualization.

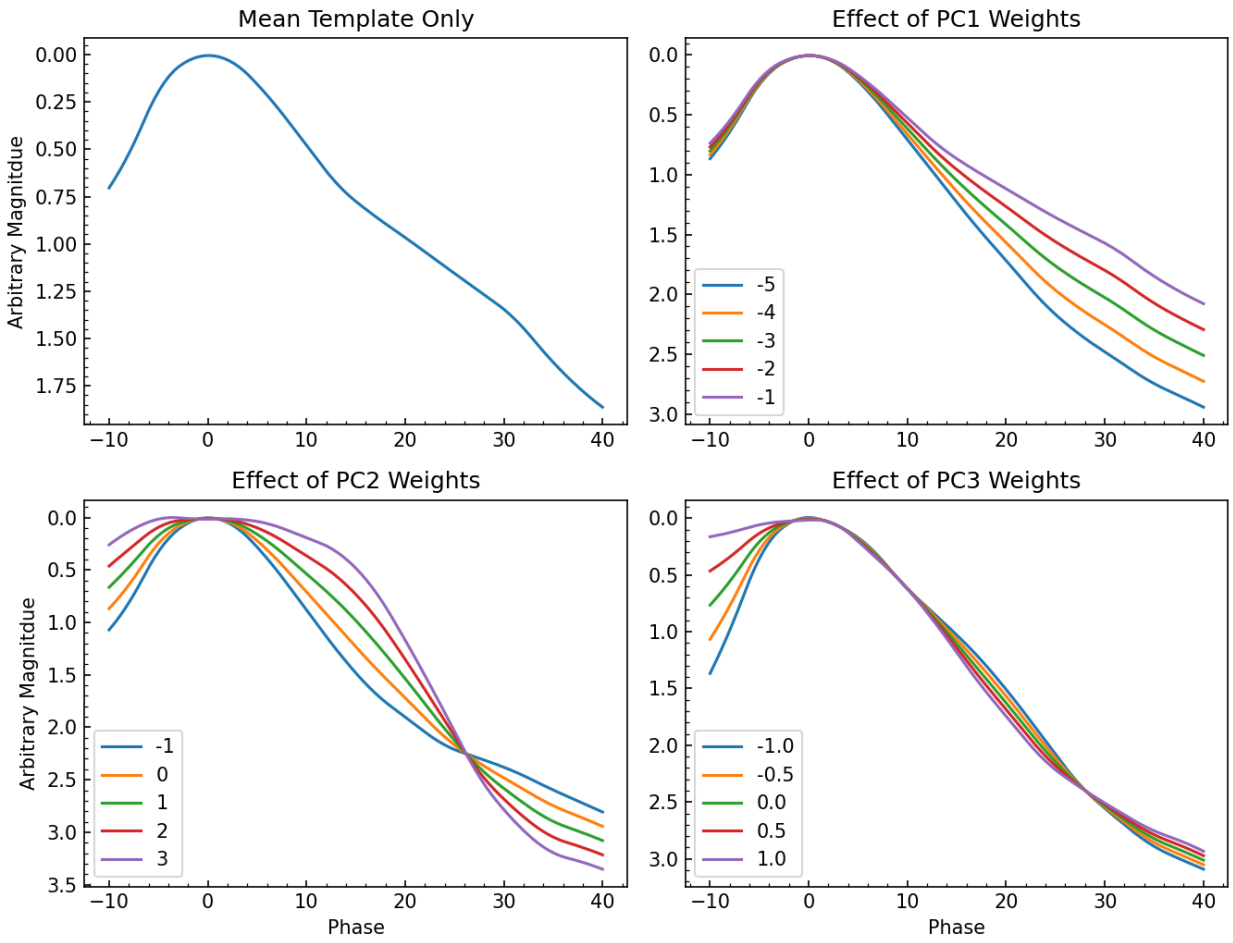

Figure 2.1: Examples of the effect that each PC template has on the light curve for a range of common B band PC score weights. The PC1 template mostly controls the late-phase decline rate, the PC2 template controls the overall stretch of the light curve and the post-peak decline rate, and the PC3 template has a plays a role in the pre-peak rise rate and the late phase flux.

2.2.3 Template Fitting

We calculated the phase of each light curve in all six filters, corrected for redshift time dilation, by using the estimated peak from the preliminary modeling as our zero point.

$$Phase_i = \frac{MJD_i - MJD_{peak}}{1+z} \tag{2.1}$$

We then removed data points that occur 10 days before the peak or 40 days after the peak,

as those are outside of the domain of the template. We ensured that there was at least one data point before the peak and one at least 15 days after the peak, and that there was a minimum of five data points. The template models were then linearly interpolated to match the phases of the observations, and linearly combined to match the observed light curve with weights for the templates determined by the `curve_fit` package from the SciPy library in python [Virtanen et al., 2020]. The program attempts to fit the function to the data by minimizing the non-linear least squared errors. Below is an example of the function,

$$LC(p) = M_{peak} + Mean_{template}(p) + \sum_{i=1}^{N} W_i * PC_i(p) \tag{2.2}$$

where p is the phase, M_{peak} is the peak magnitude (a free parameter, but given an initial guess based on the preliminary modeling estimates), $Mean_{template}$ is the mean light curve from the template, and W_i is the weight of each principal component as determined by `curve_fit`.

In total, there were 97 SNIa that had a fitted light curve in at least one filter, and 14 SNIa that had a fitted light curve in every filter. The $UVM2$ filter had the fewest well-fit light curves, due to the lower S/N of observations compared to other filters. Uncertainties in our model fits were determined by examining the full covariance matrix that results output by the `curve_fit` package. We measured the R^2 values for the modeled SNIa (Figure 2.3) as a test of goodness-of-fit, and find that the majority of SNIa behavior is well explained by our model. The U and $UVW1$ curves (which were not included in the training of the band-vague fitting) are fit with similar accuracy to the B and V band, respectively, and the PC fits explain 95% of the points for 75% of the mid-UV ($UVM2$ and $UVW2$) light curves.

2.2.4 Model Selection

To determine how many principal components were needed to ensure a good quality fit for our data set, we employed several tests of model selection. From the 14 SNIa with fits in all six bands, we selected four that had a relatively large number of observations (SN2005ke, SN2007af, SN2007on, SN2011by) to serve as test cases. Using the `train_test_split` package in the

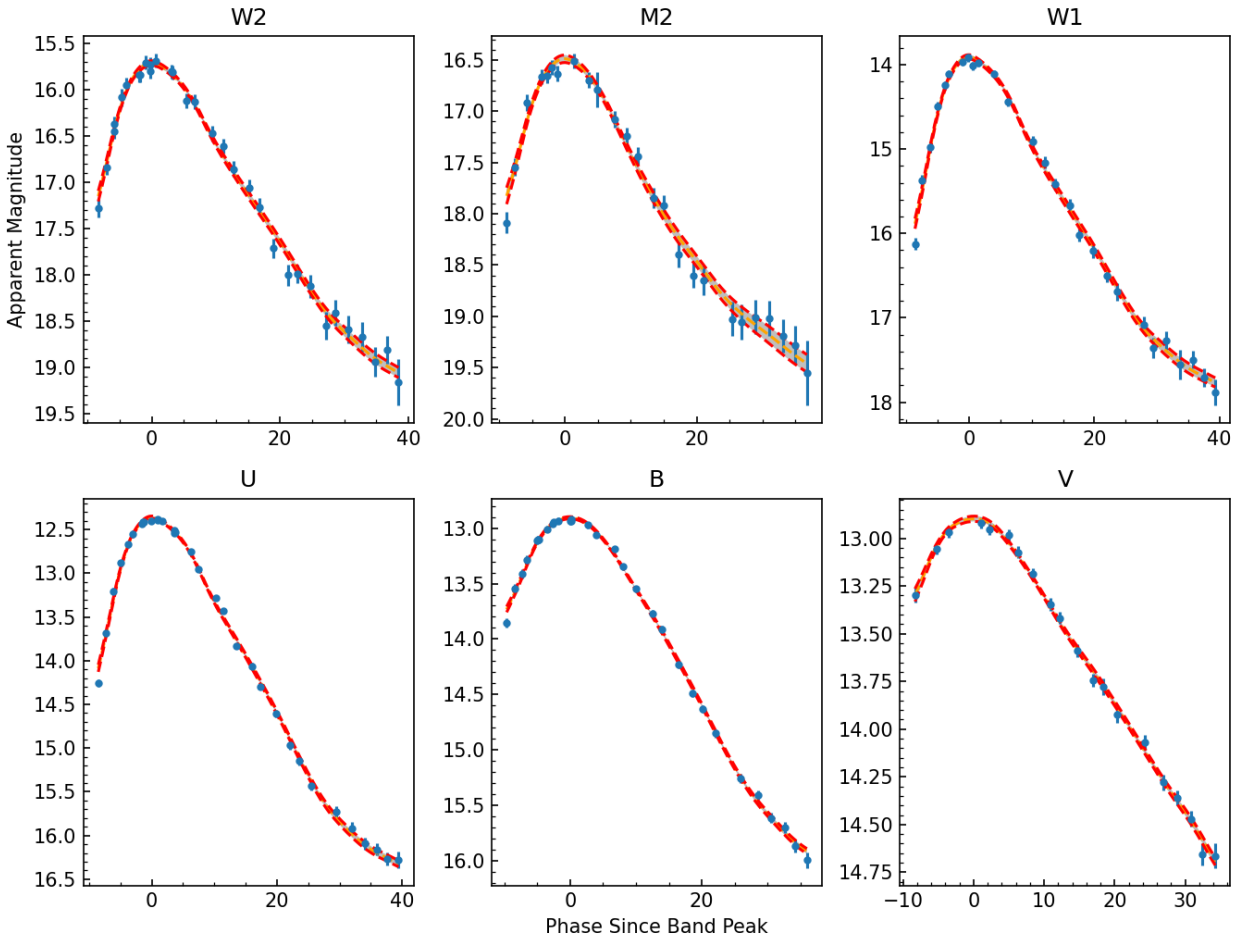

Figure 2.2: Swift observations of SN2011by (blue) and the 3 template model (orange) with 1 σ errors (red). A phase of 0 in each subplot corresponds to the date of the modeled peak brightness for each band.

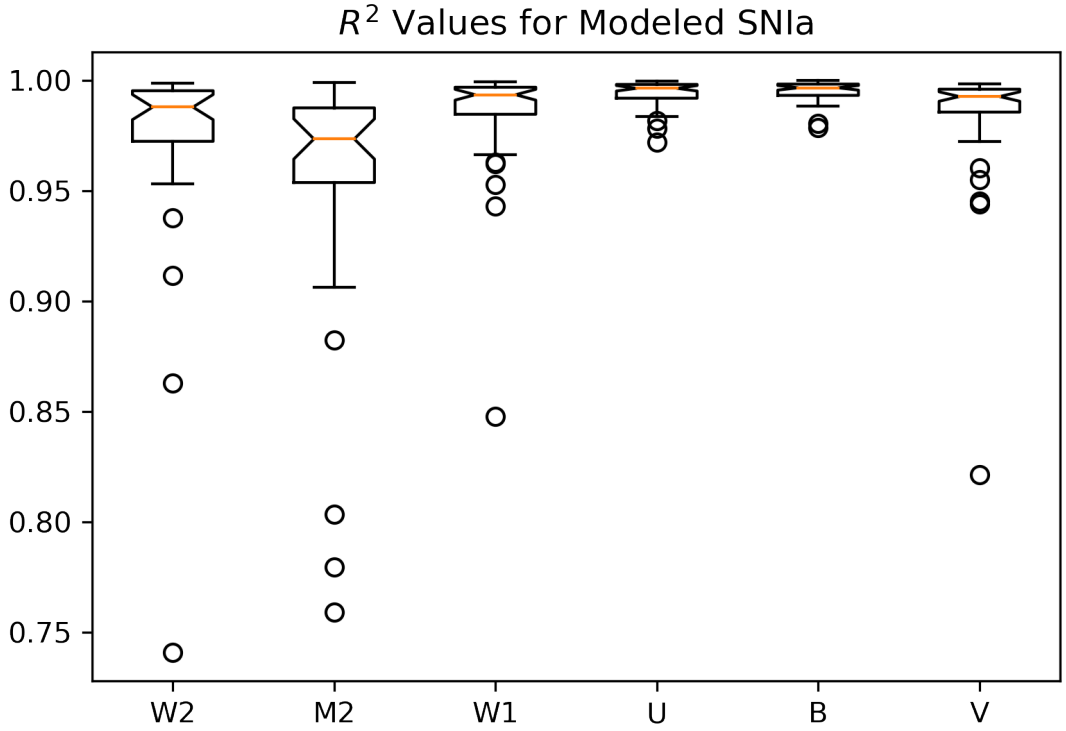

Figure 2.3: The R^2 values of modeled SNIa in each band. This value measures the amount of variance in the data that is explained by the model on a scale of 0-1. This measurement is done without accounting for the known observational error in the data, and is thus a lower limit on the true R^2 value. The notches on each box plot indicate the uncertainty in the median, and the whiskers indicate 1.5$\times$IQR distance.

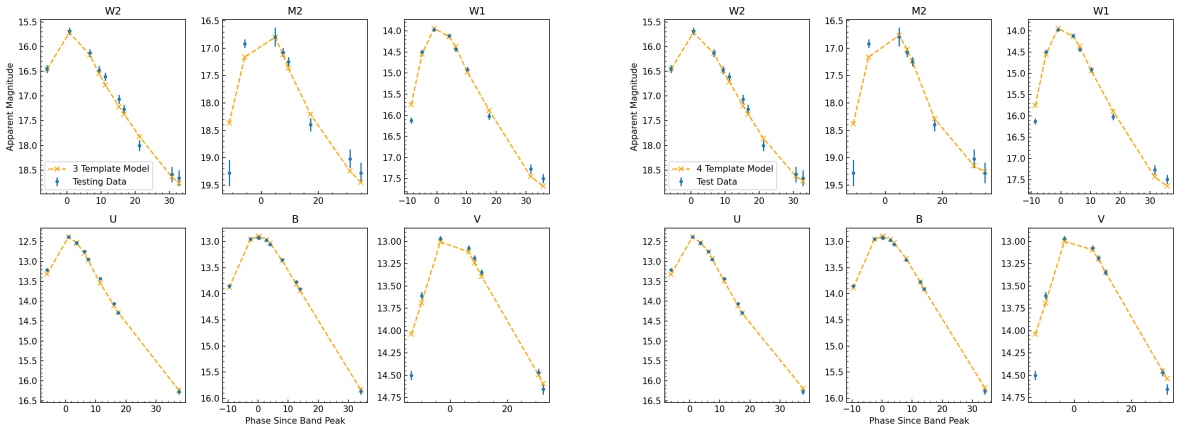

Figure 2.4: An example of one of the bootstrap samples used for estimating the robustness of a three-PC model vs a four-PC model, using SN2011by. After the model parameters are estimated using a training set, the model is then fit to a testing set and checked for goodness of fit. Increasing the number of templates used in the model from three to four does little to improve the fit of the model to the data.

scikit-learn library in Python [Pedregosa et al., 2011], we performed 100 bootstrap draws from each SNIa with a 70/30 split between the training and testing sample sizes. This allowed us to test the robustness of our fit with light curves that have sparse or inconsistent sampling, which is a more realistic case for the majority of our observations.

The Akaike Information Criterion (AIC) [Akaike, 1974] was calculated for each bootstrap sample and the mean AIC score for the two-, three-, and four-PC model were compared. The AIC score is a comparison test that measures how well a model fits a data set given a certain level of model complexity. In general, a lower AIC score indicates a better model. We employed a modified version of the AIC to account for the relatively small sample size, as shown in Equation 3.

$$\begin{aligned} AIC &= 2k - 2ln(\hat{L}) \\ AIC_{small\ sample} &= AIC + \frac{2k^2 + 2k}{n - k - 1} \end{aligned} \tag{2.3}$$

$\hat{L}$ is the maximum value of the likelihood function of the model, k is the number of parameters, and

Filter	Training Size	Testing Size	3 Temp. μ	3 Temp. σ	4 Temp. μ	4 Temp. σ
W2	22	10	5.4	0.7	12.3	0.7
M2	18	8	6.3	1.4	17.0	1.8
W1	18	9	4.9	1.3	12.8	1.4
U	23	10	3.5	1.4	10.4	1.5
B	23	10	3.0	1.7	9.6	1.9
V	16	8	4.0	1.5	14.0	1.6

Table 2.1: A comparison of the mean and standard deviation of the AIC scores taken from 100 random samples of SN2011by data. In general, a lower AIC score indicates a more favorable model.

n is the sample size. We also explored using the Bayesian Information Criterion, but determined that our sample sizes were too small for an accurate assessment.

Overall, we found that the two-PC and three-PC models had the lowest mean AIC scores in all six filters, signifying them as more appropriate models than the four PC model to use for our analysis. Between the two-PC and three-PC models, neither one had a significant difference when examining the larger data set. Future work with the FPCA template fitting could include individualized fitting for each SNIa and filter with more rigorous testing, but for uniform fitting we chose the three PC model. It added robustness to our modeling by improving our estimates of the rise of the light curves, with a minor risk of overfitting certain SNIa.

2.3 Analysis and Results

We employed a series of statistical tests to examine the similarity in the distribution of PC scores across the different bands. The Brown-Forsythe test [Brown and Forsythe, 1974] examines the differences in the variance of two data sets by examining the distribution around the median. The null hypothesis for this test is that there is no statistical difference in the variance, while a p-value below 0.05 would indicate there is a difference in variance (Appendix A).

Additionally, we visually inspected the data variability with box plots (Fig. 2.5)[Tukey, 1977]. Boxplots allow us to identify quickly and assess outliers, while also being less susceptible to issues such as sample size and skewness that may bias p-values. In particular, we examined the interquan-

tile range (IQR) of the different PC scores in each band. Similar IQR scores would suggest that the populations have similar variances. Visual analysis of the outliers revealed that many had models with acceptable fit quality, indicating that our model is capable of fitting the full diversity of our sample.

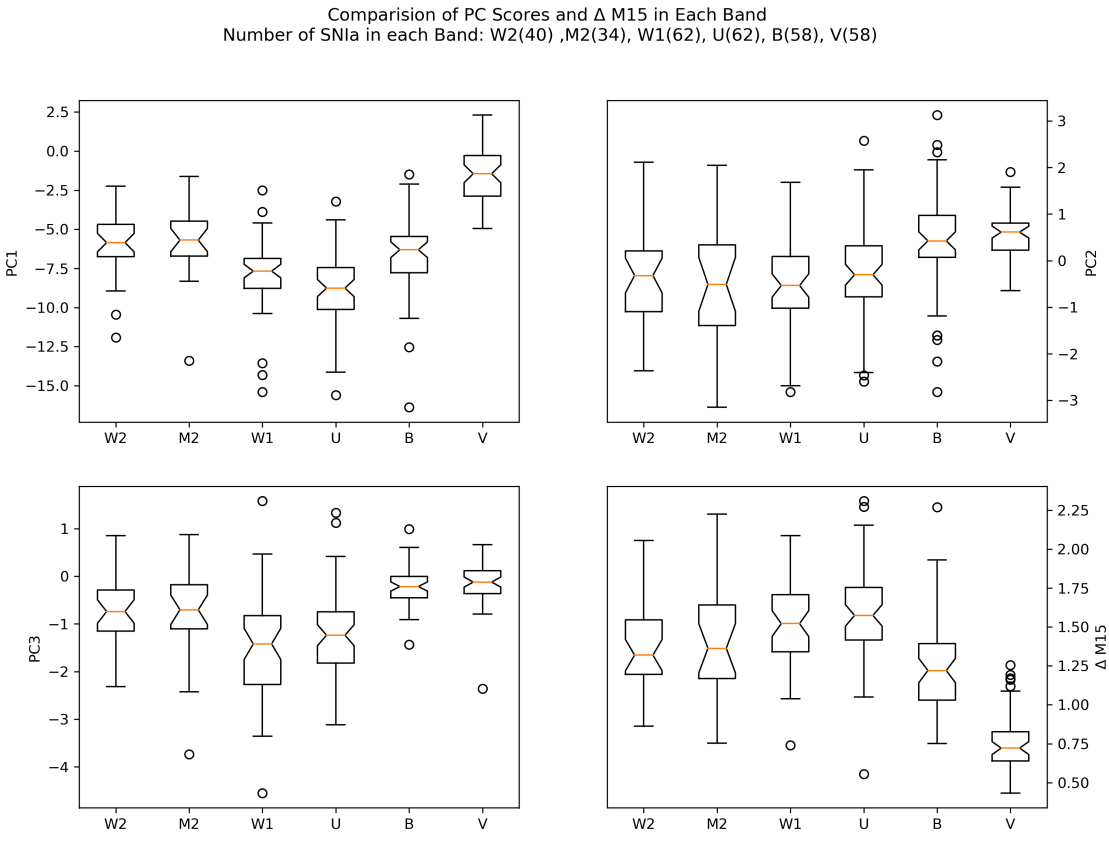

Figure 2.5: Box plots depicting the spread of parameters in each band. The notches indicate the uncertainty in the median, and the whiskers indicate 1.5×IQR distance. Light curves with parameter estimates beyond the whiskers are labeled as circles.

We find little statistical difference between the spread of PC1 and PC2 scores for both the UV and optical bands when compared to the B band PC scores. For PC3 weights, only the V band has a similar spread in values to the B band, all other bands show a much larger spread in potential

values. As both the PC1 and PC2 scores relate to the near-peak decline rate, nether can be solely used as a proxy for Δm_{15}. However the full model can be used to directly estimate the Δm_{15}, and the derived values show similar diversity with the B band values (except for the V band, which has a much tighter spread of values).

To examine the one-to-one correlations between filters, we plotted the parameter values in each filter versus the B band value. We then estimated the Spearman rank-order coefficient [Kokoska and Zwilinger, 2000], a non-parametric measure of two sets for a monotonic relationship. For parameters that have a p-value below 0.05, we test out whether a linear model can describe the relationship. While the true relationship may not be linear, having the linear fit can be a useful visual representation of the correlation and distribution of parameters. To perform this linear regression we employed the Python routine LINMIX, which uses Bayesian inference to return random draws from the posterior distribution [Kelly, 2007]. The routine uses a 1,000 iteration Markov Chain Monte Carlo procedure to converge on the posterior. The benefit of using this routine is its ability to handle uncertainties in both the independent and dependent variables as well as intrinsic scatter. From the iterations, we take the average value of the slope and intercept as our best fit parameters, and estimate the r^2 value to see how well the linear fit describes the correlation. The r^2 value is based on the total sum of squares (SS_{tot}) and the sum of squared residuals (SS_{res}) of the observed (y) and modeled (f) data, where

$$\begin{aligned} SS_{tot} &= \sum_i (y_i - \hat{y})^2 \\ SS_{res} &= \sum_i (y_i - f_i)^2 \\ r^2 &= 1 - \frac{SS_{res}}{SS_{tot}} \end{aligned} \tag{2.4}$$

We find that while the optical properties (U and V bands) are highly related to the B band properties, only the PC2 weights (Fig. A.2) show a consistent correlation between the mid-UV and near-UV bands and the B band. For PC1 (Fig. A.1), there is a strong correlation between the

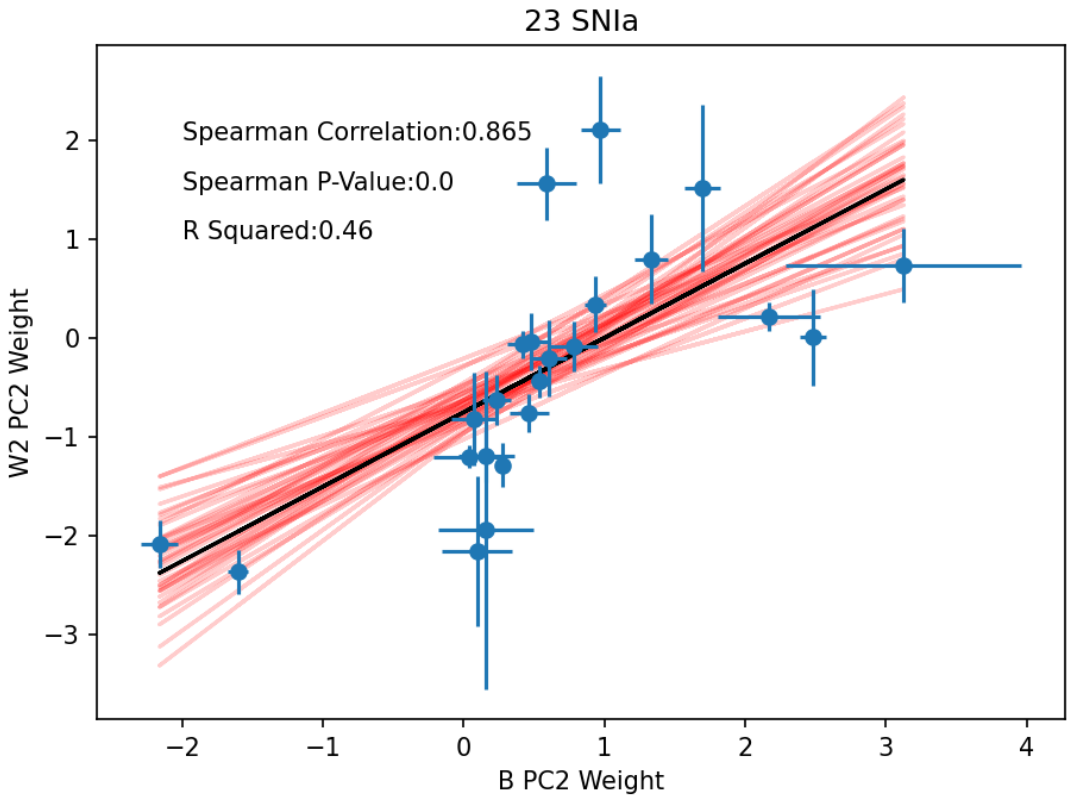

Figure 2.6: The comparison between the B band and W2 band PC2 weights for our sample of selected SNIa. The red lines indicate the range of possible regression fits from the LINMIX routine, and the black line indicates the linear fit based on the mean of the LINMIX coefficients. See Figures A.1, A.2, A.3, and A.4 in the appendix for the full set of correlated properties.

$UVW2$ band and the B band, which may be due to the relatively higher quality and quantity of data compared to the $UVM2$ and $UVW1$ bands.

There is little to no statistical correlation for the PC3 weights (Fig. A.3) between the UV bands and the B band, although the $UVW1$ could be a statistical edge case that lacks enough quality data to make a solid statement. The Δm_{15} (Fig. A.4) shows a strong correlation and a relatively tight linear relation with the B band in both the UV and the optical.

Finally, we examined the differences in the peak magnitude phase between the B band and the other filters, using a similar analysis to the PC score distributions. We find (Fig 2.7) that the U band and $UVW2$ band light curves have a tight spread of peaks phases at around 2 days before the

B band peak, and the V band has a tight spread at around 2 days after the B band peak (Figure 2.7). The $UVM2$ and $UVW1$ band light curves also seem to peak earlier than the B band light curves, although there is a much larger spread in the distribution of peak phases.

Examining the outliers, we find that SNIa that peak in the UV 4 or more days before the B band peak were more likely to be classified as over-luminous in the literature. The most extreme outliers, SN2011aa [Kamiya, 2012], SN2012dn [Copin et al., 2012], and LSQ12gdj [Scalzo et al., 2014], are all super-Chandrasekhar mass candidates. Thus, the difference in the time of peak in the UV and optical may be a useful metric for sub-type classification.

2.4 Discussion

We successfully fit UV observations of SNIa using templates constructed from functional principal component analysis of optical photometry. While the quality of fit is better for the optical observations, quality of the UV fits were sufficient to perform a statistical analysis of the SNIa light curve properties. With improved UV observations and a larger data set, it should be possible to create filter-specific UV templates that will greatly improve future analysis of SNIa light curves.

We find the the overall spread of the SNIa parameters is similar between the UV and optical bands in our sample, particularly for the PC2 template weights which are most directly tied to the stretch and decline rates of the SNIa light curve. In addition, we offer strong statistical evidence for a correlation between the UV and optical PC2 weights, suggesting that we can directly interpolate the spread of the SNIa light curve in one band based on the other. This will be highly useful with upcoming large survey telescopes such as the Rubin observatory, which is expected to find millions of SNIa at a wide range of redshifts. Interpreting the rest frame UV light from distant SNIa will require further understanding of the UV emission from nearby objects.

The lack of a strong correlation in the PC1 weights could suggest that physics behind the UV and optical light curves may be different at later phases ($\geq$20), where the PC1 weights have the largest impact. For phases immediately after the peak the PC2 weights have the strongest effect on the decline rate, resulting in the strong correlation with the Δm_{15} rates. The correlations between PC2 weights in different bands suggests a common origin for the near-peak variations in the UV

and optical light curves. Further studies with multi-epoch UV spectra of SNIa could provide more details into the emission mechanisms and the variations of SNIa light curves.

Previous work in the field has focused on rest-frame optical emission, leading to a wealth of robust models and large data sets. In comparison, there is a lack of quality observations and modeling in the UV. Our findings suggest that the UV and optical light curve properties may be more similar than previously suggested, which suggests the worth of further study into this regime. Future work will greatly constrain the true behavior of UV SNIa light curves relative to the better understood optical regime.

These correlations will be important for the study of high redshift SNIa, whose rest-frame UV and optical emission will be simultaneously observable with upcoming ground-based telescopes such as the Vera Rubin Observatory. In the case that the optical light curve is poorly sampled (regardless of distance), the UV light curve may be able to provide constraints on optical properties such as the decline rate or stretch. The UV emission's potential for sub-type classification may, with further study, also assist in standardizing the optical relations. The UV has also been shown to significantly improve estimates on the amount of reddening due to dust extinction when used in conjunction with optical and NIR data [Amanullah et al., 2015], further showing the usefulness of multi-band studies.The diversity of the UV absolute magnitudes remains poorly constrained, however, hindering cosmological studies based only on UV observations.

2.5 Conclusion

We modeled the light curves of 97 SNIa in the UV and optical from the Ultra-Violet Optical Telescope on the Neil Gehrels Swift Observatory in order to better understand the correlation of their properties in different wavelength regimes. Modeling was done using a linear combination of band-vague templates, based on functional principal component analysis (FPCA) of a sample of SNIa in the optical bands. Each principal component is associated with a different light curve property, making it a useful tool for finding correlations between the filters.

We find that the overall dispersion in the PC1 and PC2 weights in all filters were similar, suggesting that the UV light curves are not as variable as the optical light curves. There is not

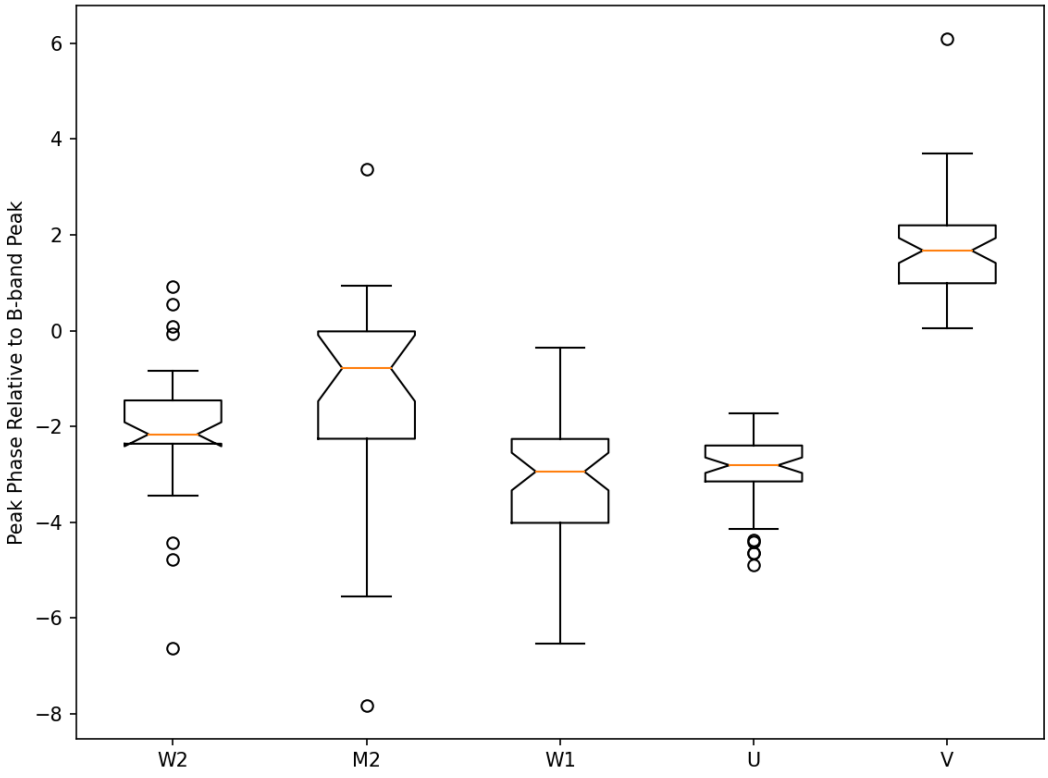

Figure 2.7: A boxplot of the peak phases for the light curves in each band relative to the B band peak phase. Both the $UVW2$ and U band light curves have a narrow distribution of peak phases at around 2 days before the B band peak phase, while the V band light curves have a narrow distribution at around 2 days after the B band peak phase. The $UVW1$ band light curves seem to peak earlier than the B band light curves, but with a larger spread in the distribution.

a strong correlation in the PC1 weights for the UV and optical filters, which would indicate the lack of a strong correlation in the late-phase decline rate. There is a statistically strong correlation between the UV and optical filters for the PC2 weights, which would suggest that the stretch of the light curves and the post-peak decline rates are correlated across the wavelength regimes. This could point to underlying physics that ties the UV and optical flux together, with the bulk of the light curve shape likely being driven by ^{56}Ni decay. The differences that do exist are likely due to wavelength-dependent metallicity effects and the opacity of the SNIa atmosphere. This is the first study to statistically show that the UV and optical light curve properties have similar variability, and that the stretch and decline rate of the UV and optical light curves are significantly correlated.

2.6 Acknowledgements

The authors are grateful for the continuing support of the Mitchell Institute for Fundamental Physics and Astrophysics. This work was supported by NASA grant 80NSSC20K0456, "SOUSA's Sequel: Improving Standard Candles by Improving UV Calibration". The authors would like to thank Minjee Kim, Jianhua, Huang, and Xiaomeng Yan for lessons learned from related work. We also thank Nicholas Suntzeff, Lauren Aldoroty, and Jiawen Yang for their assistance and expertise, as well as the anonymous referee for their helpful comments. This work made extensive use of the Python Programming language and the following community-developed/maintained software packages: Jupyter [Kluyver et al., 2016], NumPy [Harris et al., 2020], Matplotlib [Hunter, 2007], Pandas [Wes McKinney, 2010], and SciPy [Virtanen et al., 2020]. This work also used arXiv.org and NASA's Astrophysics Data System for bibliographic information.

3. MODELING THE SPECTRAL ENERGY DENSITY OF TYPE IA SUPERNOVAE

3.1 Introduction

In order to measure an object's absolute magnitude (M) based on its apparent magnitude (m), one must follow a seemingly simple formula:

$$m - M = DM(z) + A(\lambda) + K(z) \tag{3.1}$$

$$DM(z) = 5log_(10)\frac{D}{10pc} \tag{3.2}$$

where $DM(z)$ is the distance modulus for an object at distance D, and $A(\lambda)$ and $K(z)$ are corrections for the change in spectral shape due to dust extinction and redshift, respectively. If the spectral shape of the object is unknown, the $A(\lambda)$ and $K(z)$ corrections can not be made. One common method of assuming a spectral shape is to model the object's Spectral Energy Density (SED) using templates. These SEDs can be used to create synthetic photometry which are matched to the observations; the best fit model is assumed to be the relatively close to the true spectral shape of the object. Currently, programs such as SALT3 [Kenworthy et al., 2021] and BAYESN [Mandel et al., 2022] use this method to measure the optical and near-IR properties of SNe Ia.

These programs require a large training set of spectra and photometry to generate accurate SEDs. However, the current UV archival data is not large enough for accurate statistical training, thanks in part to the lower intrinsic luminosity and reduced filter transmission (Fig. 3.1). In addition, the UV spectral variability tends to be greater than the optical variability (Fig. 3.2). This is likely due to greater susceptibility of UV flux to dust extinction and metallicity effects such as Fe-group blanketing [Foley et al., 2016, Brown et al., 2017]. This variability can make it difficult to separate SNe Ia into intrinsically red vs reddened due to dust based on photometry alone. The spectral shape has a major impact the observed photometry as spectral features move into different filters; the correction for this shift is known as the $K(z)$ correction. In the nearby universe the required $K(z)$ correction in nearly 0, but as we look to higher redshifts the required correction can

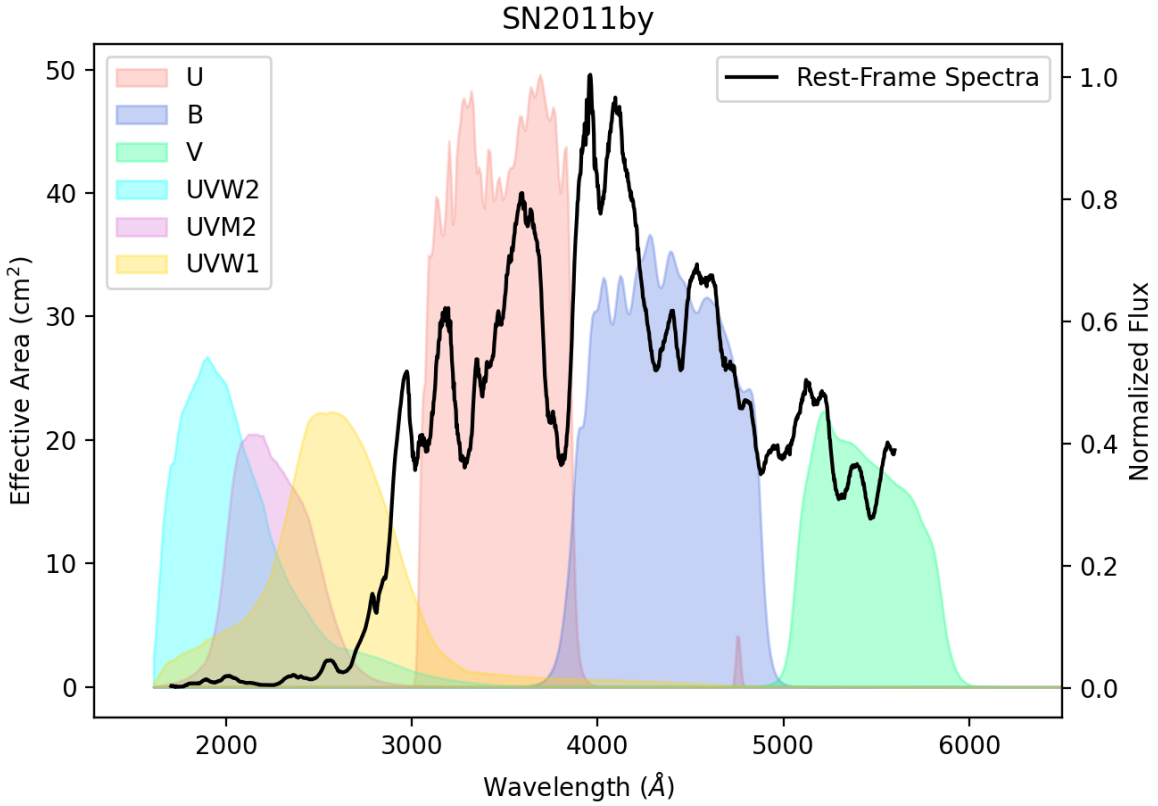

Figure 3.1: A comparison of the Swift UVOT filters and the normalized HST spectrum for SN2011by. The effective area of the UV filters are roughly half that of the U and B filters, and the UV flux is roughly a tenth that of the optical flux. This combination limits the capabilities of deep UV surveys. Note the "Red Tail" in the UVW1 and UVW2 filters, where part of the filter stretches out into the optical wavelengths. While this tail has the lowest effective area in the filter, it also spans a region with much higher incoming flux which in turn could bias UV photometry.

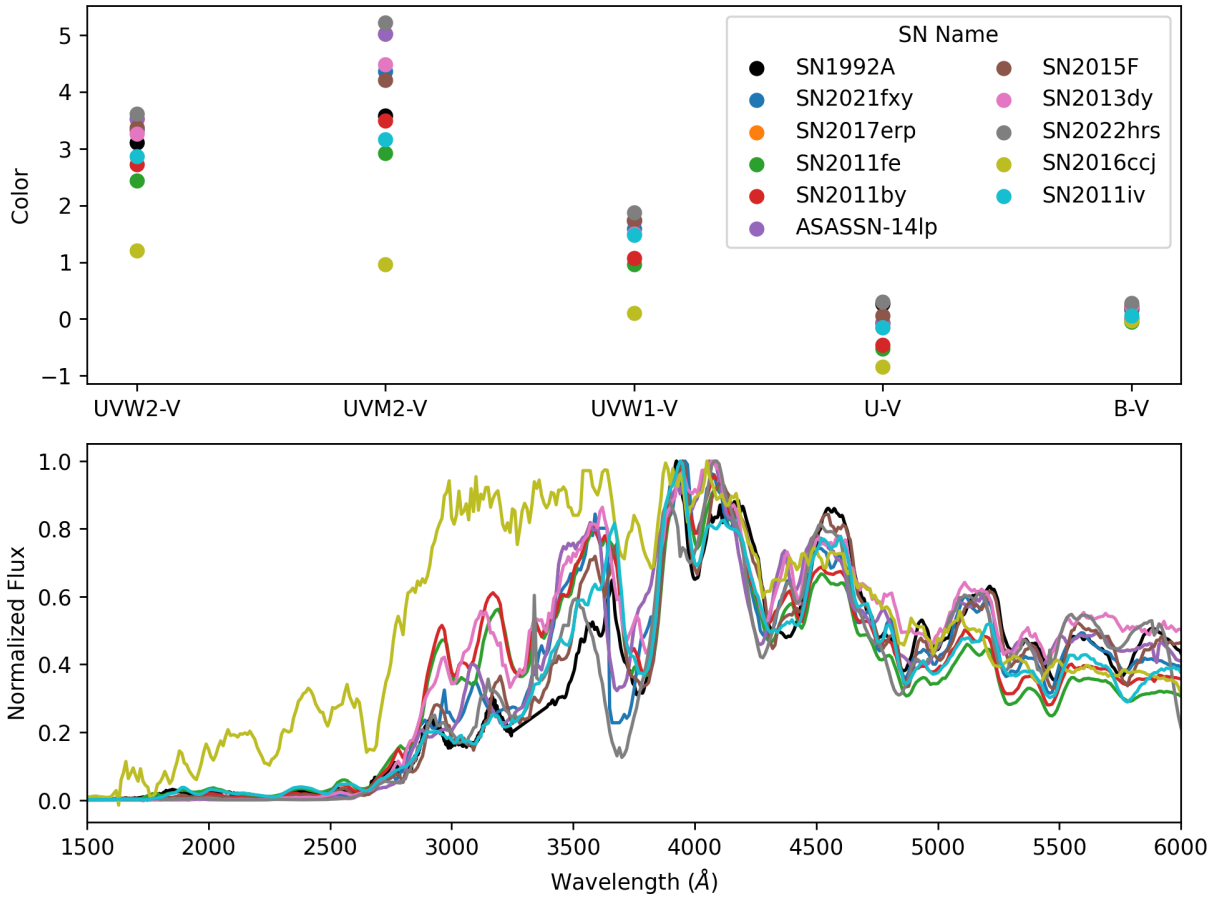

Figure 3.2: Synthetic Swift UVOT colors of 11 SNe Ia (top) based on their HST Spectra (bottom). While their B-V colors show little difference, their UV-V colors can occupy a large range due to the UV spectral diversity.

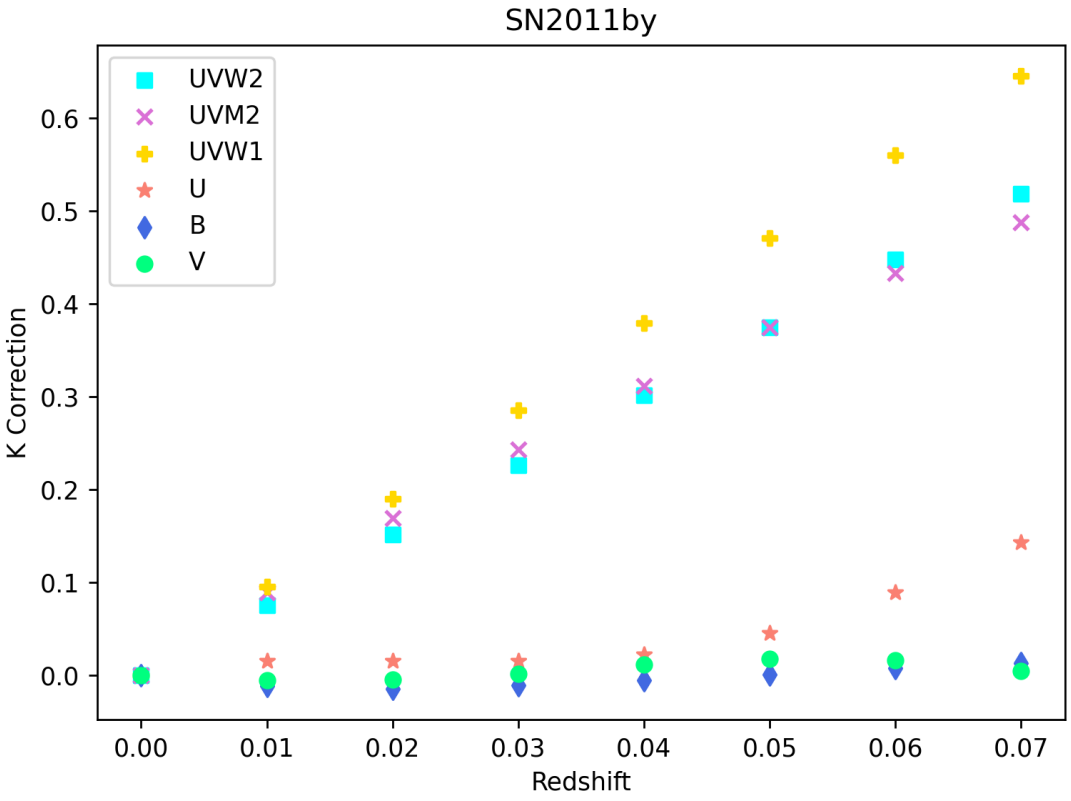

Figure 3.3: The $K(z)$ corrections for SN2011by from $0.0 \leq z \leq 0.07$. While the optical $K(z)$ corrections are small, the UV corrections can be as much as half a magnitude at higher z. After $z \sim 0.03$, any shift in an object's spectrum is dominated by the Hubble expansion, but for nearby objects there may be additional corrections due to the peculiar velocity of the object that we do not account for.

be significant (Fig. 3.3) and depends heavily on the intrinsic spectral shape of the SNe Ia (Fig. 3.4). Thus, any attempts to understand the UV $A(\lambda)$ and $K(z)$ corrections for SNe Ia using SED modeling would require a robust library of spectral templates.

3.2 Supernova Sample Selection

Our sample includes 44 SNe Ia observed with the Ultra-Violet Optical Telescope (UVOT; [Roming et al., 2005]) on the Neil Gehrels Swift Observatory [Gehrels et al., 2004] between 2005 and 2018. The observations were performed in all six medium-band UVOT filters ($UVW2$, $UVM2$, $UVW1$, U, B, and V), and were accessed from the Swift Optical Ultra-Violet Supernova

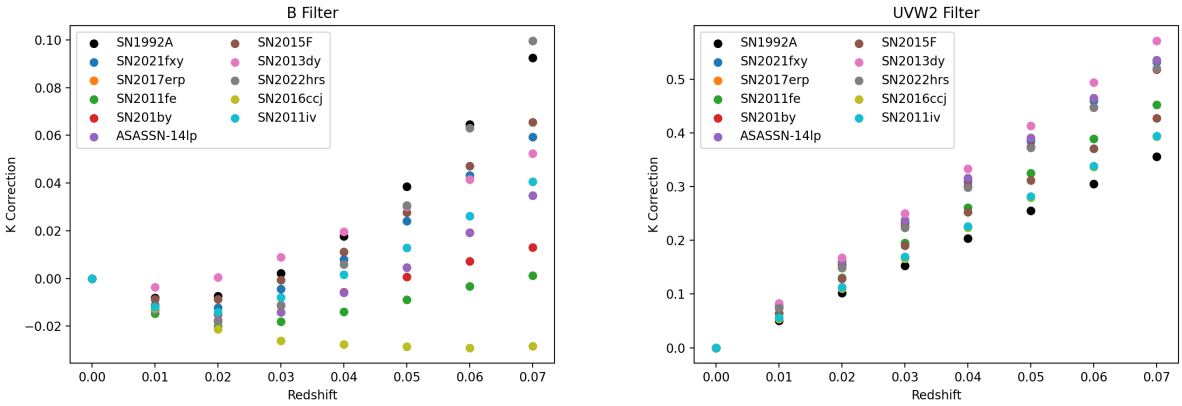

Figure 3.4: The amount of $K(z)$ correction in any particular filter depends heavily on the intrinsic spectral shape of an object. Here we show the B (left) and $UVW2$ (right) filter corrections for 11 SNe Ia (see Table 3.1). The B corrections are significantly smaller than the $UVW2$ corrections, but both show a large deviations based on spectral shape at higher z.

Archive (SOUSA; [Brown et al., 2014b]). All but one SNe were pulled from [Devarakonda and Brown, 2022] (see 2.2.1), SN2018aoz was added to this sample as part of an analysis on its early light curves [Brown et al. in prep].

The light curve $\Delta m_{15}(B)$ values were determined using the FPCA modeling technique (described in Chapter 2, [He et al., 2018, Devarakonda and Brown, 2022]). However since the FPCA technique requires observations that span a wide range of phase space to constrain the light curve behavior, it struggles to fit a peak magnitude for where there is a narrower selection of observations. This is not an issue in the B filter, but in the UV many supernovae lack enough observations to constrain the light curves with FPCA. Instead we determine the peak magnitudes with SNooPy [Burns et al., 2011], which models light curves by applying a stretch factor to templates in multiple filters. In Fig. 3.5 we compare the peak apparent magnitude (B) estimates from both fitting programs and find that they mainly agree. In the UV, SNooPy tends to favour brighter estimates for the peak magnitude, and this bias seems to increase towards the fainter SNe Ia. In the B, FPCA tends to favor slight brighter estimates, although there does not appear to be a trend with apparent magnitude. For the peak magnitudes, we prefer SNooPy for its improved ability to estimate the peak magnitude in all 6 UVOT filters compared to FPCA. We use FPCA for our $\Delta m_{15}(B)$ values

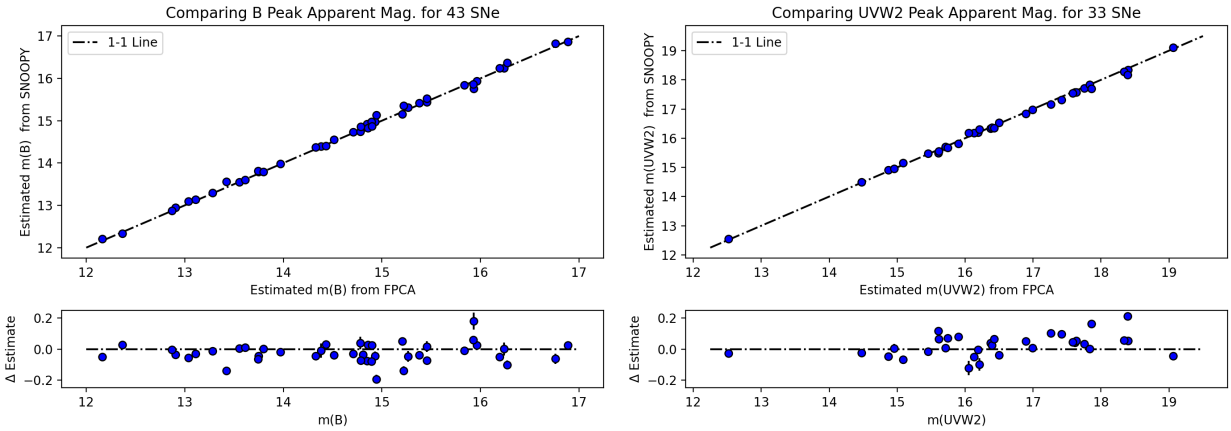

Figure 3.5: Top left: The estimated peak apparent magnitudes (B) from Snoopy and FPCA. Bottom left: The difference (FPCA-SNooPy) in the B filter peak magnitude. While both methods are in general agreement, FPCA tend to prefer slightly brigher estimates for the magnitude. Top right: The estimated peak apparent magnitudes ($UVW2$) from Snoopy and FPCA. Bottom right: The difference (FPCA-SNooPy) in the $UVW2$ filter peak magnitude. Here, SNooPy tends to prefer brighter estimates, with the discrepancy increasing for fainter SNe Ia.

to be consistent with our previous study (Chapter 2, [Devarakonda and Brown, 2022]).

3.3 Spectral Templates

Currently, there are a small number of SNe Ia with high quality UV/optical spectra near peak. For our analysis, we use the observed ultraviolet spectra of the sample of SNe Ia listed in Table 3.1. We also use the UV model from [Foley et al., 2016] as a function of $\Delta m_{15}(B)$ created at intervals of 0.1 (Fig. 3.6). The UV model was created using most of the spectra we use; in areas of $\Delta m_{15}(B)$ not sampled it provides an interpolation and in areas more densely sampled it averages over the differences of the supernovae e.g. SNe 2011by and 2011fe [Foley and Kirshner, 2013]. The addition of SN2017erp, SN2021fxy, and SN2022hrs probe the UV fainter extremes [Brown et al., 2019, DerKacy et al., 2023], and SN2016ccj matches the so-called "Super-Chandra" or SN2003fg-like SNe (Brown et al. in preparation). As the spectra will be modified by positive and negative reddening before matching to the observed photometry, we do not correct these spectra for MW or host reddening.

The photometric comparisons require spectra to cover the 1600 – 6000 Årange in both the

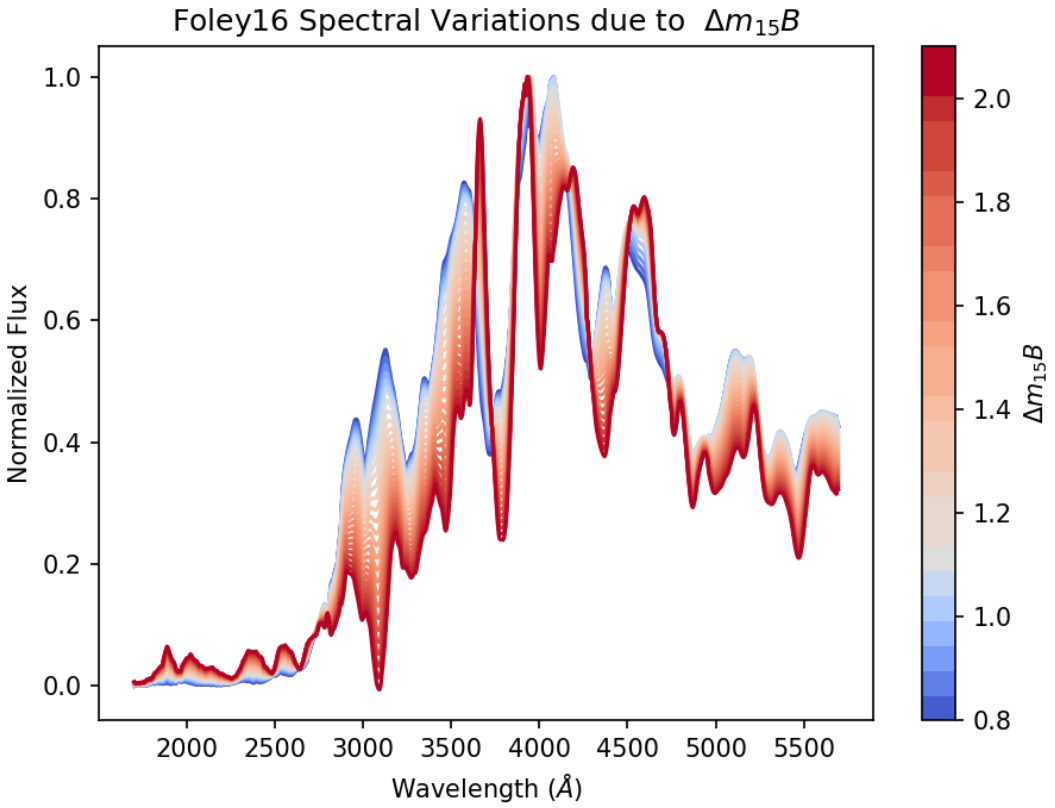

Figure 3.6: Spectral shape variations in the Foley16 template due to $\Delta m_{15}(B)$, normalized to the peak flux value. The color bar represents the $\Delta m_{15}(B)$, reflecting the shift in $B-V$ color as the $\Delta m_{15}(B)$ shifts from ~ 1.1. Generally, SNe Ia with broader, slow declining light curves tend to be bluer, while fast declining SNe Ia tend to be redder [Phillips et al., 1999].

SN Name	$\Delta m_{15}(B)$	Reference
SN2016ccj	0.67	Brown et al. in prep
ASASSN-14lp	0.80	[Shappee et al., 2016] ,[Foley et al., 2016]
SN2013dy	0.92	[Pan et al., 2015]
SN2021fxy	1.05	[DerKacy et al., 2023]
SN2011fe	1.05	[Mazzali et al., 2014]
SN2017erp	1.11	[Brown et al., 2019]
SN2011by	1.14	[Foley and Kirshner, 2013]
SN2015F	1.26	[Foley et al., 2016]
SN2022hrs	1.3	Brown et al. in prep
SN1992A	1.47	[Phillips et al., 1999],[Kirshner et al., 1993]
SN2011iv	1.77	[Gall et al., 2018]

Table 3.1: Observed Spectral Templates. If two references are given, the first refers to the $\Delta m_{15}(B)$ value and the second reference is for the UV/optical spectra.

observer frame and the corresponding rest frame of the SN. As the HST/STIS NUV-MAMA/230L or CCD/230LB response ends there, we supplement the short wavelength end by scaling the 2011 Sep 13 spectrum of SN 2011fe which included the FUV-MAMA/140L [Mazzali et al., 2014] to match the approximate flux of each SN in the 1600-1800 Årange and splice it to the near-UV spectrum. As the G430L spectra end at 5600 Å, an optical spectrum was similarly scaled and spliced at that end if a CCD/750L STIS observation is not available. The SN 1992A spectrum from [Kirshner et al., 1993] covers the whole range.

While these templates span a wide range of spectral shapes, there remain large gaps in the library that need to be filled for SED modeling. We accomplish this by inducing artificial (but physically motivated) variations in our original templates to generate new spectral shapes. These artificial variations are created by applying the Cardelli dust reddening law [Cardelli et al., 1988] (R_V = 1.8, 2.6, 3.1; -0.5 $\leq A_V \leq$ 0.5, step size = 0.1) as a smooth, wavelength-dependent flux correction factor, as in [Nugent et al., 2002] (Fig. 3.7). Intrinsic differences between the observed photometry and the templates are at least partially accounted for by the use of different spectral templates, though much of the color differences will arise from reddening differences relative to the spectral templates. The use of spline functions can be used to match multi-filter differences

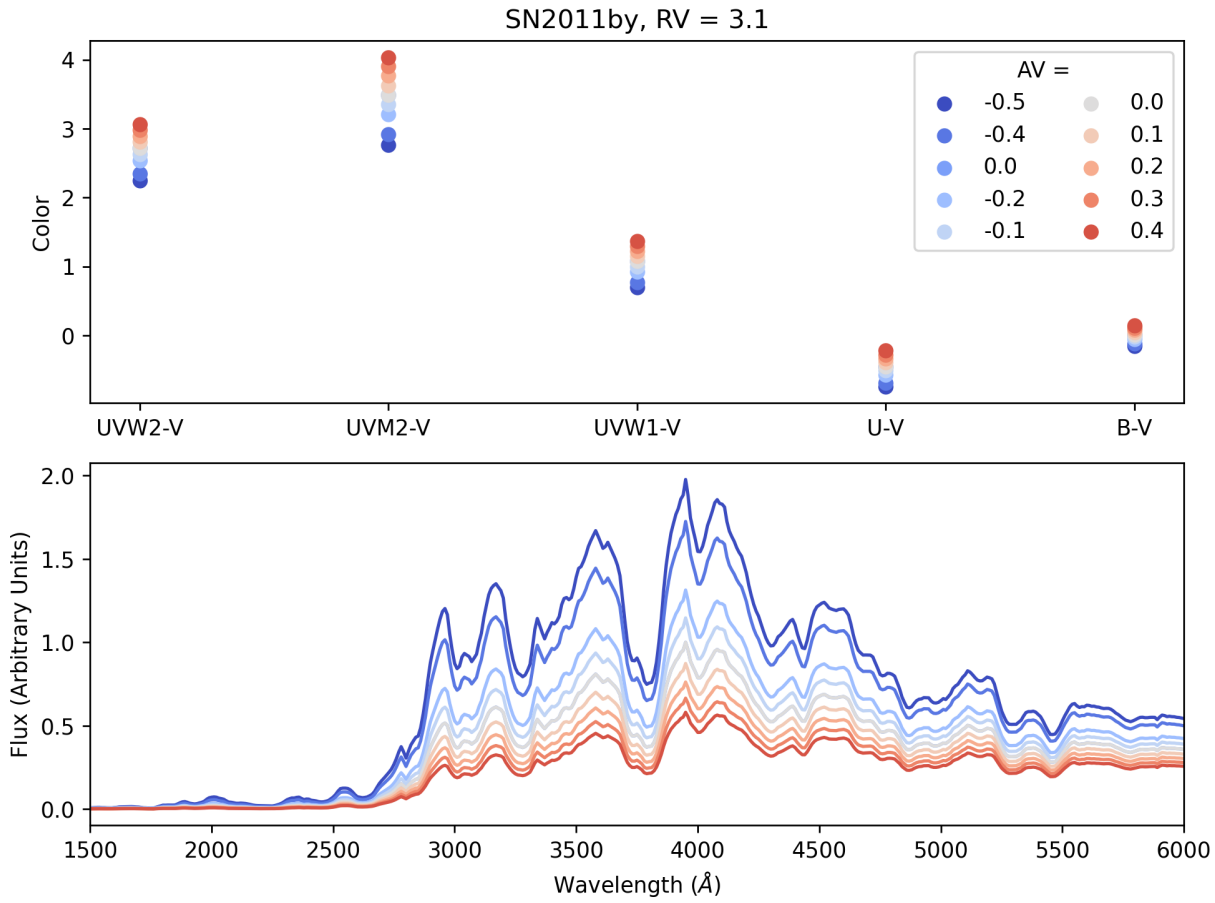

Figure 3.7: The effect of various levels of A_V on the spectral shape of SN2011by (R_V=2.6) with the CCM88 dust law. A negative A_V increases the flux of a SNe Ia by the same factor that a positive A_V reduces the flux.

[Hsiao et al., 2007]; however, the UV filters have effective wavelengths which vary with spectral shape [Brown et al., 2016] making color matching (or "mangling") via such a method problematic [Brown et al., 2010]. The choice of any specific combination of initial template and reddening is not meant to have a physical interpretation, rather it is only treated as a statistical match to a supernova's observed spectral shape.

When fitting the SEDs to our observations, we select templates from our expanded library with an initial $\Delta m_{15}(B)$ within 0.2 Mag of the measured of the $\Delta m_{15}(B)$ for the observed SNe Ia. We then shift the template spectra into the observed frame and generate synthetic UVOT photometry. The 10 templates with the lowest root mean squared deviation from the UVOT colors are selected

as the best fit models for further analysis.

3.4 Dust Extinction and K Corrections

With the chosen templates assumed to be a match for the observed spectral shape, we correct each template into the emitted frame by calculating changes in the spectra due to the Milky Way dust, redshift expansion, and Host galaxy dust (in that order). Several galactic dust laws exist that explain the reddening (slope) and extinction (amplitude) of the wavelength dependent absorption. Classically this is parameterized using the reddening and extinction in the V band (R_V and A_V, respectively), which are related to the $E(B-V)$ or color excess as [Hogg, 2022]

$$R_V = \frac{A_V}{E(B-V)} \tag{3.3}$$

$$E(B-V) = A_B - A_V. \tag{3.4}$$

For the Milky Way dust correction, we determine the E(B-V) term by using the Schlafly Milky Way Dust map [Schlafly and Finkbeiner, 2011] and apply the Cardelli dust reddening law [Cardelli et al., 1988] (CCM88) with R_V = 3.1. We also compare the O'Donnell [O'Donnell, 1994] and the Calzetti [Calzetti et al., 2000] dust laws, and find that all three are in general agreement (Fig. 3.8). Given the lack of substantial difference, we elect to apply the CCM88 law to our entire sample, although future studies may find further improvement by selecting a viewing angle/host dependent dust law.

Once the MW correction is applied, we calculate the $K(z)$ correction. We accomplish this by shifting the spectrum by the Doppler factor of (1+z) in both wavelength (redshift effect) and flux (time dilation). We then calculate the change in magnitude between the observed and emitted frame. Fig. 3.9 shows how changes in z can cause spectral features to shift into different filters, necessitating the $K(z)$ corrections. For the host galaxy dust correction, we estimate the intrinsic $B-V$ color using $\Delta m_{15}(B)$-color relation from [Phillips et al., 1999] and assume that the $E(B-V)$ after MW and $K(z)$ corrections is due to the host galaxy extinction. Although R_V values can range from 2.1-3.8 depending on the individual galaxy's properties and the sight line to the SN in

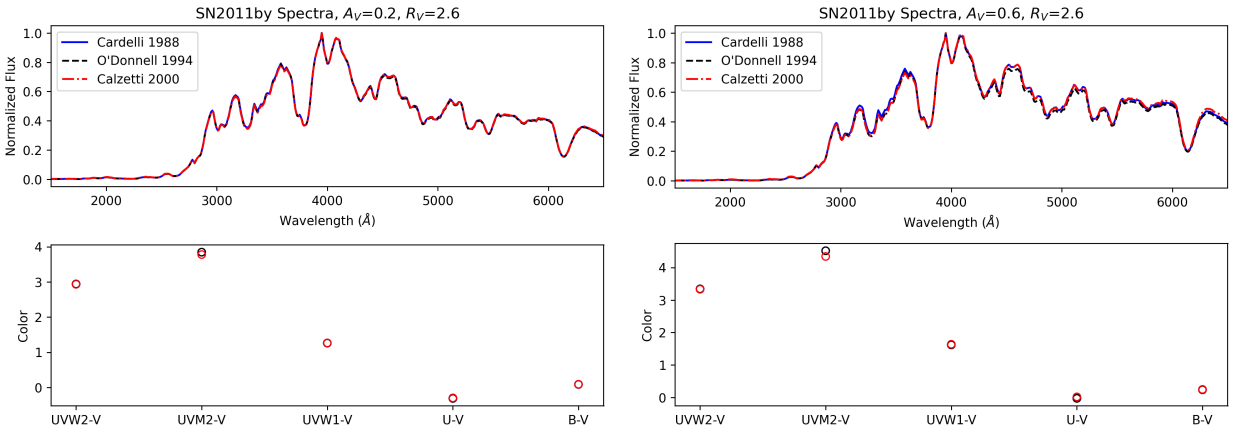

Figure 3.8: A comparison of the Cardelli (blue), O'Donnell (black), and Calzetti (red) dust laws [Cardelli et al., 1988, O'Donnell, 1994, Calzetti et al., 2000] effects on the spectrum of SN2011by, a A_V of 0.2 (left) and 0.6 (right), and a R_V of 2.6. The top plots show the direct effect on the spectrum in peak-normalized fluz, and the bottom plots show the Swift UVOT colors derived from the extincted spectrum.

the galaxy [Kulkarni et al., 2014], we assume a standard R_V = 2.6 for all of our galaxies. Future work will include galaxy-specific R_V in the modeling. For each step we take the average correction value from the 10 selected templates to be our best fit measurement, and the standard deviation of the template corrections to be the statistical error in our measurement.

In Fig. 3.10 we show an example of the deviations between the observed and fit colors for the 10 best fit templates, with a variety of template selections. The templates tend to have redder UV colors (negative deviation) and bluer $B-V$ colors (positive deviation) than the observation of SN2011by. This could be due to a variety of factors: while the observations and template spectra were each taken near the B peak, minor changes in timing could affect the spectral shape. The Foley16 models are interpolations of observed SNe spectra over a range of $\Delta m_(15(B)$ values, and the template spectra are taken from HST and supplemented in the FUV by the SN2011fe spectrum. The synthetic photometry does not account for instrumental noise or other effects that may be present in real photometry. Thus, it is unlikely that a perfect match between the observed and synthetic photometry will be found, although an improved template sample should further reduce any residuals.

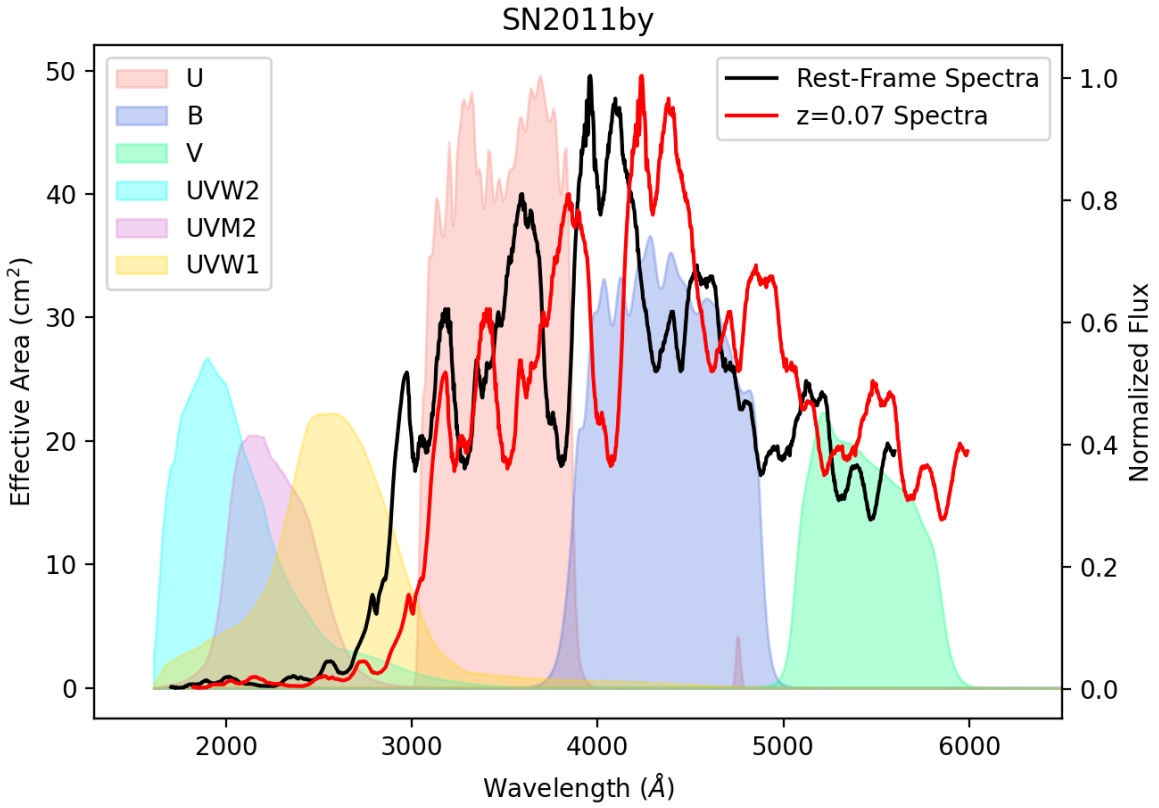

Figure 3.9: The wavelength shift of SN2011by from z=0 to z=0.07. The y-axis shows the flux normalized to the peak value. Even small changes in z can have large differences in the position of spectral features, causing them to shift into different UVOT filters.

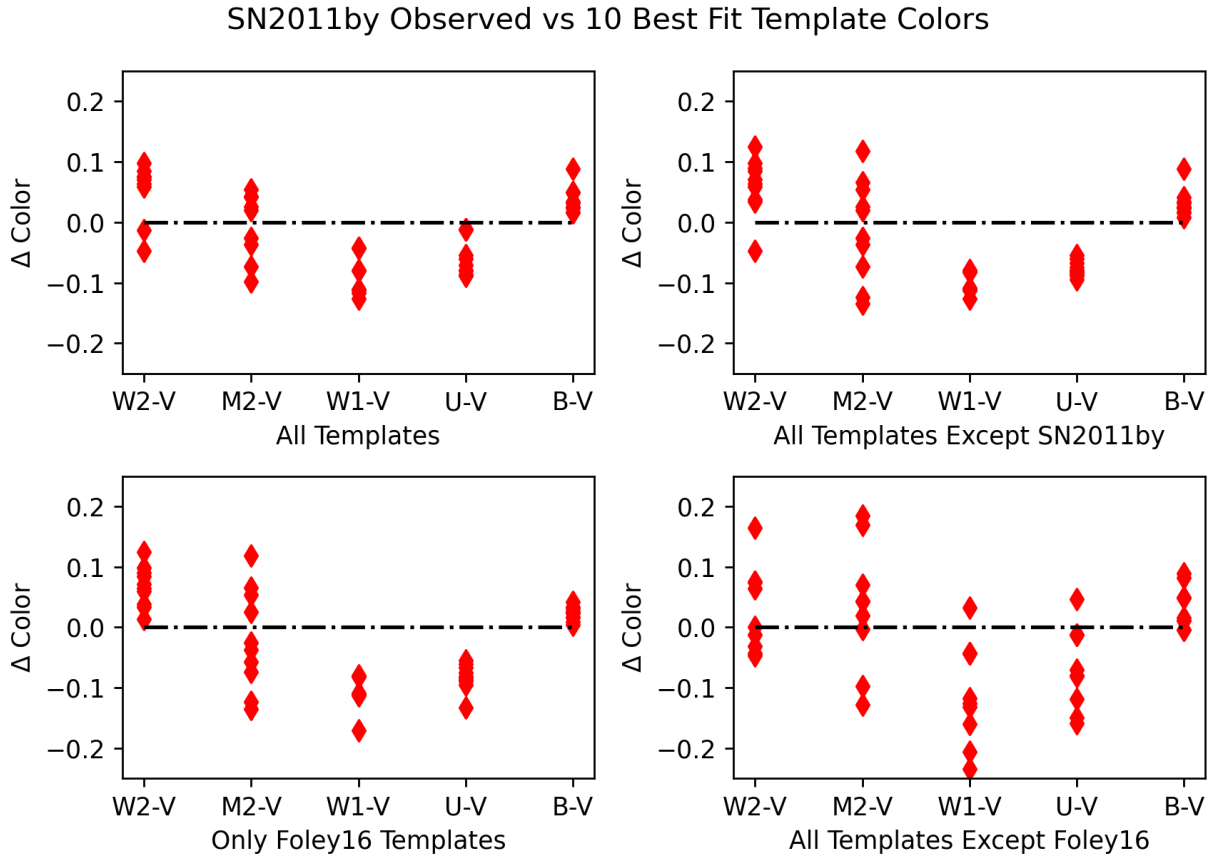

Figure 3.10: The UVOT colors of the 10 best templates based on modeling of SN2011by, in terms of their deviation from the observed colors of SN2011by. Top right includes all allowable models, top left shows the 10 best fit templates when the SN2011by template spectra are removed. Bottom shows the color deviations with only the Foley16 UV templates (left) and without those templates (right). The $UVW1 - V$ and $U - V$ colors tend to be underestimated by the templates, while the $B - V$ colors are slightly overestimated by the templates.

In Fig. 3.11 we show the change in the $B-V$ vs $UVW1-V$ colors for our sample at each stage of correction. Broadly, the $K(z)$ corrections are the smallest due to the low z of our sample. The majority of the SNe Ia are observed out of the plane of the Milky Way, so those corrections are also small. The host dust extinction dominates our corrections, and its assumed dependence on the color-decline law [Phillips et al., 1999] may add additional uncertainty that we do not capture, as non-normal SNe Ia may not follow that relation as precisely.

In Fig. 3.12 we compare the coverage in color space of our sample and our templates. We are able to match the observed colors of nearly all the SNe Ia in our sample. For SNe Ia with an average root mean squared deviation ≥ 1.5, we remove them from the sample: SN2005ke [Bufano et al., 2009] and SN2007cv [González-Gaitán et al., 2014] are 91bg-like sub-luminous SNe while SN2007on is a transitional SN (between normal and sub-luminous) [Gall et al., 2018]. SN2008hs is labled as a fast decliner [Dhawan et al., 2017]. SN2010Y is the fastest decliner in our sample ($\Delta m_{15}(B)$ = 2.27) and is classified as an abnormally cool and faint SN [Parrent et al., 2011]. These fast-declining, sub-luminous SNe are known to deviate significantly from the standard P99 relation [Garnavich et al., 2004]. SN2012V and SN2013bs are the only removed objects to not be described in the literature as known oddities.

3.5 Phillips Relation

The intrinsic optical color and luminosity of SNe Ia are strongly related to their light curve shape, usually parameterized as their post-peak decline rate (often the 15 day decline rate in the B filter, or $\Delta m_{15}(B)$) or stretch. SNe Ia with a $\Delta m_{15}(B)$ = 1.1 are generally held as the standard for determining the absolute magnitude [Hamuy et al., 1996a], and deviations from that decline rate are used to standardize the color and luminosity. The color-decline and luminosity-decline relations (often called the "Phillips Relations") were originally given as [Phillips et al., 1999] (hereafter P99):

$$B_{peak} - V_{peak} = 0.114 * (\Delta m_{15}(B) - 1.1) - 0.07 \tag{3.5}$$

$$M(B_{peak}) = 0.633 * (\Delta m_{15}(B) - 1.1)^2 + 0.786(\Delta m_{15}(B) - 1.1) - 19.3. \tag{3.6}$$

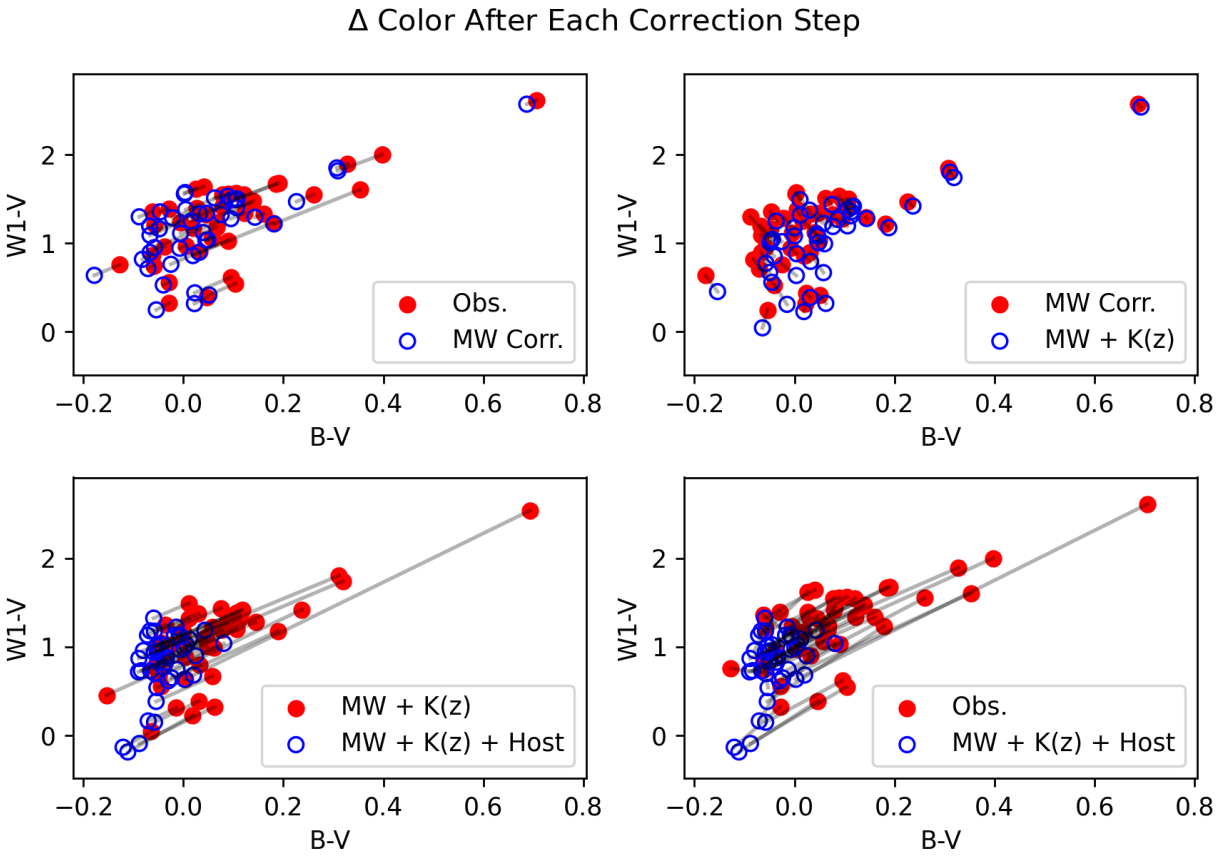

Figure 3.11: The shift in color before (red) and after (blue) each correction is applied. The black lines connect the pre- and post-correction colors for individual SNe Ia. From top left going clockwise: observed color $\rightarrow$ Milky Way dust corrected color, MW dust corrected color $\rightarrow$ MW+ $K(z)$ corrected color, MW+$K(z)$ corrected color $\rightarrow$ MW+$K(z)$+ host galaxy dust corrected color, observed color $\rightarrow$ color after all correction steps. The $K(z)$ has the smallest effect on color, as most of our SNe Ia are at relatively low z, while the estimated host dust correction has the largest effect on color.

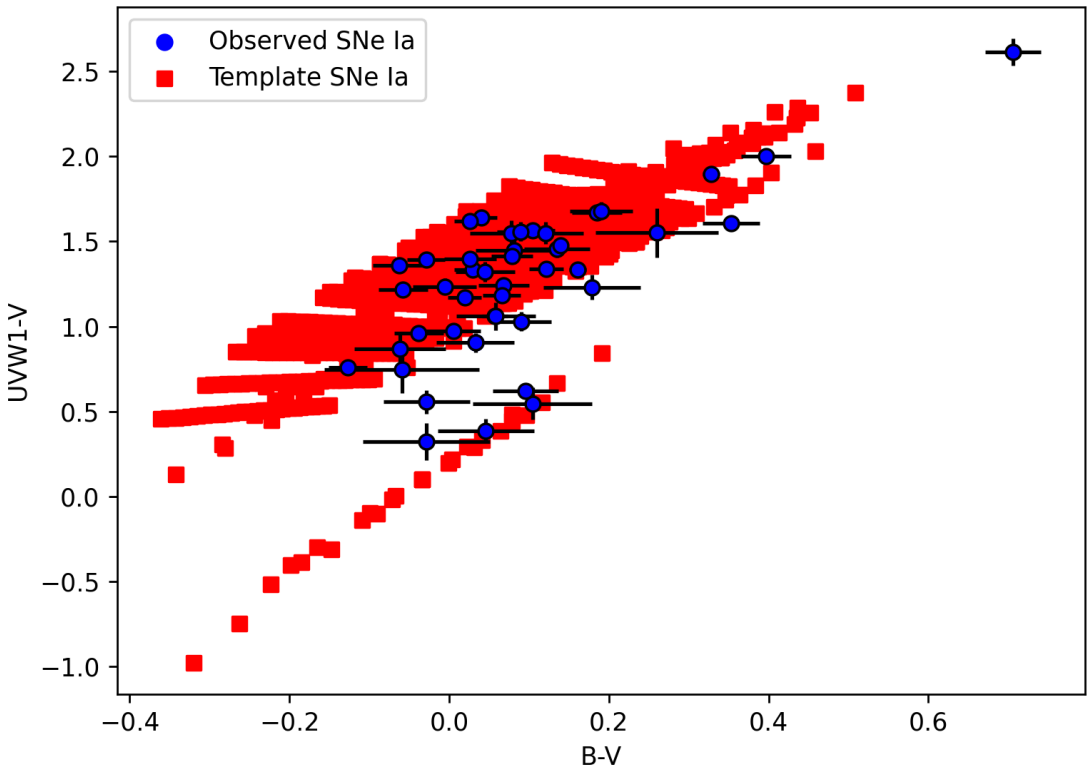

Figure 3.12: The $B - V$ and $UVW1 - V$ colors of our observed sample (blue) and our template suite (red). The templates are able to match the colors of almost all of our sample.

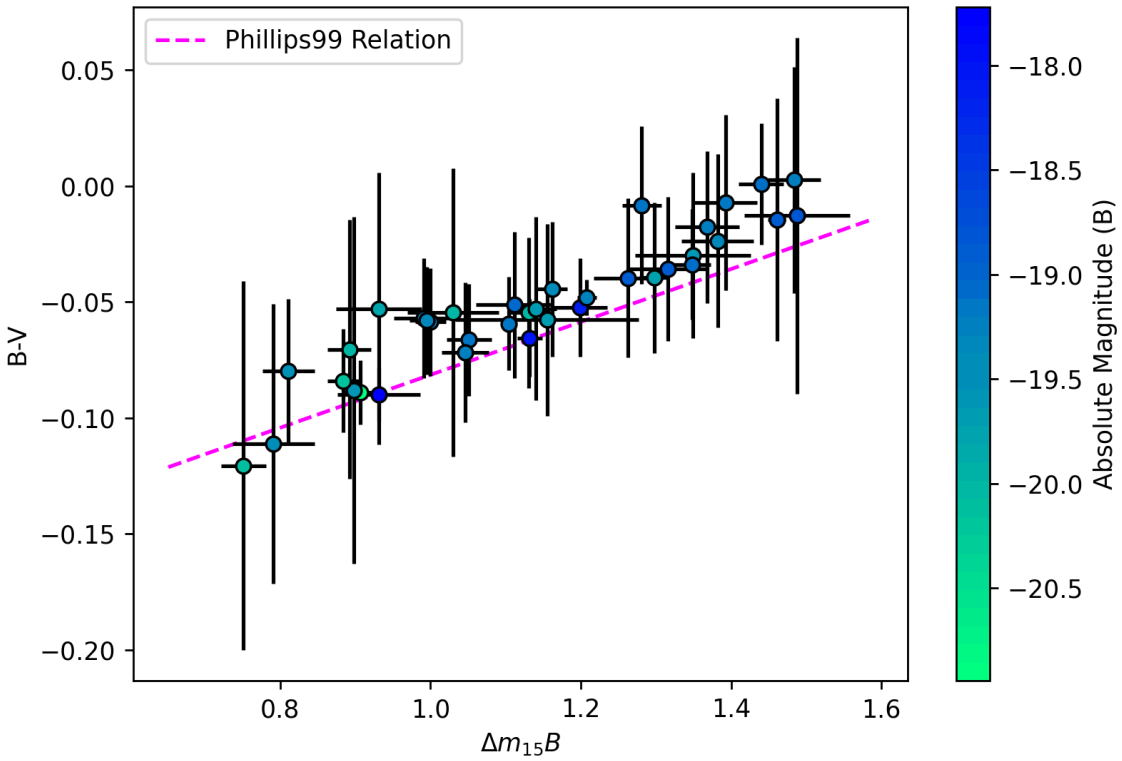

Figure 3.13: The $\Delta m_{15}(B)$ vs $B - V$ colors of our sample, color coded by their M(B). The magenta line shows the P99 relation.

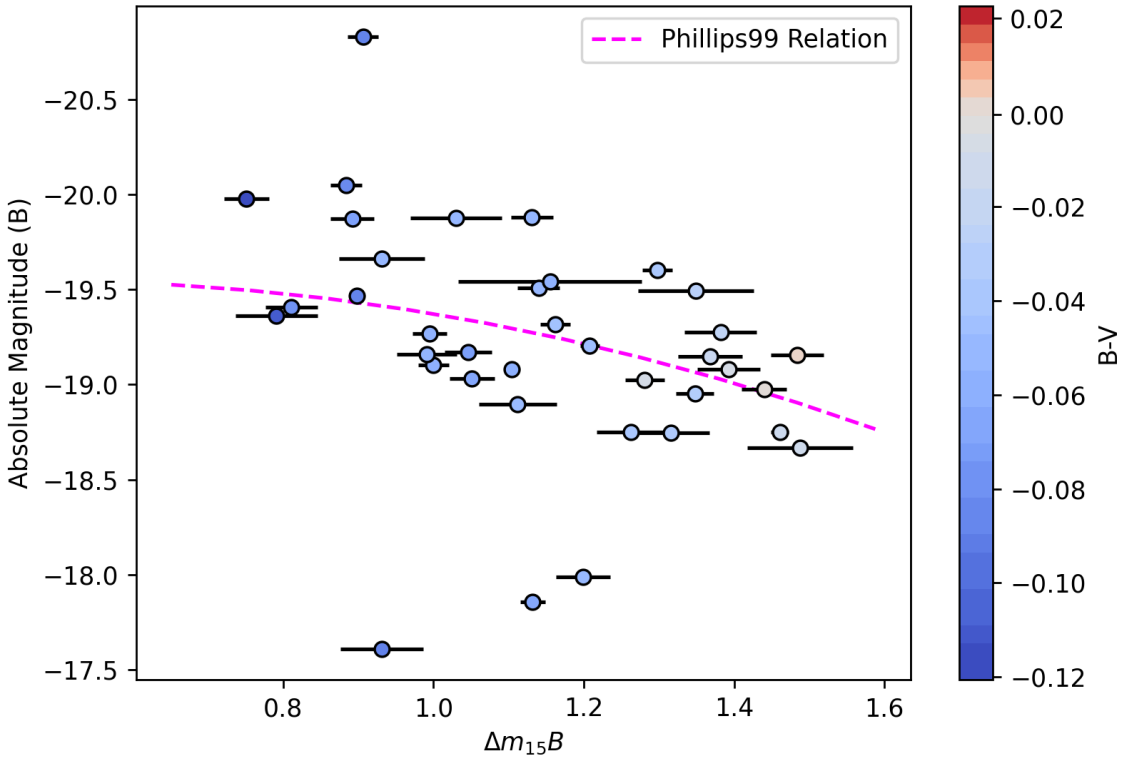

Figure 3.14: The $\Delta m_{15}(B)$ vs M(B) colors of our sample, color coded by their $B-V$. The magenta line shows the P99 relation. The three SNe Ia with the lowest magnitudes are SN2012ht, SN2011by, and SN2012cg, in descending order. SN2011by is known to have substantial uncertainty in it's distance estimate between host galaxy redshift measurements and Cepheid measurements [Foley et al., 2020]. Here we use the host galaxy redshift to estimate distance, it's possible that a Cepheid distance would shift the estimated absolute magnitude back to the P99 relation. This is likely what is causing the scatter in SN2012ht, SN2012cg, and other offset SNe in the figure.

Our color-decline estimates have similar slope to the original P99 relation, but are offset to slightly redder colors. This maybe due to a systemic over-correction in reddening, or other unaddressed correction factors. Our luminosity-decline estimates diverges somewhat from P99, likely due to uncertainties in the distance modulus. We determine the distance modulus term using the host galaxy redshift, however for galaxies that are not in the Hubble Flow ($z \leq 0.03$) the peculiar velocity may add considerable uncertainty. Improved distance estimates from Cepheid analysis may reduce this scatter [Foley et al., 2020]. We also do not remove non-normal SNe Ia from our sample when fitting the relations, which may skew the results. More diverse templates, a more nuanced approach to host extinction, and improved outlier selection may reduce the scatter in our estimates.

3.6 UV-Optical Relations

Studies have suggested that SNe Ia with standardized optical colors can be placed into two different categories based on their NUV properties: "NUV-red" and "NUV-Blue" [Milne et al., 2013, Brown et al., 2017]. In Fig. 3.15 we examine the $B - V$ and $UVW1 - V$ colors of our sample after correction and find that normal SNe Ia occupy a range of NUV colors with no bimodality. Super-C type SNe (SN2011aa, Sn2011de, and SN2012dn [Brown, 2014]) do tend to have bluer colors than normal, as expected [Brown et al., 2014b]. This UV excess may be due to a variety of factors such as early UV flux from shock interactions [Scalzo et al., 2010, Noebauer et al., 2016] or compositional effects that cause the UV light curves to be much broader and peak earlier than expected from optical analysis [Brown et al., 2014b, Devarakonda and Brown, 2022].

While the $B - V$ color is roughly standard, the UV-optical and UV-UV colors may show more diversity. We examine the relation between the colors and absolute magnitudes of our sample (Fig. 3.16), and find that UV-optical color-color and color-magnitude relations are fairly linear. We fit the linear relations using the $Scipy\ curvefit$ module [Virtanen et al., 2019], with the best fit value and uncertainties from the mean and standard deviation of 1000 Monte Carlo Gaussian draws of our estimated peak values. We focus our analysis on the $UVM2$ data, as the $UVW1$ and $UVW2$ filters are susceptible to bias from their red filter tails.

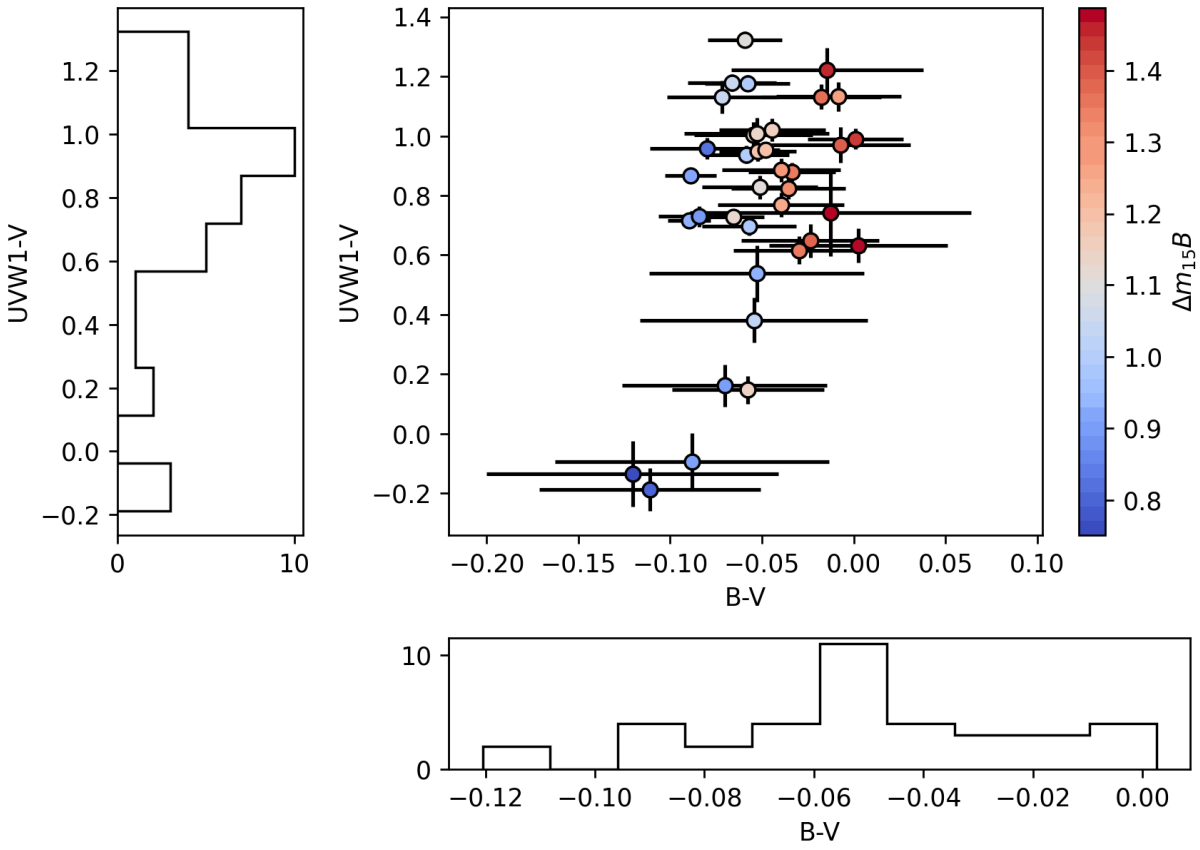

Figure 3.15: The $B - V$ vs $UVW1 - V$ colors after corrections, with histograms showing the distribution of SNe Ia in each color space. While a few of the Super-C type objects lie on the blue end of the diagram, the normal SNe Ia show no evidence of a NUV-blue/NUV-red population.

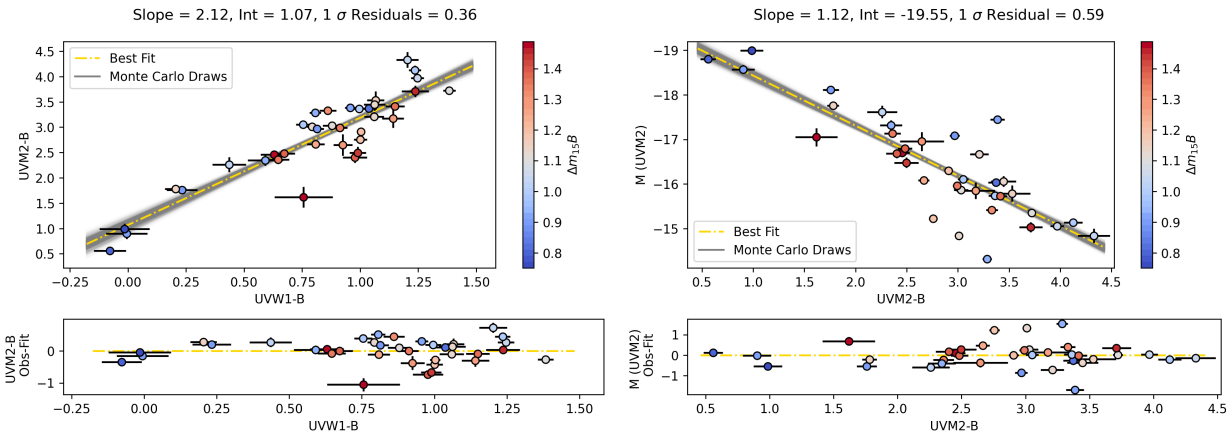

Figure 3.16: Left: The $UVW1 - B$ vs $UVM2 - B$ colors for our sample, with the best fit linear relation (gold) and Monte Carlo draws (gray). Below are the residuals from comparing the observations to the best fit relation, the 1 σ dispersion from the residuals is $\sim$ 0.36 mag. Right: The $UVM2 - B$ color vs M($UWM2$) for our sample, with the best fit linear relation (gold) and Monte Carlo draws (gray). Below are the residuals from comparing the observations to the best fit relation, the 1 σ dispersion from the residuals is $\sim$ 0.59 mag.

The color-color relations particularly show a tight linear relation in the various possible combinations. While the idea that "blue things are blue" isn't novel, the tightness of the correlations suggests that intrinsic differences, such as metallicity effects [Foley et al., 2016], shift the flux somewhat uniformly across the UV. In addition, the Super-C objects do not show significant deviation from the relation, which may suggest that the physical cause of UV flux differences is not dependent on sub-type. The color-magnitude relation shows a linear increase in UV luminosity for bluer UV-optical colors, as expected, however the dispersion around the relation is much larger than the color-color relations. Most of this dispersion is from the fainter, redder SNe Ia, so the scatter may be driven by increased observational uncertainties that we are not accounting for or by inaccurate dust corrections.

When comparing the magnitudes across filter (Fig. 3.17), we again find a linear relation. The dispersion around the fit decreases as the distance between filters decrease. While this dispersion is higher than dispersion in the optical luminosity-width relation [Hamuy et al., 1996b, Phillips et al., 1999], it does open the door to UV standardization. Rather than using any one relation, a

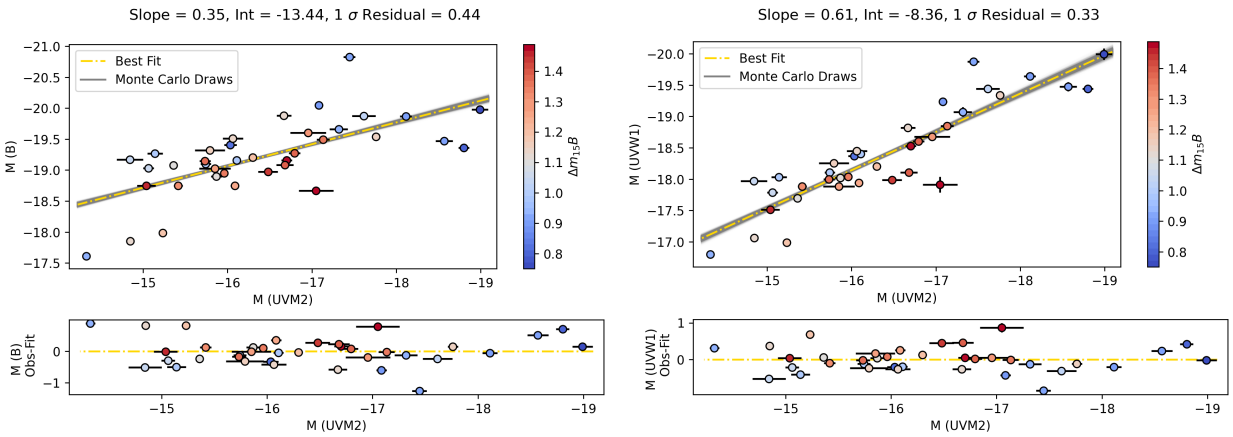

Figure 3.17: Left: The M(B) vs M($UVM2$) for our sample, with the best fit linear relation (gold) and Monte Carlo draws (gray). Below are the residuals from comparing the observations to the best fit relation, the 1 σ dispersion from the residuals is $\sim$ 0.44 mag. Right: The M($UVW1$) vs M($UWM2$) for our sample, with the best fit linear relation (gold) and Monte Carlo draws (gray). Below are the residuals from comparing the observations to the best fit relation, the 1 σ dispersion from the residuals is $\sim$ 0.33 mag.

statistical model could chain the relations together across filters, vastly improving standardization in the UV. With optical calibration and a sufficient training sample, such a model could possibly compute the intrinsic luminosities of SNe Ia with only UV data. In addition, deviations from the expected color relations can provide estimates for $K(z)$ and dust extinction independent of the $\Delta m_{15}(B)$-derived color corrections. The Rubin Observatory is expected to find thousands of SNe Ia over the course of its planned survey. This includes SNe Ia as far as $z \sim 1$, at which point Rubin would be observing their rest-frame NUV and MUV emission. These object will likely be too faint to be detected beyond their peak, so models capable of standardizing with limited epochs of UV observations will be crucial for studying these objects.

3.7 The SIRAH Project

While multi-color statistical light curve models and high-z SNe Ia from Rubin are not available yet, there is plenty to be done with available data of high-z SNe Ia and light curve models. The "Supernovae in the Infrared avec Hubble" or SIRAH project [Jha et al., 2019] measured the NIR properties of 24 SNe Ia with the HST WFC3/IR. These SNe lie in the nearby "Hubble Flow"

($0.02 \leq z \leq 0.07$), a cosmological region where an objects velocity due to the expansion of the universe dominates over its peculiar velocity. Such observations are crucial for addressing the discrepancy between local measurements of the Hubble constant and measurements derived from studies of the CMB [Planck Collaboration et al., 2018, Freedman et al., 2019]. Ground based optical observations from programs such as ASAS-SN, ATLAS, and ZTF will supplement this data set. UVOT observations with Swift will expand this program into the UV. This will result in the first cosmological study of UV SNe Ia and will act as a precursor for future Rubin Observatory surveys.

SNe Ia are difficult to observe in the UV due to their intrinsic faintness and the Swift UV transmission function (see 3.1); at higher redshifts the UV emission may only be visible at epochs near peak. Models such as SNooPy [Burns et al., 2011] and FPCA [He et al., 2018, Devarakonda and Brown, 2022] are unable to fit such sparse data sets. To address this issue, we explore the use of a simple stretch based fitting method in order to estimate the peak magnitudes of the SNe Ia with as few as 3 observations near peak in the Swift UVOT filters.

3.8 Stretch Based Modeling

We first create a template by fitting a smoothed spline function ($Scipy\ UnivariateSpline$, [Virtanen et al., 2019]) to synthetic UVOT light curves generated from spectrophotometric observations of SN2011fe [Pereira et al., 2013] (Fig. 3.18). This spline template is then stretched to match the observations using the $Scipy\ CurveFit$ program, which uses a least squares method of regression [Virtanen et al., 2019] to fit defined models to data. Our fitting function is defined as:

$$Flux = spline(\frac{T}{A}) + C, \tag{3.7}$$

where T is the phase of observation relative to the peak and $A,\ C$ are free parameters. The key assumption for this method is the time of peak, which can drastically affect the fit profile. We initially estimate the time of peak as the time of the brightest B band observation. Then we sample peak time estimates using a random normal distribution, centered around our initial

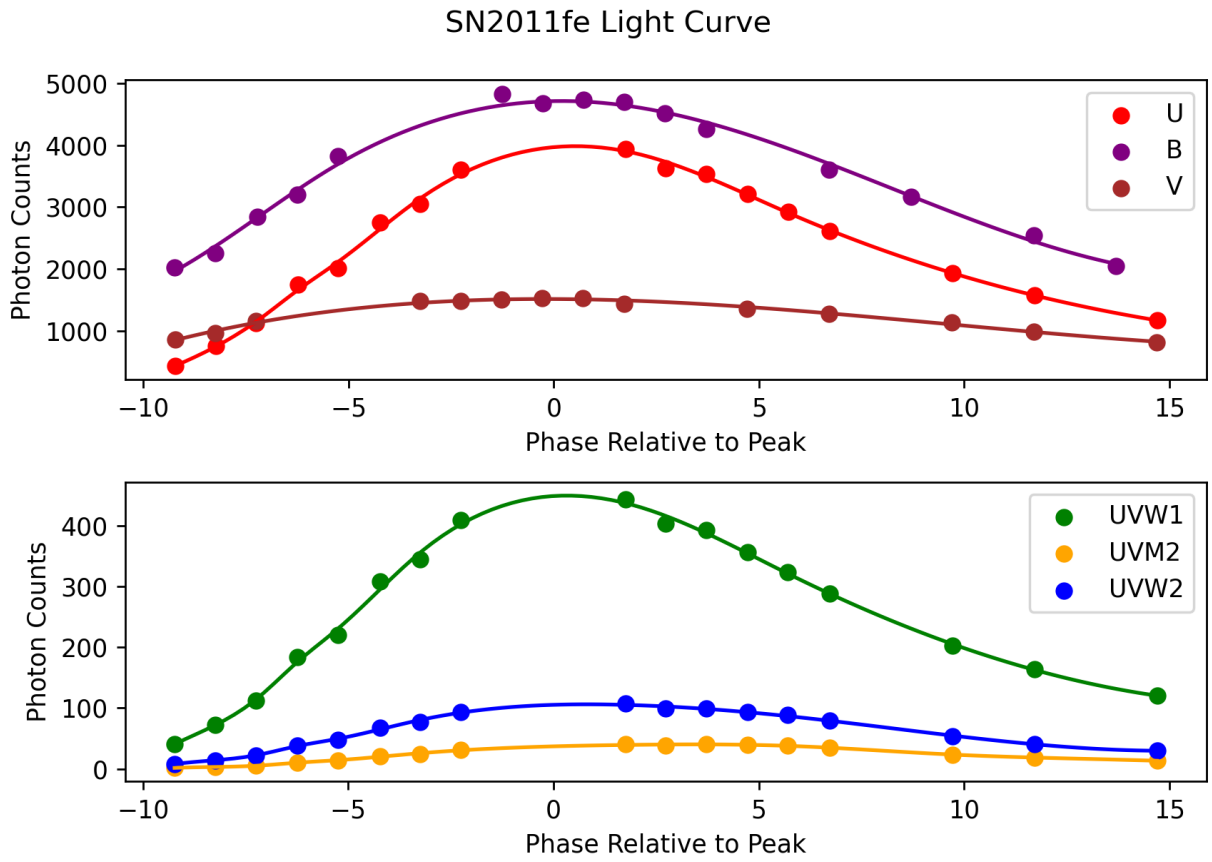

Figure 3.18: The UVOT light curves of SN2011fe, based on spline fitting (solid lines) of spectrophotometric data (solid points) from [Pereira et al., 2013].

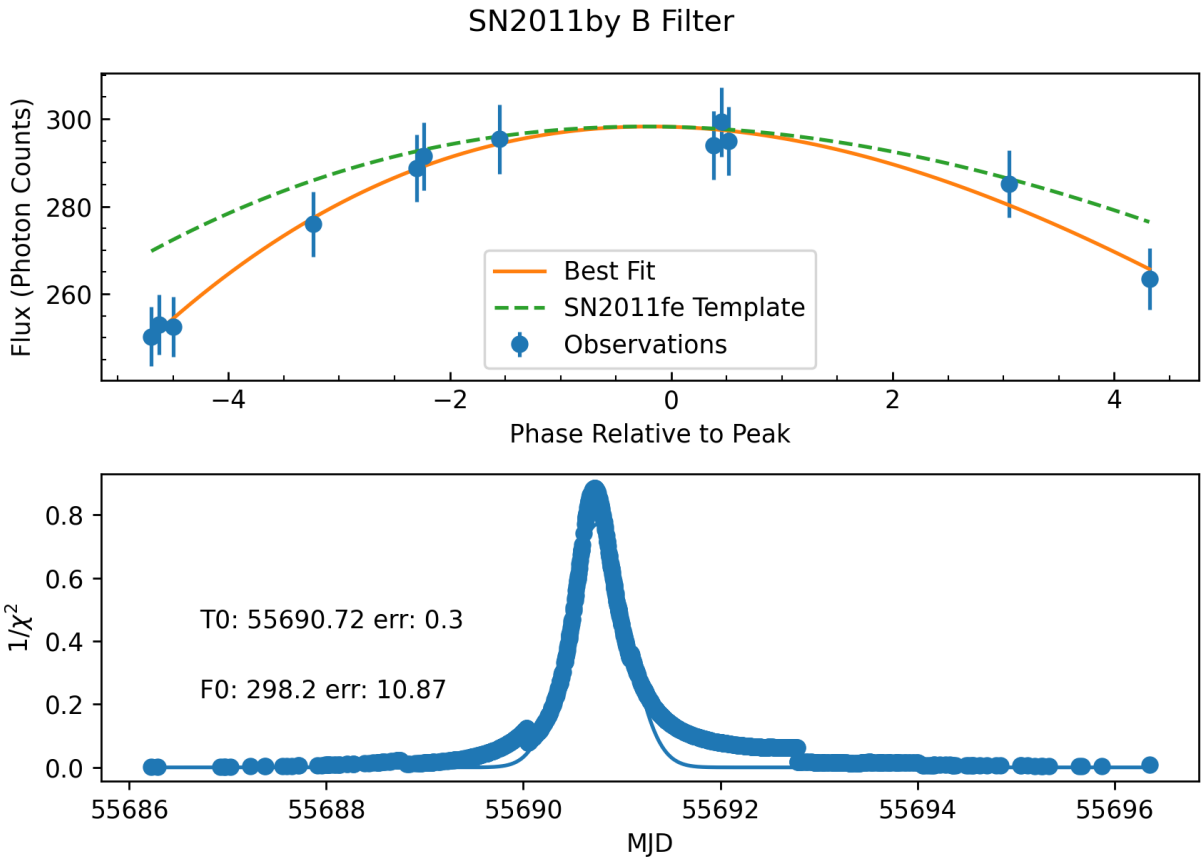

Figure 3.19: Top: An example of the stretch based fitting routine, with the B filter observations of SN2011by (blue points). The orange line shows the best fit light curve for SN2011by, and the green line shows the unmodified SN2011fe light curve for comparison. Bottom: Blue points show the $1/\chi^2$ values from each random draw of the peak phase estimate. The blue line shows the Gaussian fit to this distribution. The estimate for the peak phase (T0) and peak photon count (P0) with uncertainties are also shown.

estimate (σ=1.5, n=1000). The χ^2 distribution from our draws resembles a Gaussian distribution, which we then fit to estimate the peak time (μ), the uncertainty on the peak time (σ), and the uncertainty on the photon counts at peak. Figure 3.19 shows an example of this fitting routine with B filter observations of SN2011by. See Figures B.1, B.2, B.3, B.4, and B.5 in Appendix B for examples of the fitting routine with the other UVOT filters.

We test the capabilities of this method by applying it to the SNe Ia in our SNooPy/FPCA sample (see 3.2), and find the resulting peak magnitudes to be in agreement (Fig. 3.20). Many of

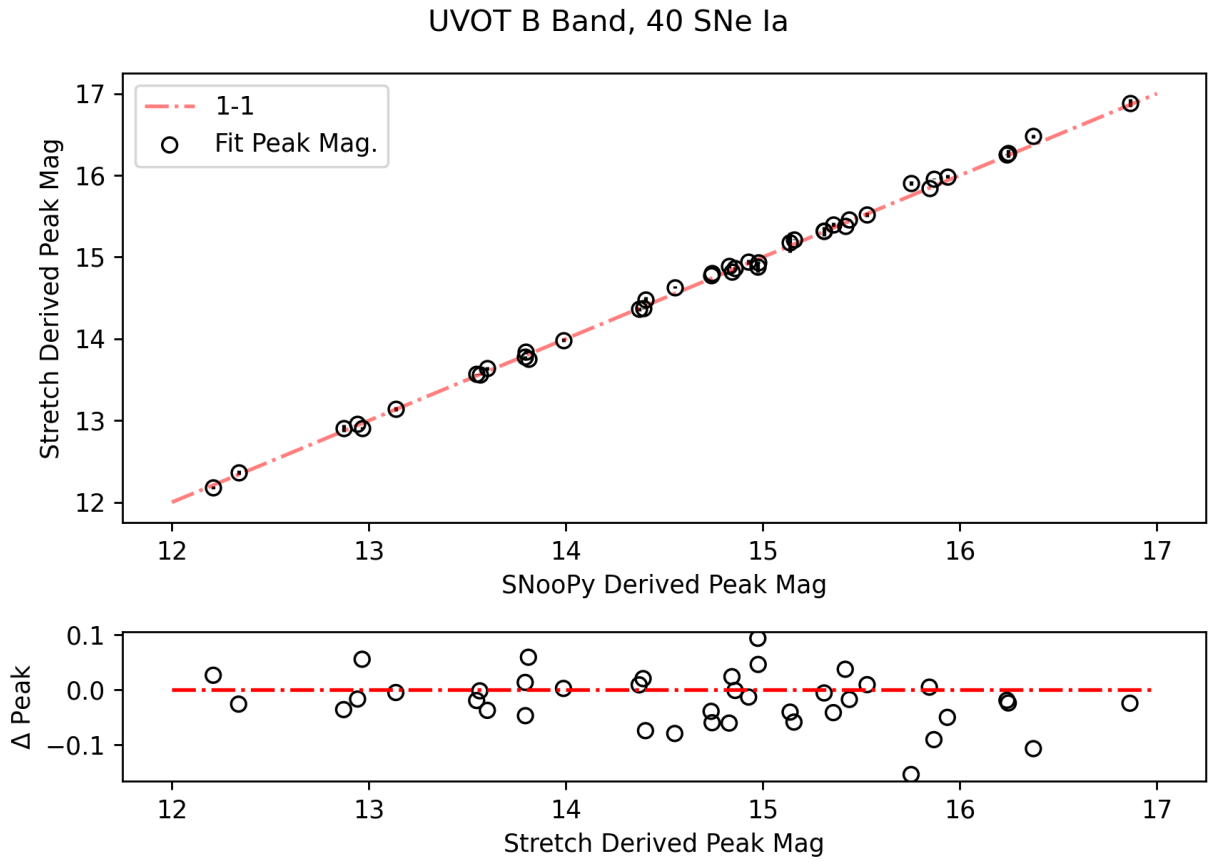

Figure 3.20: Top: The B filter peak magnitude estimates for 40 SNe Ia from the Chapter 3 sample (black circles). The x-axis shows the best fit values from SNooPy, and the y-axis shows the best fit values from the stretch fitting. Uncertainties from the fitting routines are shown as black error bars. The red line demonstrates the 1-1 relation. Bottom: The difference between the SNoopy and stretch fit estimates for peak magnitude.

the supernovae in that sample are well observed, more so than expected for our high-z sample. For further testing, we sub-sample the observations and re-fit the light curves. This sub-sampling is done two ways, by filtering out every other observation for each supernova (low cadence) and by limiting the observations to be within 5 days of the estimated peak (limited epochs). In both cases, the peak magnitudes from sub-sampling agree with the full sample (Fig. 3.21).

With this light curve fitting method and the SED analysis, we will be able to craft the first UV Hubble diagram. Combined with the optical and IR data, this sample will have the widest wavelength coverage of any SNe Ia cosmology study to date.

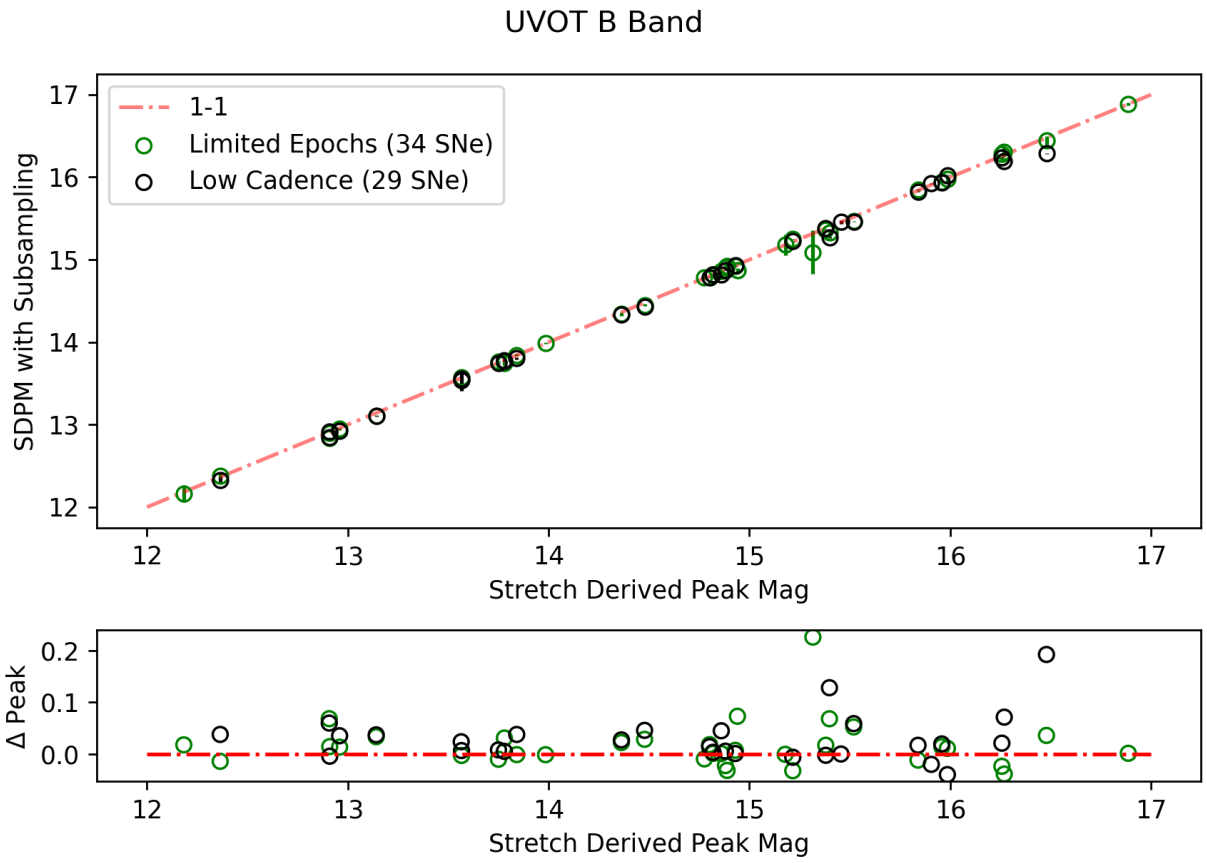

Figure 3.21: Top: The B filter peak magnitude estimates using the stretch fitting, with an unmodified sample (x-axis) and two different sub-sampling methods to simulate the SIRAH observations. Green circles show the 34 SNe which were fit using only observations within 5 days of peak, while black circles show SNe for which every other observations was omitted. The red line demonstrates the 1-1 relation. Bottom: The difference in the stretch fit estimates for peak magnitude between the unmodified and modified samples.

4. SUMMARY AND CONCLUSION

Every now and then, a white dwarf accretes too much mass and explodes spectacularly as a Type Ia supernova. These remarkable objects offer a glimpse into the origin of elements and the history of the universe. The progenitors of these explosions could be binary white dwarf systems or white dwarf/red giant pairs, whose interactions lead to a thermonuclear detonation. At their brightest they outshine all of the stars in their host galaxy as the tremendous amounts of radioactive material they produce decay away. Their decay rate is tied closely to their optical luminosity, leading to their use as "standard candles" to determine distances to far away objects. Their use as candles led to the discovery of dark energy, as well as the great tension in modern cosmology over the expansion rate of the universe and the nature of dark energy. Beyond the optical, their infrared light curves have proven to be highly standard and their ultraviolet properties may reveal their hidden structure. Modeling their light curve behavior across all wavelengths is key to their study, and multiple methods have been devised over the years for this purpose.

4.1 Summary

In Chapter 2 I described the analysis of the largest published sample of UVOT SNe Ia to date. We examined the light curves of 97 nearby SNe with a band-vague light curve model derived from FPCA analysis of BVRI SNe Ia. We found that the post-peak light curves of UV and optical SNe show statistically similar behavior, indicating a physical link to the UV and optical properties at those epochs. This is likely due to the expansion of the ejecta reaching a phase where both the UV and optical photons are able to travel freely. However the pre-peak light curve behaviors are not statistically related, from the previous scenario this would suggest that the photons in one or both wavelength regimes are still being restricted by the ejecta material.

In Chapter 3 I described a method to recover the intrinsic luminosities of SNe Ia by correcting for dust extinction and redshift effects, using SED modeling. The process uses various spectral templates generated from real observations and modeled SNe that are matched up to the observed

colors of SNe. The matched templates are then corrected for the predicted dust extinction and $K(z)$ corrections. With this we produce the largest sample to date of SNe Ia absolute magnitudes and intrinsic colors in the UV and optical. We show that for fixed $B-V$ colors, SNe Ia exhibit a range of NUV colors rather than being split into a NUV-red and NUV-blue subclass. We characterize the linear relations between the colors and absolute magnitudes in the UV and optical, and demonstrate the possibility for multi-color models that can standardize the UV properties of SNe Ia. At the end of Chapter 3, we introduce the SIRAH project and describe a light curve fitting method that stretches a template to match as little as 3 observations near peak, which will open to door to high-z studies of SNe Ia.

4.2 The Future

As part of the analysis for the SIRAH project, we will create the first Hubble Diagram to use UV observations of SNe Ia. This will be an important step to anchoring the cosmological distance ladder, and will set up future high-z surveys with the Vera C. Rubin Observatory and the Nancy Grace Roman Space Telescope. Further improvements to the SED modeling process such as a more diverse range of templates, a color-based extinction correction, and a statistical model for multi-color standardization will greatly enhance future surveys. These models are especially important as the aforementioned high-z will require a deeper understanding of the rest-frame UV diversity.

REFERENCES

[Akaike, 1974] Akaike, H. (1974). A new look at the statistical model identification. *IEEE Transactions on Automatic Control*, 19(6):716–723.

[Aldoroty et al., 2022] Aldoroty, L., Wang, L., Hoeflich, P., Yang, J., Suntzeff, N., Aldering, G., Antilogus, P., Aragon, C., Bailey, S., Baltay, C., Bongard, S., Boone, K., Buton, C., Copin, Y., Dixon, S., Fouchez, D., Gangler, E., Gupta, R., Hayden, B., Karmen, M., Kim, A. G., Kowalski, M., Küsters, D., Léget, P. F., Mondon, F., Nordin, J., Pain, R., Pecontal, E., Pereira, R., Perlmutter, S., Ponder, K. A., Rabinowitz, D., Rigault, M., Rubin, D., Runge, K., Saunders, C., Smadja, G., Suzuki, N., Tao, C., Thomas, R. C., and Vincenzi, M. (2022). Bump Morphology of the CMAGIC Diagram. *arXiv e-prints*, page arXiv:2210.06708.

[Amanullah et al., 2015] Amanullah, R., Johansson, J., Goobar, A., Ferretti, R., Papadogiannakis, S., Petrushevska, T., Brown, P. J., Cao, Y., Contreras, C., Dahle, H., Elias-Rosa, N., Fynbo, J. P. U., Gorosabel, J., Guaita, L., Hangard, L., Howell, D. A., Hsiao, E. Y., Kankare, E., Kasliwal, M., Leloudas, G., Lundqvist, P., Mattila, S., Nugent, P., Phillips, M. M., Sandberg, A., Stanishev, V., Sullivan, M., Taddia, F., Östlin, G., Asadi, S., Herrero-Illana, R., Jensen, J. J., Karhunen, K., Lazarevic, S., Varenius, E., Santos, P., Sridhar, S. S., Wallström, S. H. J., and Wiegert, J. (2015). Diversity in extinction laws of Type Ia supernovae measured between 0.2 and 2 μm. , 453:3300–3328.

[Arcones and Thielemann, 2023] Arcones, A. and Thielemann, F.-K. (2023). Origin of the elements. , 31(1):1.

[Avelino et al., 2019] Avelino, A., Friedman, A. S., Mandel, K. S., Jones, D. O., Challis, P. J., and Kirshner, R. P. (2019). Type Ia Supernovae Are Excellent Standard Candles in the Near-infrared. , 887(1):106.

[Branch, 1998] Branch, D. (1998). Type IA Supernovae and the Hubble Constant. *ARAA*, 36:17–56.

[Breeveld et al., 2011] Breeveld, A. A., Landsman, W., Holland, S. T., Roming, P., Kuin, N. P. M., and Page, M. J. (2011). An Updated Ultraviolet Calibration for the Swift/UVOT. In McEnery, J. E., Racusin, J. L., and Gehrels, N., editors, *GAMMA RAY BURSTS 2010. AIP Conference Proceedings*, volume 1358 of *American Institute of Physics Conference Series*, pages 373–376.

[Brown and Forsythe, 1974] Brown, M. B. and Forsythe, A. B. (1974). Robust tests for the equality of variances. *Journal of the American Statistical Association*, 69(346):364–367.

[Brown, 2014] Brown, P. J. (2014). The Ultraviolet Brightest Type Ia Supernova 2011de. *ApJL*, 796:L18.

[Brown et al., 2015] Brown, P. J., Baron, E., Milne, P., Roming, P. W. A., and Wang, L. (2015). Theoretical Clues to the Ultraviolet Diversity of Type Ia Supernovae. , 809:37.

[Brown et al., 2016] Brown, P. J., Breeveld, A., Roming, P. W. A., and Siegel, M. (2016). Interpreting Flux from Broadband Photometry. , 152:102.

[Brown et al., 2014a] Brown, P. J., Breeveld, A. A., Holland, S., Kuin, P., and Pritchard, T. (2014a). SOUSA: the Swift Optical/Ultraviolet Supernova Archive. *A&SS*, 354:89–96.

[Brown and Crumpler, 2020] Brown, P. J. and Crumpler, N. R. (2020). A Photometric Analysis of the Relationship between the UV flux of Type Ia Supernovae and Host-galaxy Metallicity. , 890(1):45.

[Brown et al., 2012a] Brown, P. J., Dawson, K. S., de Pasquale, M., Gronwall, C., Holland, S., Immler, S., Kuin, P., Mazzali, P., Milne, P., Oates, S., and Siegel, M. (2012a). A Swift Look at SN 2011fe: The Earliest Ultraviolet Observations of a Type Ia Supernova. *ApJ*, 753:22.

[Brown et al., 2012b] Brown, P. J., Dawson, K. S., Harris, D. W., Olmstead, M., Milne, P., and Roming, P. W. A. (2012b). Constraints on Type Ia Supernova Progenitor Companions from Early Ultraviolet Observations with Swift. *ApJ*, 749:18.

[Brown et al., 2019] Brown, P. J., Hosseinzadeh, G., Jha, S. W., Sand, D., Vieira, E., Wang, X., Dai, M., Dettman, K. G., Mould, J., Uddin, S., Wang, L., Arcavi, I., Bento, J., Burns, C. R., Diamond, T., Hiramatsu, D., Howell, D. A., Hsiao, E. Y., Marion, G. H., McCully, C., Milne,

P. A., Mirzaqulov, D., Ruiter, A. J., Valenti, S., and Xiang, D. (2019). Red and Reddened: Ultraviolet through Near-infrared Observations of Type Ia Supernova 2017erp. , 877(2):152.

[Brown et al., 2014b] Brown, P. J., Kuin, P., Scalzo, R., Smitka, M. T., de Pasquale, M., Holland, S., Krisciunas, K., Milne, P., and Wang, L. (2014b). Ultraviolet Observations of Super-Chandrasekhar Mass Type Ia Supernova Candidates with Swift UVOT. *ApJ*, 787:29.

[Brown et al., 2017] Brown, P. J., Landez, N. J., Milne, P. A., and Stritzinger, M. D. (2017). Reddened, Redshifted, or Intrinsically Red? Understanding Near-ultraviolet Colors of Type Ia Supernovae. , 836:232.

[Brown et al., 2018] Brown, P. J., Perry, J. M., Beeny, B. A., Milne, P. A., and Wang, X. (2018). The Ultraviolet Colors of Type Ia Supernovae and their Photospheric Velocities. *ArXiv e-prints*.

[Brown et al., 2010] Brown, P. J., Roming, P. W. A., Milne, P., Bufano, F., Ciardullo, R., Elias-Rosa, N., Filippenko, A. V., Foley, R. J., Gehrels, N., Gronwall, C., Hicken, M., Holland, S. T., Hoversten, E. A., Immler, S., Kirshner, R. P., Li, W., Mazzali, P., Phillips, M. M., Pritchard, T., Still, M., Turatto, M., and Vanden Berk, D. (2010). The Absolute Magnitudes of Type Ia Supernovae in the Ultraviolet. *ApJ*, 721:1608–1626.

[Bufano et al., 2009] Bufano, F., Immler, S., Turatto, M., Landsman, W., Brown, P., Benetti, S., Cappellaro, E., Holland, S. T., Mazzali, P., Milne, P., Panagia, N., Pian, E., Roming, P., Zampieri, L., Breeveld, A. A., and Gehrels, N. (2009). Ultraviolet Spectroscopy of Supernovae: The First Two Years of Swift Observations. *ApJ*, 700:1456–1472.

[Burke et al., 2022] Burke, J., Howell, D. A., Sand, D. J., and Hosseinzadeh, G. (2022). Companion Shocking Fits to the 2018 ZTF Sample of SNe Ia Are Consistent with Single-Degenerate Progenitor Systems. *arXiv e-prints*, page arXiv:2208.11201.

[Burke et al., 2021] Burke, J., Howell, D. A., Sarbadhicary, S. K., Sand, D. J., Amaro, R. C., Hiramatsu, D., McCully, C., Pellegrino, C., Andrews, J. E., Brown, P. J., Itagaki, K., Shahbandeh, M., Bostroem, K. A., Chomiuk, L., Hsiao, E. Y., Smith, N., and Valenti, S. (2021). A Bright Ultraviolet Excess in the Transitional 02es-like Type Ia Supernova 2019yvq. , 919(2):142.

[Burns et al., 2011] Burns, C. R., Stritzinger, M., Phillips, M. M., Kattner, S., Persson, S. E., Madore, B. F., Freedman, W. L., Boldt, L., Campillay, A., Contreras, C., Folatelli, G., Gonzalez, S., Krzeminski, W., Morrell, N., Salgado, F., and Suntzeff, N. B. (2011). The Carnegie Supernova Project: Light-curve Fitting with SNooPy. , 141:19.

[Calzetti et al., 2000] Calzetti, D., Armus, L., Bohlin, R. C., Kinney, A. L., Koornneef, J., and Storchi-Bergmann, T. (2000). The Dust Content and Opacity of Actively Star-forming Galaxies. , 533(2):682–695.

[Camacho-Neves et al., 2023] Camacho-Neves, Y., Jha, S. W., Barna, B., Dai, M., Filippenko, A. V., Foley, R. J., Hosseinzadeh, G., Howell, D. A., Johansson, J., Kelly, P., Kerzendorf, W. E., Kwok, L. A., Larison, C., Magee, M. R., McCully, C., O'Brien, J. T., Pan, Y.-C., Pandya, V., Singhal, J., Stahl, B. E., Szalai, T., Wieber, M., and Williamson, M. (2023). Over 500 Days in the Life of the Photosphere of the Type Iax Supernova SN 2014dt. *arXiv e-prints*, page arXiv:2302.03105.

[Cardelli et al., 1988] Cardelli, J. A., Clayton, G. C., and Mathis, J. S. (1988). The determination of ultraviolet extinction from the optical and near-infrared. *ApJL*, 329:L33–L37.

[Chandrasekhar, 1931] Chandrasekhar, S. (1931). The Maximum Mass of Ideal White Dwarfs. , 74:81.

[Chen et al., 2023] Chen, N. M., Tucker, M. A., Hoyer, N., Jha, S. W., Kwok, L. A., Leroy, A. K., Rosolowsky, E., Ashall, C., Anand, G., Bigiel, F., Boquien, M., Burns, C., Dale, D., DerKacy, J. M., Egorov, O. V., Galbany, L., Grasha, K., Hassani, H., Hoeflich, P., Hsiao, E., Klessen, R. S., Lopez, L. A., Lu, J., Morrell, N., Orellana, M., Pinna, F., Sarbadhicary, S. K., Schinnerer, E., Shahbandeh, M., Stritzinger, M., Thilker, D. A., and Williams, T. G. (2023). Serendipitous Nebular-phase JWST Imaging of SN Ia SN 2021aefx: Testing the Confinement of ^{56}Co Decay Energy. , 944(2):L28.

[Cheng et al., 2020] Cheng, S., Cummings, J. D., Ménard, B., and Toonen, S. (2020). Double White Dwarf Merger Products among High-mass White Dwarfs. , 891(2):160.

[Claeys et al., 2014] Claeys, J. S. W., Pols, O. R., Izzard, R. G., Vink, J., and Verbunt, F. W. M. (2014). Theoretical uncertainties of the Type Ia supernova rate. , 563:A83.

[Copin et al., 2012] Copin, Y., Gangler, E., Pereira, R., Rigault, M., Smadja, G., Aldering, G., Birchall, D., Childress, M., Fakhouri, H., Kim, A., Nordin, J., Nugent, P., Perlmutter, S., Runge, K., Saunders, C., Suzuki, N., Thomas, R. C., Pecontal, E., Buton, C., Feindt, U., Kerschhaggl, M., Kowalski, M., Benitez, S., Hillebrandt, W., Kromer, M., Sasdelli, M., Sternberg, A., Taubenberger, S., Baugh, D., Chen, J., Chotard, N., Wu, C., Tao, C., Fouchez, D., Tilquin, A., Hadjiyska, E., Rabinowitz, D., Baltay, C., Ellman, N., McKinnon, R., Effron, A., Cellier-Holzem, F., Canto, A., Antilogus, P., Bongard, S., and Pain, R. (2012). Spectroscopic classification of PSN J20233626-2816434 as an early peculiar type Ia supernova by the Nearby Supernova Factory II. *The Astronomer's Telegram*, 4253:1.

[DerKacy et al., 2023] DerKacy, J. M., Ashall, C., Hoeflich, P., Baron, E., Shappee, B. J., Baade, D., Andrews, J., Bostroem, K. A., Brown, P. J., Burns, C. R., Burrow, A., Cikota, A., de Jaeger, T., Do, A., Dong, Y., Dominguez, I., Galbany, L., Hsiao, E. Y., Karamehmetoglu, E., Krisciunas, K., Kumar, S., Lu, J., Mera Evans, T. B., Maund, J. R., Mazzali, P., Medler, K., Morrell, N., Patat, F., Phillips, M. M., Shahbandeh, M., Stangl, S., Stevens, C. P., Stritzinger, M. D., Suntzeff, N. B., Telesco, C. M., Tucker, M. A., Valenti, S., Wang, L., Yang, Y., Jha, S. W., and Kwok, L. A. (2023). JWST Low-Resolution MIRI Spectral Observations of SN∼2021aefx: High-density Burning in a Type Ia Supernova. *arXiv e-prints*, page arXiv:2301.03647.

[DerKacy et al., 2020] DerKacy, J. M., Baron, E., Branch, D., Hoeflich, P., Hauschildt, P., Brown, P. J., and Wang, L. (2020). Ultraviolet Line Identifications and Spectral Formation Near Max Light in Type Ia Supernova 2011fe. , 901(1):86.

[Dettman et al., 2021] Dettman, K. G., Jha, S. W., Dai, M., Foley, R. J., Rest, A., Scolnic, D. M., Siebert, M. R., Chambers, K. C., Coulter, D. A., Huber, M. E., Johnson, E., Jones, D. O., Kilpatrick, C. D., Kirshner, R. P., Pan, Y. C., Riess, A. G., and Shultz, A. S. B. (2021). The Foundation Supernova Survey: Photospheric Velocity Correlations in Type Ia Supernovae. ,

923(2):267.

[Devarakonda and Brown, 2022] Devarakonda, Y. and Brown, P. J. (2022). Comparisons of Type Ia Supernova Light Curves in the UV and Optical with the Swift Ultra-violet/Optical Telescope. , 163(6):258.

[Dhawan et al., 2018] Dhawan, S., Jha, S. W., and Leibundgut, B. (2018). Measuring the Hubble constant with Type Ia supernovae as near-infrared standard candles. , 609:A72.

[Dhawan et al., 2017] Dhawan, S., Leibundgut, B., Spyromilio, J., and Blondin, S. (2017). Two classes of fast-declining Type Ia supernovae. , 602:A118.

[Drozdov et al., 2015] Drozdov, D., Leising, M. D., Milne, P. A., Pearcy, J., Riess, A. G., Macri, L. M., Bryngelson, G. L., and Garnavich, P. M. (2015). Detection of a Light Echo from the Otherwise Normal SN 2007af. , 805(1):71.

[Elias-Rosa et al., 2021] Elias-Rosa, N., Chen, P., Benetti, S., Dong, S., Prieto, J. L., Cappellaro, E., Kollmeier, J. A., Morrell, N., Piro, A. L., and Phillips, M. M. (2021). Nebular Hα emission in Type Ia supernova 2016jae. , 652:A115.

[Foley et al., 2020] Foley, R. J., Hoffmann, S. L., Macri, L. M., Riess, A. G., Brown, P. J., Filippenko, A. V., Graham, M. L., and Milne, P. A. (2020). Significant luminosity differences of two twin Type Ia supernovae. , 491(4):5991–5999.

[Foley and Kasen, 2011] Foley, R. J. and Kasen, D. (2011). Measuring Ejecta Velocity Improves Type Ia Supernova Distances. , 729:55.

[Foley and Kirshner, 2013] Foley, R. J. and Kirshner, R. P. (2013). Metallicity Differences in Type Ia Supernova Progenitors Inferred from Ultraviolet Spectra. *ApJL*, 769:L1.

[Foley et al., 2016] Foley, R. J., Pan, Y.-C., Brown, P., Filippenko, A. V., Fox, O. D., Hillebrandt, W., Kirshner, R. P., Marion, G. H., Milne, P. A., Parrent, J. T., Pignata, G., and Stritzinger, M. D. (2016). Ultraviolet diversity of Type Ia Supernovae. , 461:1308–1316.

[Foley et al., 2015] Foley, R. J., Van Dyk, S. D., Jha, S. W., Clubb, K. I., Filippenko, A. V., Mauerhan, J. C., Miller, A. A., and Smith, N. (2015). On the Progenitor System of the Type Iax Supernova 2014dt in M61. , 798(2):L37.

[Freedman et al., 2019] Freedman, W. L., Madore, B. F., Hatt, D., Hoyt, T. J., Jang, I. S., Beaton, R. L., Burns, C. R., Lee, M. G., Monson, A. J., Neeley, J. R., Phillips, M. M., Rich, J. A., and Seibert, M. (2019). The Carnegie-Chicago Hubble Program. VIII. An Independent Determination of the Hubble Constant Based on the Tip of the Red Giant Branch. , 882(1):34.

[Gall et al., 2018] Gall, C., Stritzinger, M. D., Ashall, C., Baron, E., Burns, C. R., Hoeflich, P., Hsiao, E. Y., Mazzali, P. A., Phillips, M. M., Filippenko, A. V., Anderson, J. P., Benetti, S., Brown, P. J., Campillay, A., Challis, P., Contreras, C., Elias de la Rosa, N., Folatelli, G., Foley, R. J., Fraser, M., Holmbo, S., Marion, G. H., Morrell, N., Pan, Y.-C., Pignata, G., Suntzeff, N. B., Taddia, F., Torres Robledo, S., and Valenti, S. (2018). Two transitional type Ia supernovae located in the Fornax cluster member NGC 1404: SN 2007on and SN 2011iv. , 611:A58.

[Garnavich et al., 2004] Garnavich, P. M., Bonanos, A. Z., Krisciunas, K., Jha, S., Kirshner, R. P., Schlegel, E. M., Challis, P., Macri, L. M., Hatano, K., Branch, D., Bothun, G. D., and Freedman, W. L. (2004). The Luminosity of SN 1999by in NGC 2841 and the Nature of "Peculiar" Type Ia Supernovae. *ApJ*, 613:1120–1132.

[Gehrels, 1997] Gehrels, N. (1997). Use of νF spectral energy distributions for multiwavelength astronomy. *Nuovo Cimento B Serie*, 112:11–15.

[Gehrels et al., 2004] Gehrels, N., Chincarini, G., Giommi, P., Mason, K. O., Nousek, J. A., Wells, A. A., White, N. E., Barthelmy, S. D., Burrows, D. N., Cominsky, L. R., Hurley, K. C., Marshall, F. E., Mészáros, P., Roming, P. W. A., Angelini, L., Barbier, L. M., Belloni, T., Campana, S., Caraveo, P. A., Chester, M. M., Citterio, O., Cline, T. L., Cropper, M. S., Cummings, J. R., Dean, A. J., Feigelson, E. D., Fenimore, E. E., Frail, D. A., Fruchter, A. S., Garmire, G. P., Gendreau, K., Ghisellini, G., Greiner, J., Hill, J. E., Hunsberger, S. D., Krimm, H. A., Kulkarni, S. R., Kumar, P., Lebrun, F., Lloyd-Ronning, N. M., Markwardt, C. B., Mattson, B. J.,

Mushotzky, R. F., Norris, J. P., Osborne, J., Paczynski, B., Palmer, D. M., Park, H.-S., Parsons, A. M., Paul, J., Rees, M. J., Reynolds, C. S., Rhoads, J. E., Sasseen, T. P., Schaefer, B. E., Short, A. T., Smale, A. P., Smith, I. A., Stella, L., Tagliaferri, G., Takahashi, T., Tashiro, M., Townsley, L. K., Tueller, J., Turner, M. J. L., Vietri, M., Voges, W., Ward, M. J., Willingale, R., Zerbi, F. M., and Zhang, W. W. (2004). The Swift Gamma-Ray Burst Mission. *ApJ*, 611:1005–1020.

[Goldhaber et al., 2001] Goldhaber, G., Groom, D. E., Kim, A., Aldering, G., Astier, P., Conley, A., Deustua, S. E., Ellis, R., Fabbro, S., Fruchter, A. S., Goobar, A., Hook, I., Irwin, M., Kim, M., Knop, R. A., Lidman, C., McMahon, R., Nugent, P. E., Pain, R., Panagia, N., Pennypacker, C. R., Perlmutter, S., Ruiz-Lapuente, P., Schaefer, B., Walton, N. A., and York, T. (2001). Timescale Stretch Parameterization of Type Ia Supernova B-Band Light Curves. *ApJ*, 558:359–368.

[González-Gaitán et al., 2014] González-Gaitán, S., Hsiao, E. Y., Pignata, G., Förster, F., Gutiérrez, C. P., Bufano, F., Galbany, L., Folatelli, G., Phillips, M. M., Hamuy, M., Anderson, J. P., and de Jaeger, T. (2014). Defining Photometric Peculiar Type Ia Supernovae. , 795(2):142.

[Graham et al., 2019] Graham, M. L., Harris, C. E., Nugent, P. E., Maguire, K., Sullivan, M., Smith, M., Valenti, S., Goobar, A., Fox, O. D., Shen, K. J., Kelly, P. L., McCully, C., Brink, T. G., and Filippenko, A. V. (2019). Delayed Circumstellar Interaction for Type Ia SN 2015cp Revealed by an HST Ultraviolet Imaging Survey. , 871:62.

[Graham et al., 2022] Graham, M. L., Kennedy, T. D., Kumar, S., Amaro, R. C., Sand, D. J., Jha, S. W., Galbany, L., Vinko, J., Wheeler, J. C., Hsiao, E. Y., Bostroem, K. A., Burke, J., Hiramatsu, D., Hosseinzadeh, G., McCully, C., Howell, D. A., Diamond, T., Hoeflich, P., Wang, X., and Li, W. (2022). Nebular-phase spectra of Type Ia supernovae from the Las Cumbres Observatory Global Supernova Project. , 511(3):3682–3707.

[Graur et al., 2018] Graur, O., Zurek, D. R., Rest, A., Seitenzahl, I. R., Shappee, B. J., Fisher, R., Guillochon, J., Shara, M. M., and Riess, A. G. (2018). Observations of SN 2015F Suggest

a Correlation between the Intrinsic Luminosity of Type Ia Supernovae and the Shape of Their Light Curves >900 Days after Explosion. , 859(2):79.

[Hamuy et al., 1996a] Hamuy, M., Phillips, M. M., Suntzeff, N. B., Schommer, R. A., Maza, J., and Aviles, R. (1996a). The Absolute Luminosities of the Calan/Tololo Type IA Supernovae. *AJ*, 112:2391–+.

[Hamuy et al., 1996b] Hamuy, M., Phillips, M. M., Suntzeff, N. B., Schommer, R. A., Maza, J., Smith, R. C., Lira, P., and Aviles, R. (1996b). The Morphology of Type IA Supernovae Light Curves. *AJ*, 112:2438–+.

[Harris et al., 2020] Harris, C. R., Millman, K. J., van der Walt, S. J., Gommers, R., Virtanen, P., Cournapeau, D., Wieser, E., Taylor, J., Berg, S., Smith, N. J., Kern, R., Picus, M., Hoyer, S., van Kerkwijk, M. H., Brett, M., Haldane, A., del Río, J. F., Wiebe, M., Peterson, P., Gérard-Marchant, P., Sheppard, K., Reddy, T., Weckesser, W., Abbasi, H., Gohlke, C., and Oliphant, T. E. (2020). Array programming with NumPy. *Nature*, 585(7825):357–362.

[He et al., 2018] He, S., Wang, L., and Huang, J. Z. (2018). Characterization of Type Ia Supernova Light Curves Using Principal Component Analysis of Sparse Functional Data. , 857(2):110.

[Hillebrandt and Niemeyer, 2000] Hillebrandt, W. and Niemeyer, J. C. (2000). Type IA Supernova Explosion Models. , 38:191–230.

[Höflich et al., 1996] Höflich, P., Khokhlov, A., Wheeler, J. C., Phillips, M. M., Suntzeff, N. B., and Hamuy, M. (1996). Maximum Brightness and Postmaximum Decline of Light Curves of Type IA Supernovae: A Comparison of Theory and Observations. *ApJL*, 472:L81+.

[Hogg, 2022] Hogg, D. W. (2022). Magnitudes, distance moduli, bolometric corrections, and so much more. *arXiv e-prints*, page arXiv:2206.00989.

[Hosseinzadeh et al., 2022] Hosseinzadeh, G., Sand, D. J., Lundqvist, P., Andrews, J. E., Bostroem, K. A., Dong, Y., Janzen, D., Jencson, J. E., Lundquist, M., Meza Retamal, N. E., Pearson, J., Valenti, S., Wyatt, S., Burke, J., Howell, D. A., McCully, C., Newsome, M., Gonzalez, E. P., Pellegrino, C., Terreran, G., Kwok, L. A., Jha, S. W., Strader, J., Kundu, E., Ryder,

S. D., Haislip, J., Kouprianov, V., and Reichart, D. E. (2022). Constraining the Progenitor System of the Type Ia Supernova 2021aefx. , 933(2):L45.

[Howell et al., 2006] Howell, D. A., Sullivan, M., Nugent, P. E., Ellis, R. S., Conley, A. J., Le Borgne, D., Carlberg, R. G., Guy, J., Balam, D., Basa, S., Fouchez, D., Hook, I. M., Hsiao, E. Y., Neill, J. D., Pain, R., Perrett, K. M., and Pritchet, C. J. (2006). The type Ia supernova SNLS-03D3bb from a super-Chandrasekhar-mass white dwarf star. *Nature*, 443:308–311.

[Hsiao et al., 2007] Hsiao, E. Y., Conley, A., Howell, D. A., Sullivan, M., Pritchet, C. J., Carlberg, R. G., Nugent, P. E., and Phillips, M. M. (2007). K-Corrections and Spectral Templates of Type Ia Supernovae. *ApJ*, 663:1187–1200.

[Hsiao et al., 2020] Hsiao, E. Y., Hoeflich, P., Ashall, C., Lu, J., Contreras, C., Burns, C. R., Phillips, M. M., Galbany, L., Anderson, J. P., Baltay, C., Baron, E., Castellón, S., Davis, S., Freedman, W. L., Gall, C., Gonzalez, C., Graham, M. L., Hamuy, M., Holoien, T. W. S., Karamehmetoglu, E., Krisciunas, K., Kumar, S., Kuncarayakti, H., Morrell, N., Moriya, T. J., Nugent, P. E., Perlmutter, S., Persson, S. E., Piro, A. L., Rabinowitz, D., Roth, M., Shahbandeh, M., Shappee, B. J., Stritzinger, M. D., Suntzeff, N. B., Taddia, F., and Uddin, S. A. (2020). Carnegie Supernova Project II: The Slowest Rising Type Ia Supernova LSQ14fmg and Clues to the Origin of Super-Chandrasekhar/03fg-like Events. , 900(2):140.

[Hunter, 2007] Hunter, J. D. (2007). Matplotlib: A 2d graphics environment. *Computing in Science & Engineering*, 9(3):90–95.

[Jha et al., 2006] Jha, S., Kirshner, R. P., Challis, P., Garnavich, P. M., Matheson, T., Soderberg, A. M., Graves, G. J. M., Hicken, M., Alves, J. F., Arce, H. G., Balog, Z., Barmby, P., Barton, E. J., Berlind, P., Bragg, A. E., Briceño, C., Brown, W. R., Buckley, J. H., Caldwell, N., Calkins, M. L., Carter, B. J., Concannon, K. D., Donnelly, R. H., Eriksen, K. A., Fabricant, D. G., Falco, E. E., Fiore, F., Garcia, M. R., Gómez, M., Grogin, N. A., Groner, T., Groot, P. J., Haisch, Jr., K. E., Hartmann, L., Hergenrother, C. W., Holman, M. J., Huchra, J. P., Jayawardhana, R., Jerius, D., Kannappan, S. J., Kim, D.-W., Kleyna, J. T., Kochanek, C. S., Koranyi, D. M.,

Krockenberger, M., Lada, C. J., Luhman, K. L., Luu, J. X., Macri, L. M., Mader, J. A., Mahdavi, A., Marengo, M., Marsden, B. G., McLeod, B. A., McNamara, B. R., Megeath, S. T., Moraru, D., Mossman, A. E., Muench, A. A., Muñoz, J. A., Muzerolle, J., Naranjo, O., Nelson-Patel, K., Pahre, M. A., Patten, B. M., Peters, J., Peters, W., Raymond, J. C., Rines, K., Schild, R. E., Sobczak, G. J., Spahr, T. B., Stauffer, J. R., Stefanik, R. P., Szentgyorgyi, A. H., Tollestrup, E. V., Väisänen, P., Vikhlinin, A., Wang, Z., Willner, S. P., Wolk, S. J., Zajac, J. M., Zhao, P., and Stanek, K. Z. (2006). UBVRI Light Curves of 44 Type Ia Supernovae. *AJ*, 131:527–554.

[Jha et al., 2007] Jha, S., Riess, A. G., and Kirshner, R. P. (2007). Improved Distances to Type Ia Supernovae with Multicolor Light-Curve Shapes: MLCS2k2. *ApJ*, 659:122–148.

[Jha et al., 2019] Jha, S. W., Avelino, A., Burns, C., Camacho-Neves, Y., Dai, M., Dettman, K., Dhawan, S., Filippenko, A. V., Foley, R., Friedman, A., Galbany, L., Garnavich, P. M., Hlozek, R., Holoien, T., Hounsell, R., Hsiao, E., Jones, D. O., Kelly, P., Kessler, R., Kirshner, R. P., Mandel, K., Matheson, T., Narayan, G., Phillips, M. M., Ponder, K., Rest, A., Riess, A., Roberts-Pierel, J., Rodney, S., Sand, D. J., Scolnic, D., Stritzinger, M., Strolger, L.-G., and Valenti, S. (2019). Supernovae in the Infrared avec Hubble. HST Proposal. Cycle 27, ID. #15889.

[Kamiya, 2012] Kamiya, Y. (2012). Light curve model for sn 2011aa, poster presented at supernovae illuminating the universe: from individuals to populations, september 10–14, garching bei muenchen, germany. Poster presented at Supernovae Illuminating the Universe: from Individuals to Populations, September 10–14, Garching bei Muenchen, Germany.

[Kasen, 2010] Kasen, D. (2010). Seeing the Collision of a Supernova with Its Companion Star. *ApJ*, 708:1025–1031.

[Kasen and Woosley, 2007] Kasen, D. and Woosley, S. E. (2007). On the Origin of the Type Ia Supernova Width-Luminosity Relation. *ApJ*, 656:661–665.

[Kattner et al., 2012] Kattner, S., Leonard, D. C., Burns, C. R., Phillips, M. M., Folatelli, G., Morrell, N., Stritzinger, M. D., Hamuy, M., Freedman, W. L., Persson, S. E., Roth, M., and

Suntzeff, N. B. (2012). The Standardizability of Type Ia Supernovae in the Near-Infrared: Evidence for a Peak-Luminosity Versus Decline-Rate Relation in the Near-Infrared. *PASP*, 124:114–127.

[Kelly, 2007] Kelly, B. C. (2007). Some Aspects of Measurement Error in Linear Regression of Astronomical Data. , 665:1489–1506.

[Kenworthy et al., 2021] Kenworthy, W. D., Jones, D. O., Dai, M., Kessler, R., Scolnic, D., Brout, D., Siebert, M. R., Pierel, J. D. R., Dettman, K. G., Dimitriadis, G., Foley, R. J., Jha, S. W., Pan, Y. C., Riess, A., Rodney, S., and Rojas-Bravo, C. (2021). SALT3: An Improved Type Ia Supernova Model for Measuring Cosmic Distances. *arXiv e-prints*, page arXiv:2104.07795.

[Kessler et al., 2009] Kessler, R., Becker, A. C., Cinabro, D., Vanderplas, J., Frieman, J. A., Marriner, J., Davis, T. M., Dilday, B., Holtzman, J., Jha, S. W., Lampeitl, H., Sako, M., Smith, M., Zheng, C., Nichol, R. C., Bassett, B., Bender, R., Depoy, D. L., Doi, M., Elson, E., Filippenko, A. V., Foley, R. J., Garnavich, P. M., Hopp, U., Ihara, Y., Ketzeback, W., Kollatschny, W., Konishi, K., Marshall, J. L., McMillan, R. J., Miknaitis, G., Morokuma, T., Mörtsell, E., Pan, K., Prieto, J. L., Richmond, M. W., Riess, A. G., Romani, R., Schneider, D. P., Sollerman, J., Takanashi, N., Tokita, K., van der Heyden, K., Wheeler, J. C., Yasuda, N., and York, D. (2009). First-Year Sloan Digital Sky Survey-II Supernova Results: Hubble Diagram and Cosmological Parameters. *ApJs*, 185:32–84.

[Kilic et al., 2021] Kilic, M., Bergeron, P., Blouin, S., and Bédard, A. (2021). The most massive white dwarfs in the solar neighbourhood. , 503(4):5397–5408.

[Kirshner et al., 1993] Kirshner, R. P., Jeffery, D. J., Leibundgut, B., Challis, P. M., Sonneborn, G., Phillips, M. M., Suntzeff, N. B., Smith, R. C., Winkler, P. F., Winge, C., Hamuy, M., Hunter, D. A., Roth, K. C., Blades, J. C., Branch, D., Chevalier, R. A., Fransson, C., Panagia, N., Wagoner, R. V., Wheeler, J. C., and Harkness, R. P. (1993). SN 1992A: Ultraviolet and Optical Studies Based on HST, IUE, and CTIO Observations. *ApJ*, 415:589–+.

[Kluyver et al., 2016] Kluyver, T., Ragan-Kelley, B., Pérez, F., Granger, B., Bussonnier, M., Frederic, J., Kelley, K., Hamrick, J., Grout, J., Corlay, S., Ivanov, P., Avila, D., Abdalla, S., Willing, C., and development team, J. (2016). Jupyter notebooks ? a publishing format for reproducible computational workflows. In Loizides, F. and Scmidt, B., editors, *Positioning and Power in Academic Publishing: Players, Agents and Agendas*, pages 87–90. IOS Press.

[Kokoska and Zwilinger, 2000] Kokoska, S. and Zwilinger, D. (2000). CRC Standard Probability and Statistics Tables and Formulae. *Chapman & Hall: New York*.

[Krisciunas et al., 2000] Krisciunas, K., Hastings, N. C., Loomis, K., McMillan, R., Rest, A., Riess, A. G., and Stubbs, C. (2000). Uniformity of (V-Near-Infrared) Color Evolution of Type Ia Supernovae and Implications for Host Galaxy Extinction Determination. *ApJ*, 539:658–674.

[Kulkarni et al., 2014] Kulkarni, S., Sahu, D. K., Chaware, L., Chakradhari, N. K., and Pandey, S. K. (2014). Study of dust and ionized gas in early-type galaxies. , 30:51–63.

[Kwok et al., 2023] Kwok, L. A., Jha, S. W., Temim, T., Fox, O. D., Larison, C., Camacho-Neves, Y., Brenner Newman, M. J., Pierel, J. D. R., Foley, R. J., Andrews, J. E., Badenes, C., Barna, B., Bostroem, K. A., Deckers, M., Flörs, A., Garnavich, P., Graham, M. L., Graur, O., Hosseinzadeh, G., Howell, D. A., Hughes, J. P., Johansson, J., Kendrew, S., Kerzendorf, W. E., Maeda, K., Maguire, K., McCully, C., O'Brien, J. T., Rest, A., Sand, D. J., Shahbandeh, M., Strolger, L.-G., Szalai, T., Ashall, C., Baron, E., Burns, C. R., DerKacy, J. M., Evans, T. M., Fisher, A., Galbany, L., Hoeflich, P., Hsiao, E., de Jaeger, T., Karamehmetoglu, E., Krisciunas, K., Kumar, S., Lu, J., Maund, J., Mazzali, P. A., Medler, K., Morrell, N., Phillips, M. M., Shappee, B. J., Stritzinger, M., Suntzeff, N., Telesco, C., Tucker, M., and Wang, L. (2023). A JWST Near- and Mid-infrared Nebular Spectrum of the Type Ia Supernova 2021aefx. , 944(1):L3.

[Lee et al., 2022] Lee, J. C., Sandstrom, K. M., Leroy, A. K., Thilker, D. A., Schinnerer, E., Rosolowsky, E., Larson, K. L., Egorov, O. V., Williams, T. G., Schmidt, J., Emsellem, E., Anand, G. S., Barnes, A. T., Belfiore, F., Beslic, I., Bigiel, F., Blanc, G. A., Bolatto, A. D., Boquien, M., den Brok, J., Cao, Y., Chandar, R., Chastenet, J., Chevance, M., Chiang, I.-D.,

Congiu, E., Dale, D. A., Deger, S., Eibensteiner, C., Faesi, C. M., Glover, S. C. O., Grasha, K., Groves, B., Hassani, H., Henny, K. F., Henshaw, J. D., Hoyer, N., Hughes, A., Jeffreson, S., Jimenez-Donaire, M. J., Kim, J., Kim, H., Klessen, R. S., Koch, E. W., Kreckel, K., Kruijssen, J. M. D., Li, J., Liu, D., Lopez, L. A., Maschmann, D., Mayker Chen, N., Meidt, S. E., Murphy, E. J., Neumann, J., Neumayer, N., Pan, H.-A., Pessa, I., Pety, J., Querejeta, M., Pinna, F., Jimena Rodrıguez, M., Saito, T., Sanchez-Blazquez, P., Santoro, F., Sardone, A., Smith, R. J., Sormani, M. C., Scheuermann, F., Stuber, S. K., Sutter, J., Sun, J., Teng, Y.-H., Tress, R. G., Usero, A., Watkins, E. J., Whitmore, B. C., and Razza, A. (2022). The PHANGS-JWST Treasury Survey: Star Formation, Feedback, and Dust Physics at High Angular resolution in Nearby GalaxieS. *arXiv e-prints*, page arXiv:2212.02667.

[Leibundgut, 2001] Leibundgut, B. (2001). Cosmological Implications from Observations of Type Ia Supernovae. *ARAA*, 39:67–98.

[Li et al., 2019] Li, C.-J., Kerzendorf, W. E., Chu, Y.-H., Chen, T.-W., Do, T., Gruendl, R. A., Holmes, A., Ishioka, R., Leibundgut, B., Pan, K.-C., Ricker, P. M., and Weisz, D. (2019). Search for Surviving Companions of Progenitors of Young LMC SN Ia Remnants. , 886(2):99.

[Maeda, 2022] Maeda, K. (2022). Stellar evolution, SN explosion, and nucleosynthesis. *arXiv e-prints*, page arXiv:2210.00326.

[Maeda and Terada, 2016] Maeda, K. and Terada, Y. (2016). Progenitors of type Ia supernovae. *International Journal of Modern Physics D*, 25(10):1630024.

[Mandel et al., 2011] Mandel, K. S., Narayan, G., and Kirshner, R. P. (2011). Type Ia Supernova Light Curve Inference: Hierarchical Models in the Optical and Near-infrared. , 731:120.

[Mandel et al., 2022] Mandel, K. S., Thorp, S., Narayan, G., Friedman, A. S., and Avelino, A. (2022). A hierarchical Bayesian SED model for Type Ia supernovae in the optical to near-infrared. , 510(3):3939–3966.

[Maoz and Hallakoun, 2017] Maoz, D. and Hallakoun, N. (2017). The binary fraction, separation distribution, and merger rate of white dwarfs from SPY. , 467(2):1414–1425.

[Mazzali et al., 2001] Mazzali, P. A., Nomoto, K., Cappellaro, E., Nakamura, T., Umeda, H., and Iwamoto, K. (2001). Can Differences in the Nickel Abundance in Chandrasekhar-Mass Models Explain the Relation between the Brightness and Decline Rate of Normal Type IA Supernovae? *ApJ*, 547:988–994.

[Mazzali et al., 2007] Mazzali, P. A., Röpke, F. K., Benetti, S., and Hillebrandt, W. (2007). A Common Explosion Mechanism for Type Ia Supernovae. *Science*, 315:825–.

[Mazzali et al., 2014] Mazzali, P. A., Sullivan, M., Hachinger, S., Ellis, R. S., Nugent, P. E., Howell, D. A., Gal-Yam, A., Maguire, K., Cooke, J., Thomas, R., Nomoto, K., and Walker, E. S. (2014). Hubble Space Telescope spectra of the Type Ia supernova SN 2011fe: a tail of low-density, high-velocity material with Z less than $Z_{\odot}$. *MNRAS*, 439:1959–1979.

[Milne et al., 2013] Milne, P. A., Brown, P. J., Roming, P. W. A., Bufano, F., and Gehrels, N. (2013). Grouping Normal Type Ia Supernovae by UV to Optical Color Differences. *ApJ*, 779:23.

[Milne et al., 2010] Milne, P. A., Brown, P. J., Roming, P. W. A., Holland, S. T., Immler, S., Filippenko, A. V., Ganeshalingam, M., Li, W., Stritzinger, M., Phillips, M. M., Hicken, M., Kirshner, R. P., Challis, P. J., Mazzali, P., Schmidt, B. P., Bufano, F., Gehrels, N., and Vanden Berk, D. (2010). Near-ultraviolet Properties of a Large Sample of Type Ia Supernovae as Observed with the Swift UVOT. *ApJ*, 721:1627–1655.

[Noebauer et al., 2016] Noebauer, U. M., Taubenberger, S., Blinnikov, S., Sorokina, E., and Hillebrandt, W. (2016). Type Ia supernovae within dense carbon- and oxygen-rich envelopes: a model for 'Super-Chandrasekhar' explosions? , 463(3):2972–2985.

[Nugent et al., 2002] Nugent, P., Kim, A., and Perlmutter, S. (2002). K-Corrections and Extinction Corrections for Type Ia Supernovae. *PASP*, 114:803–819.

[Nugent et al., 1995] Nugent, P., Phillips, M., Baron, E., Branch, D., and Hauschildt, P. (1995). Evidence for a Spectroscopic Sequence among Type 1a Supernovae. *ApJL*, 455:L147+.

[O'Donnell, 1994] O'Donnell, J. E. (1994). R v-dependent Optical and Near-Ultraviolet Extinction. , 422:158.

[Pan et al., 2020] Pan, Y. C., Foley, R. J., Jones, D. O., Filippenko, A. V., and Kuin, N. P. M. (2020). Swift UVOT grism observations of nearby Type Ia supernovae - II. Probing the progenitor metallicity of SNe Ia with ultraviolet spectra. , 491(4):5897–5910.

[Pan et al., 2015] Pan, Y.-C., Foley, R. J., Kromer, M., Fox, O. D., Zheng, W., Challis, P., Clubb, K. I., Filippenko, A. V., Folatelli, G., Graham, M. L., Hillebrandt, W., Kirshner, R. P., Lee, W. H., Pakmor, R., Patat, F., Phillips, M. M., Pignata, G., Röpke, F., Seitenzahl, I., Silverman, J. M., Simon, J. D., Sternberg, A., Stritzinger, M. D., Taubenberger, S., Vinko, J., and Wheeler, J. C. (2015). 500 days of SN 2013dy: spectra and photometry from the ultraviolet to the infrared. , 452:4307–4325.

[Parrent et al., 2011] Parrent, J. T., Thomas, R. C., Fesen, R. A., Marion, G. H., Challis, P., Garnavich, P. M., Milisavljevic, D., Vinkò, J., and Wheeler, J. C. (2011). A Study of Carbon Features in Type Ia Supernova Spectra. *ApJ*, 732:30.

[Pedregosa et al., 2011] Pedregosa, F., Varoquaux, G., Gramfort, A., Michel, V., Thirion, B., Grisel, O., Blondel, M., Prettenhofer, P., Weiss, R., Dubourg, V., Vanderplas, J., Passos, A., Cournapeau, D., Brucher, M., Perrot, M., and Édouard Duchesnay (2011). Scikit-learn: Machine learning in python. *Journal of Machine Learning Research*, 12(85):2825–2830.

[Pereira et al., 2013] Pereira, R., Thomas, R. C., Aldering, G., Antilogus, P., Baltay, C., Benitez-Herrera, S., Bongard, S., Buton, C., Canto, A., Cellier-Holzem, F., Chen, J., Childress, M., Chotard, N., Copin, Y., Fakhouri, H. K., Fink, M., Fouchez, D., Gangler, E., Guy, J., Hillebrandt, W., Hsiao, E. Y., Kerschhaggl, M., Kowalski, M., Kromer, M., Nordin, J., Nugent, P., Paech, K., Pain, R., Pécontal, E., Perlmutter, S., Rabinowitz, D., Rigault, M., Runge, K., Saunders, C., Smadja, G., Tao, C., Taubenberger, S., Tilquin, A., and Wu, C. (2013). Spectrophotometric time series of SN 2011fe from the Nearby Supernova Factory. *A&A*, 554:A27.

[Perlmutter et al., 1999] Perlmutter, S., Aldering, G., Goldhaber, G., Knop, R. A., Nugent, P., Castro, P. G., Deustua, S., Fabbro, S., Goobar, A., Groom, D. E., Hook, I. M., Kim, A. G., Kim, M. Y., Lee, J. C., Nunes, N. J., Pain, R., Pennypacker, C. R., Quimby, R., Lidman, C., Ellis, R. S., Irwin, M., McMahon, R. G., Ruiz-Lapuente, P., Walton, N., Schaefer, B., Boyle, B. J., Filippenko, A. V., Matheson, T., Fruchter, A. S., Panagia, N., Newberg, H. J. M., Couch, W. J., and The Supernova Cosmology Project (1999). Measurements of Omega and Lambda from 42 High-Redshift Supernovae. *ApJ*, 517:565–586.

[Phillips, 1993] Phillips, M. M. (1993). The absolute magnitudes of Type IA supernovae. *ApJL*, 413:L105–L108.

[Phillips et al., 1999] Phillips, M. M., Lira, P., Suntzeff, N. B., Schommer, R. A., Hamuy, M., and Maza, J. (1999). The Reddening-Free Decline Rate Versus Luminosity Relationship for Type IA Supernovae. *AJ*, 118:1766–1776.

[Pierel et al., 2022] Pierel, J. D. R., Jones, D. O., Kenworthy, W. D., Dai, M., Kessler, R., Ashall, C., Do, A., Peterson, E. R., Shappee, B. J., Siebert, M. R., Barna, T., Brink, T. G., Burke, J., Calamida, A., Camacho-Neves, Y., de Jaeger, T., Filippenko, A. V., Foley, R. J., Galbany, L., Fox, O. D., Gomez, S., Hiramatsu, D., Hounsell, R., Howell, D. A., Jha, S. W., Kwok, L. A., Pérez-Fournon, I., Poidevin, F., Rest, A., Rubin, D., Scolnic, D. M., Shirley, R., Strolger, L. G., Tinyanont, S., and Wang, Q. (2022). SALT3-NIR: Taking the Open-source Type Ia Supernova Model to Longer Wavelengths for Next-generation Cosmological Measurements. , 939(1):11.

[Piro and Nakar, 2014] Piro, A. L. and Nakar, E. (2014). Constraints on Shallow ^{56}Ni from the Early Light Curves of Type Ia Supernovae. , 784(1):85.

[Planck Collaboration et al., 2018] Planck Collaboration, Aghanim, N., Akrami, Y., Ashdown, M., Aumont, J., Baccigalupi, C., Ballardini, M., Banday, A. J., Barreiro, R. B., Bartolo, N., Basak, S., Battye, R., Benabed, K., Bernard, J. P., Bersanelli, M., Bielewicz, P., Bock, J. J., Bond, J. R., Borrill, J., Bouchet, F. R., Boulanger, F., Bucher, M., Burigana, C., Butler, R. C., Calabrese, E., Cardoso, J. F., Carron, J., Challinor, A., Chiang, H. C., Chluba, J., Colombo,

L. P. L., Combet, C., Contreras, D., Crill, B. P., Cuttaia, F., de Bernardis, P., de Zotti, G., Delabrouille, J., Delouis, J. M., Di Valentino, E., Diego, J. M., Doré, O., Douspis, M., Ducout, A., Dupac, X., Dusini, S., Efstathiou, G., Elsner, F., Enßlin, T. A., Eriksen, H. K., Fantaye, Y., Farhang, M., Fergusson, J., Fernandez-Cobos, R., Finelli, F., Forastieri, F., Frailis, M., Fraisse, A. A., Franceschi, E., Frolov, A., Galeotta, S., Galli, S., Ganga, K., Génova-Santos, R. T., Gerbino, M., Ghosh, T., González-Nuevo, J., Górski, K. M., Gratton, S., Gruppuso, A., Gudmundsson, J. E., Hamann, J., Handley, W., Hansen, F. K., Herranz, D., Hildebrandt, S. R., Hivon, E., Huang, Z., Jaffe, A. H., Jones, W. C., Karakci, A., Keihänen, E., Keskitalo, R., Kiiveri, K., Kim, J., Kisner, T. S., Knox, L., Krachmalnicoff, N., Kunz, M., Kurki-Suonio, H., Lagache, G., Lamarre, J. M., Lasenby, A., Lattanzi, M., Lawrence, C. R., Le Jeune, M., Lemos, P., Lesgourgues, J., Levrier, F., Lewis, A., Liguori, M., Lilje, P. B., Lilley, M., Lindholm, V., López-Caniego, M., Lubin, P. M., Ma, Y. Z., Macías-Pérez, J. F., Maggio, G., Maino, D., Mandolesi, N., Mangilli, A., Marcos-Caballero, A., Maris, M., Martin, P. G., Martinelli, M., Martínez-González, E., Matarrese, S., Mauri, N., McEwen, J. D., Meinhold, P. R., Melchiorri, A., Mennella, A., Migliaccio, M., Millea, M., Mitra, S., Miville-Deschênes, M. A., Molinari, D., Montier, L., Morgante, G., Moss, A., Natoli, P., Nørgaard-Nielsen, H. U., Pagano, L., Paoletti, D., Partridge, B., Patanchon, G., Peiris, H. V., Perrotta, F., Pettorino, V., Piacentini, F., Polastri, L., Polenta, G., Puget, J. L., Rachen, J. P., Reinecke, M., Remazeilles, M., Renzi, A., Rocha, G., Rosset, C., Roudier, G., Rubiño-Martín, J. A., Ruiz-Granados, B., Salvati, L., Sandri, M., Savelainen, M., Scott, D., Shellard, E. P. S., Sirignano, C., Sirri, G., Spencer, L. D., Sunyaev, R., Suur-Uski, A. S., Tauber, J. A., Tavagnacco, D., Tenti, M., Toffolatti, L., Tomasi, M., Trombetti, T., Valenziano, L., Valiviita, J., Van Tent, B., Vibert, L., Vielva, P., Villa, F., Vittorio, N., Wand elt, B. D., Wehus, I. K., White, M., White, S. D. M., Zacchei, A., and Zonca, A. (2018). Planck 2018 results. VI. Cosmological parameters. *arXiv e-prints*, page arXiv:1807.06209.

[Poole et al., 2008] Poole, T. S., Breeveld, A. A., Page, M. J., Landsman, W., Holland, S. T., Roming, P., Kuin, N. P. M., Brown, P. J., Gronwall, C., Hunsberger, S., Koch, S., Mason, K. O., Schady, P., vanden Berk, D., Blustin, A. J., Boyd, P., Broos, P., Carter, M., Chester, M. M.,

Cucchiara, A., Hancock, B., Huckle, H., Immler, S., Ivanushkina, M., Kennedy, T., Marshall, F., Morgan, A., Pandey, S. B., de Pasquale, M., Smith, P. J., and Still, M. (2008). Photometric calibration of the Swift ultraviolet/optical telescope. *MNRAS*, 383:627–645.

[Pskovskii, 1977] Pskovskii, I. P. (1977). Light curves, color curves, and expansion velocity of type I supernovae as functions of the rate of brightness decline. *Soviet Astronomy*, 21:675–682.

[Riess et al., 1998] Riess, A. G., Filippenko, A. V., Challis, P., Clocchiatti, A., Diercks, A., Garnavich, P. M., Gilliland, R. L., Hogan, C. J., Jha, S., Kirshner, R. P., Leibundgut, B., Phillips, M. M., Reiss, D., Schmidt, B. P., Schommer, R. A., Smith, R. C., Spyromilio, J., Stubbs, C., Suntzeff, N. B., and Tonry, J. (1998). Observational Evidence from Supernovae for an Accelerating Universe and a Cosmological Constant. *AJ*, 116:1009–1038.

[Riess et al., 1996] Riess, A. G., Press, W. H., and Kirshner, R. P. (1996). A Precise Distance Indicator: Type IA Supernova Multicolor Light-Curve Shapes. *ApJ*, 473:88–+.

[Rigby et al., 2022] Rigby, J., Perrin, M., McElwain, M., Kimble, R., Friedman, S., Lallo, M., Doyon, R., Feinberg, L., Ferruit, P., Glasse, A., Rieke, M., Rieke, G., Wright, G., Willott, C., Colon, K., Milam, S., Neff, S., Stark, C., Valenti, J., Abell, J., Abney, F., Abul-Huda, Y., Acton, D. S., Adams, E., Adler, D., Aguilar, J., Ahmed, N., Albert, L., Alberts, S., Aldridge, D., Allen, M., Altenburg, M., Alvarez Marquez, J., Alves de Oliveira, C., Andersen, G., Anderson, H., Anderson, S., Argyriou, I., Armstrong, A., Arribas, S., Artigau, E., Arvai, A., Atkinson, C., Bacon, G., Bair, T., Banks, K., Barrientes, J., Barringer, B., Bartosik, P., Bast, W., Baudoz, P., Beatty, T., Bechtold, K., Beck, T., Bergeron, E., Bergkoetter, M., Bhatawdekar, R., Birkmann, S., Blazek, R., Blome, C., Boccaletti, A., Boeker, T., Boia, J., Bonaventura, N., Bond, N., Bosley, K., Boucarut, R., Bourque, M., Bouwman, J., Bower, G., Bowers, C., Boyer, M., Bradley, L., Brady, G., Braun, H., Breda, D., Bresnahan, P., Bright, S., Britt, C., Bromenschenkel, A., Brooks, B., Brooks, K., Brown, B., Brown, M., Brown, P., Bunker, A., Burger, M., Bushouse, H., Cale, S., Cameron, A., Cameron, P., Canipe, A., Caplinger, J., Caputo, F., Cara, M., Carey, L., Carniani, S., Carrasquilla, M., Carruthers, M., Case, M., Catherine, R., Chance, D., Chap-

man, G., Charlot, S., Charlow, B., Chayer, P., Chen, B., Cherinka, B., Chichester, S., Chilton, Z., Chonis, T., Clampin, M., Clark, C., Clark, K., Coe, D., Coleman, B., Comber, B., Comeau, T., Connolly, D., Cooper, J., Cooper, R., Coppock, E., Correnti, M., Cossou, C., Coulais, A., Coyle, L., Cracraft, M., Curti, M., Cuturic, S., Davis, K., Davis, M., Dean, B., DeLisa, A., de-Meester, W., Dencheva, N., Dencheva, N., DePasquale, J., Deschenes, J., Hunor Detre, Ö., Diaz, R., Dicken, D., DiFelice, A., Dillman, M., Dixon, W., Doggett, J., Donaldson, T., Douglas, R., DuPrie, K., Dupuis, J., Durning, J., Easmin, N., Eck, W., Edeani, C., Egami, E., Ehrenwinkler, R., Eisenhamer, J., Eisenhower, M., Elie, M., Elliott, J., Elliott, K., Ellis, T., Engesser, M., Espinoza, N., Etienne, O., Etxaluze, M., Falini, P., Feeney, M., Ferry, M., Filippazzo, J., Fincham, B., Fix, M., Flagey, N., Florian, M., Flynn, J., Fontanella, E., Ford, T., Forshay, P., Fox, O., Franz, D., Fu, H., Fullerton, A., Galkin, S., Galyer, A., Garcia Marin, M., Gardner, J., Gardner, L., Garland, D., Garrett, B., Gasman, D., Gaspar, A., Gaudreau, D., Gauthier, P., Geers, V., Geithner, P., Gennaro, M., Giardino, G., Girard, J., Giuliano, M., Glassmire, K., Glauser, A., Glazer, S., Godfrey, J., Golimowski, D., Gollnitz, D., Gong, F., Gonzaga, S., Gordon, M., Gordon, K., Goudfrooij, P., Greene, T., Greenhouse, M., Grimaldi, S., Groebner, A., Grundy, T., Guillard, P., Gutman, I., Ha, K. Q., Haderlein, P., Hagedorn, A., Hainline, K., Haley, C., Hami, M., Hamilton, F., Hammel, H., Hansen, C., Harkins, T., Harr, M., Hart, J., Hart, Q., Hartig, G., Hashimoto, R., Haskins, S., Hathaway, W., Havey, K., Hayden, B., Hecht, K., Heller-Boyer, C., Henriques, C., Henry, A., Hermann, K., Hernandez, S., Hesman, B., Hicks, B., Hilbert, B., Hines, D., Hoffman, M., Holfeltz, S., Holler, B. J., Hoppa, J., Hott, K., Howard, J., Howard, R., Hunter, A., Hunter, D., Hurst, B., Husemann, B., Hustak, L., Ilinca Ignat, L., Illingworth, G., Irish, S., Jackson, W., Jahromi, A., Jakobsen, P., James, L., James, B., Januszewski, W., Jenkins, A., Jirdeh, H., Johnson, P., Johnson, T., Jones, V., Jones, R., Jones, D., Jones, O., Jordan, I., Jordan, M., Jurczyk, S., Jurling, A., Kaleida, C., Kalmanson, P., Kammerer, J., Kang, H., Kao, S.-H., Karakla, D., Kavanagh, P., Kelly, D., Kendrew, S., Kennedy, H., Kenny, D., Keski-kuha, R., Keyes, C., Kidwell, R., Kinzel, W., Kirk, J., Kirkpatrick, M., Kirshenblat, D., Klaassen, P., Knapp, B., Knight, J. S., Knollenberg, P., Koehler, R., Koekemoer, A., Kovacs, A.,

Kulp, T., Kumari, N., Kyprianou, M., La Massa, S., Labador, A., Labiano Ortega, A., Lagage, P.-O., Lajoie, C.-P., Lallo, M., Lam, M., Lamb, T., Lambros, S., Lampenfield, R., Langston, J., Larson, K., Law, D., Lawrence, J., Lee, D., Leisenring, J., Lepo, K., Leveille, M., Levenson, N., Levine, M., Levy, Z., Lewis, D., Lewis, H., Libralato, M., Lightsey, P., Link, M., Liu, L., Lo, A., Lockwood, A., Logue, R., Long, C., Long, D., Loomis, C., Lopez-Caniego, M., Alvarez, J. L., Love-Pruitt, J., Lucy, A., Luetzgendorf, N., Maghami, P., Maiolino, R., Major, M., Malla, S., Malumuth, E., Manjavacas, E., Mannfolk, C., Marrione, A., Marston, A., Martel, A., Maschmann, M., Masci, G., Masciarelli, M., Maszkiewicz, M., Mather, J., McKenzie, K., McLean, B., McMaster, M., Melbourne, K., Meléndez, M., Menzel, M., Merz, K., Meyett, M., Meza, L., Miskey, C., Misselt, K., Moller, C., Morrison, J., Morse, E., Moseley, H., Mosier, G., Mountain, M., Mueckay, J., Mueller, M., Mullally, S., Murphy, J., Murray, K., Murray, C., Mustelier, D., Muzerolle, J., Mycroft, M., Myers, R., Myrick, K., Nanavati, S., Nance, E., Nayak, O., Naylor, B., Nelan, E., Nickson, B., Nielson, A., Nieto-Santisteban, M., Nikolov, N., Noriega-Crespo, A., O'Shaughnessy, B., O'Sullivan, B., Ochs, W., Ogle, P., Oleszczuk, B., Olmsted, J., Osborne, S., Ottens, R., Owens, B., Pacifici, C., Pagan, A., Page, J., Park, S., Parrish, K., Patapis, P., Paul, L., Pauly, T., Pavlovsky, C., Pedder, A., Peek, M., Pena-Guerrero, M., Pennanen, K., Perez, Y., Perna, M., Perriello, B., Phillips, K., Pietraszkiewicz, M., Pinaud, J.-P., Pirzkal, N., Pitman, J., Piwowar, A., Platais, V., Player, D., Plesha, R., Pollizi, J., Polster, E., Pontoppidan, K., Porterfield, B., Proffitt, C., Pueyo, L., Pulliam, C., Quirt, B., Quispe Neira, I., Ramos Alarcon, R., Ramsay, L., Rapp, G., Rapp, R., Rauscher, B., Ravindranath, S., Rawle, T., Regan, M., Reichard, T. A., Reis, C., Ressler, M. E., Rest, A., Reynolds, P., Rhue, T., Richon, K., Rickman, E., Ridgaway, M., Ritchie, C., Rix, H.-W., Robberto, M., Robinson, G., Robinson, M., Robinson, O., Rock, F., Rodriguez, D., Rodriguez Del Pino, B., Roellig, T., Rohrbach, S., Roman, A., Romelfanger, F., Rose, P., Roteliuk, A., Roth, M., Rothwell, B., Rowlands, N., Roy, A., Royer, P., Royle, P., Rui, C., Rumler, P., Runnels, J., Russ, M., Rustamkulov, Z., Ryden, G., Ryer, H., Sabata, M., Sabatke, D., Sabbi, E., Samuelson, B., Sapp, B., Sappington, B., Sargent, B., Sauer, A., Scheithauer, S., Schlawin, E., Schlitz, J., Schmitz, T., Schneider, A., Schreiber,

J., Schulze, V., Schwab, R., Scott, J., Sembach, K., Shanahan, C., Shaughnessy, B., Shaw, R., Shawger, N., Shay, C., Sheehan, E., Shen, S., Sherman, A., Shiao, B., Shih, H.-Y., Shivaei, I., Sienkiewicz, M., Sing, D., Sirianni, M., Sivaramakrishnan, A., Skipper, J., Sloan, G., Slocum, C., Slowinski, S., Smith, E., Smith, E., Smith, D., Smith, C., Snyder, G., Soh, W., Sohn, T., Soto, C., Spencer, R., Stallcup, S., Stansberry, J., Starr, C., Starr, E., Stewart, A., Stiavelli, M., Straughn, A., Strickland, D., Stys, J., Summers, F., Sun, F., Sunnquist, B., Swade, D., Swam, M., Swaters, R., Swoish, R., Taylor, J. M., Taylor, R., Te Plate, M., Tea, M., Teague, K., Telfer, R., Temim, T., Thatte, D., Thompson, C., Thompson, L., Thomson, S., Tikkanen, T., Tippet, W., Todd, C., Toolan, S., Tran, H., Trejo, E., Truong, J., Tsukamoto, C., Tustain, S., Tyra, H., Ubeda, L., Underwood, K., Uzzo, M., Van Campen, J., Vandal, T., Vandenbussche, B., Vila, B., Volk, K., Wahlgren, G., Waldman, M., Walker, C., Wander, M., Warfield, C., Warner, G., Wasiak, M., Watkins, M., Weaver, A., Weilert, M., Weiser, N., Weiss, B., Weissman, S., Welty, A., West, G., Wheate, L., Wheatley, E., Wheeler, T., White, R., Whiteaker, K., Whitehouse, P., Whiteleather, J., Whitman, W., Williams, C., Willmer, C., Willoughby, S., Wilson, A., Wirth, G., Wislowski, E., Wolf, E., Wolfe, D., Wolff, S., Workman, B., Wright, R., Wu, C., Wu, R., Wymer, K., Yates, K., Yeager, C., Yeates, J., Yerger, E., Yoon, J., Young, A., Yu, S., Zak, D., Zeidler, P., Zhou, J., Zielinski, T., Zincke, C., and Zonak, S. (2022). The Science Performance of JWST as Characterized in Commissioning. *arXiv e-prints*, page arXiv:2207.05632.

[Roming et al., 2005] Roming, P. W. A., Kennedy, T. E., Mason, K. O., Nousek, J. A., Ahr, L., Bingham, R. E., Broos, P. S., Carter, M. J., Hancock, B. K., Huckle, H. E., Hunsberger, S. D., Kawakami, H., Killough, R., Koch, T. S., McLelland, M. K., Smith, K., Smith, P. J., Soto, J. C., Boyd, P. T., Breeveld, A. A., Holland, S. T., Ivanushkina, M., Pryzby, M. S., Still, M. D., and Stock, J. (2005). The Swift Ultra-Violet/Optical Telescope. *Space Science Reviews*, 120:95–142.

[Roy et al., 2022] Roy, N. C., Tiwari, V., Bobrick, A., Kosakowski, D., Fisher, R., Perets, H. B., Kashyap, R., Lorén-Aguilar, P., and García-Berro, E. (2022). 3D Hydrodynamical Simulations of Helium-ignited Double-degenerate White Dwarf Mergers. , 932(2):L24.

[Scalzo et al., 2010] Scalzo, R. A., Aldering, G., Antilogus, P., Aragon, C., Bailey, S., Baltay, C., Bongard, S., Buton, C., Childress, M., Chotard, N., Copin, Y., Fakhouri, H. K., Gal-Yam, A., Gangler, E., Hoyer, S., Kasliwal, M., Loken, S., Nugent, P., Pain, R., Pécontal, E., Pereira, R., Perlmutter, S., Rabinowitz, D., Rau, A., Rigaudier, G., Runge, K., Smadja, G., Tao, C., Thomas, R. C., Weaver, B., and Wu, C. (2010). Nearby Supernova Factory Observations of SN 2007if: First Total Mass Measurement of a Super-Chandrasekhar-Mass Progenitor. *ApJ*, 713:1073–1094.

[Scalzo et al., 2014] Scalzo, R. A., Childress, M., Tucker, B., Yuan, F., Schmidt, B., Brown, P. J., Contreras, C., Morrell, N., Hsiao, E., Burns, C., Phillips, M. M., Campillay, A., Gonzalez, C., Krisciunas, K., Stritzinger, M., Graham, M. L., Parrent, J., Valenti, S., Lidman, C., Schaefer, B., Scott, N., Fraser, M., Gal-Yam, A., Inserra, C., Maguire, K., Smartt, S. J., Sollerman, J., Sullivan, M., Taddia, F., Yaron, O., Young, D. R., Taubenberger, S., Baltay, C., Ellman, N., Feindt, U., Hadjiyska, E., McKinnon, R., Nugent, P. E., Rabinowitz, D., and Walker, E. S. (2014). Early ultraviolet emission in the Type Ia supernova LSQ12gdj: No evidence for ongoing shock interaction. *MNRAS*, 445:30–48.

[Schlafly and Finkbeiner, 2011] Schlafly, E. F. and Finkbeiner, D. P. (2011). Measuring Reddening with Sloan Digital Sky Survey Stellar Spectra and Recalibrating SFD. *ApJ*, 737:103.

[Shappee et al., 2016] Shappee, B. J., Piro, A. L., Holoien, T. W.-S., Prieto, J. L., Contreras, C., Itagaki, K., Burns, C. R., Kochanek, C. S., Stanek, K. Z., Alper, E., Basu, U., Beacom, J. F., Bersier, D., Brimacombe, J., Conseil, E., Danilet, A. B., Dong, S., Falco, E., Grupe, D., Hsiao, E. Y., Kiyota, S., Morrell, N., Nicolas, J., Phillips, M. M., Pojmanski, G., Simonian, G., Stritzinger, M., Szczygieł, D. M., Taddia, F., Thompson, T. A., Thorstensen, J., Wagner, M. R., and Woźniak, P. R. (2016). The Young and Bright Type Ia Supernova ASASSN-14lp: Discovery, Early-time Observations, First-light Time, Distance to NGC 4666, and Progenitor Constraints. , 826:144.

[Stahl et al., 2019] Stahl, B. E., Zheng, W., de Jaeger, T., Filippenko, A. V., Bigley, A., Blanchard,

K., Blanchard, P. K., Brink, T. G., Cargill, S. K., Casper, C., Channa, S., Choi, B. Y., Choksi, N., Chu, J., Clubb, K. I., Cohen, D. P., Ellison, M., Falcon, E., Fazeli, P., Fuller, K., Ganeshalingam, M., Gates, E. L., Gould, C., Halevi, G., Hayakawa, K. T., Hestenes, J., Jeffers, B. T., Joubert, N., Kandrashoff, M. T., Kim, M., Kim, H., Kislak, M. E., Kleiser, I., Kong, J. J., de Kouchkovsky, M., Krishnan, D., Kumar, S., Leja, J., Leonard, E. J., Li, G. Z., Li, W., Lu, P., Mason, M. N., Molloy, J., Pina, K., Rex, J., Ross, T. W., Stegman, S., Tang, K., Thrasher, P., Wang, X., Wilkins, A., Yuk, H., Yunus, S., and Zhang, K. (2019). Lick Observatory Supernova Search follow-up program: photometry data release of 93 Type Ia supernovae. , 490(3):3882–3907.

[Tucker et al., 2022] Tucker, M. A., Ashall, C., Shappee, B. J., Kochanek, C. S., Stanek, K. Z., and Garnavich, P. (2022). A Rapid Ionization Change in the Nebular-phase Spectra of the Type Ia SN 2011fe. , 926(2):L25.

[Tukey, 1977] Tukey, J. W. (1977). *Exploratory Data Analysis*. Addison-Wesley.

[Uddin et al., 2020] Uddin, S. A., Burns, C. R., Phillips, M. M., Suntzeff, N. B., Contreras, C., Hsiao, E. Y., Morrell, N., Galbany, L., Stritzinger, M., Hoeflich, P., Ashall, C., Piro, A. L., Freedman, W. L., Persson, S. E., Krisciunas, K., and Brown, P. (2020). The Carnegie Supernova Project-I: Correlation between Type Ia Supernovae and Their Host Galaxies from Optical to Near-infrared Bands. , 901(2):143.

[Virtanen et al., 2019] Virtanen, P., Gommers, R., Oliphant, T. E., Haberland, M., Reddy, T., Cournapeau, D., Burovski, E., Peterson, P., Weckesser, W., Bright, J., van der Walt, S. J., Brett, M., Wilson, J., Jarrod Millman, K., Mayorov, N., Nelson, A. R. J., Jones, E., Kern, R., Larson, E., Carey, C., Polat, İ., Feng, Y., Moore, E. W., Vand erPlas, J., Laxalde, D., Perktold, J., Cimrman, R., Henriksen, I., Quintero, E. A., Harris, C. R., Archibald, A. M., Ribeiro, A. H., Pedregosa, F., van Mulbregt, P., and Contributors, S. . . (2019). SciPy 1.0–Fundamental Algorithms for Scientific Computing in Python. *arXiv e-prints*, page arXiv:1907.10121.

[Virtanen et al., 2020] Virtanen, P., Gommers, R., Oliphant, T. E., Haberland, M., Reddy, T., Cournapeau, D., Burovski, E., Peterson, P., Weckesser, W., Bright, J., van der Walt, S. J.,

Brett, M., Wilson, J., Millman, K. J., Mayorov, N., Nelson, A. R. J., Jones, E., Kern, R., Larson, E., Carey, C. J., Polat, İ., Feng, Y., Moore, E. W., Vand erPlas, J., Laxalde, D., Perktold, J., Cimrman, R., Henriksen, I., Quintero, E. A., Harris, C. R., Archibald, A. M., Ribeiro, A. H., Pedregosa, F., van Mulbregt, P., and SciPy 1. 0 Contributors (2020). SciPy 1.0: fundamental algorithms for scientific computing in Python. *Nature Methods*, 17:261–272.

[Virtanen et al., 2020] Virtanen, P., Gommers, R., Oliphant, T. E., Haberland, M., Reddy, T., Cournapeau, D., Burovski, E., Peterson, P., Weckesser, W., Bright, J., van der Walt, S. J., Brett, M., Wilson, J., Millman, K. J., Mayorov, N., Nelson, A. R. J., Jones, E., Kern, R., Larson, E., Carey, C. J., Polat, İ., Feng, Y., Moore, E. W., VanderPlas, J., Laxalde, D., Perktold, J., Cimrman, R., Henriksen, I., Quintero, E. A., Harris, C. R., Archibald, A. M., Ribeiro, A. H., Pedregosa, F., van Mulbregt, P., and SciPy 1.0 Contributors (2020). SciPy 1.0: Fundamental Algorithms for Scientific Computing in Python. *Nature Methods*, 17:261–272.

[Wang et al., 2003] Wang, L., Goldhaber, G., Aldering, G., and Perlmutter, S. (2003). Multicolor Light Curves of Type Ia Supernovae on the Color-Magnitude Diagram: A Novel Step toward More Precise Distance and Extinction Estimates. *ApJ*, 590:944–970.

[Wang et al., 2019] Wang, X., Chen, J., Wang, L., Hu, M., Xi, G., Yang, Y., Zhao, X., and Li, W. (2019). The Cold and Dusty Circumstellar Matter around Fast-expanding Type Ia Supernovae. , 882(2):120.

[Wes McKinney, 2010] Wes McKinney (2010). Data Structures for Statistical Computing in Python. In Stéfan van der Walt and Jarrod Millman, editors, *Proceedings of the 9th Python in Science Conference*, pages 56 – 61.

[Whelan and Iben, 1973] Whelan, J. and Iben, Jr., I. (1973). Binaries and Supernovae of Type I. *ApJ*, 186:1007–1014.

[Wood-Vasey et al., 2008] Wood-Vasey, W. M., Friedman, A. S., Bloom, J. S., Hicken, M., Modjaz, M., Kirshner, R. P., Starr, D. L., Blake, C. H., Falco, E. E., Szentgyorgyi, A. H., Challis,

P., Blondin, S., Mandel, K. S., and Rest, A. (2008). Type Ia Supernovae Are Good Standard Candles in the Near Infrared: Evidence from PAIRITEL. , 689:377–390.

APPENDIX A

Band	Interquartile Range	Brown-Forsythe Test Statistic	Brown-Forsythe P-Value
W2	2.062	0.169	0.682
M2	2.235	0.012	0.913
W1	1.913	0.112	0.738
U	2.679	0.118	0.732
B	2.320	-	-
V	2.597	1.516	0.221

Table A.1: A comparison of the variability in the PC1 values as compared to the B band. Similar IQR scores and P values > 0.05 would suggest that there is not statistical difference in the variability between the bands.

Band	Interquartile Range	Brown-Forsythe Test Statistic	Brown-Forsythe P-Value
W2	1.304	0.426	0.516
M2	1.731	3.118	0.082
W1	1.110	0.359	0.550
U	1.095	0	0.983
B	0.900	-	-
V	0.581	10.731	0.001

Table A.2: A comparison of the variability in the PC2 values as compared to the B band. Similar IQR scores and P values > 0.05 would suggest that there is not statistical difference in the variability between the bands.

Band	Interquartile Range	Brown-Forsythe Test Statistic	Brown-Forsythe P-Value
W2	0.861	7.804	0.007
M2	0.925	13.237	0.001
W1	1.444	28.489	0
U	1.075	21.533	0
B	0.448	-	-
V	0.481	0.062	0.804

Table A.3: A comparison of the variability in the PC3 values as compared to the B band. Similar IQR scores and P values > 0.05 would suggest that there is not statistical difference in the variability between the bands.

Band	Interquartile Range	Brown-Forsythe Test Statistic	Brown-Forsythe P-Value
W2	0.350	0.008	0.930
M2	0.473	0.107	0.745
W1	0.367	1.533	0.219
U	0.337	0.031	0.861
B	0.363	-	-
V	0.188	9.904	0.002

Table A.4: A comparison of the variability in the Δm_{15} values as compared to the B band. Similar IQR scores and P values > 0.05 would suggest that there is not statistical difference in the variability between the bands.

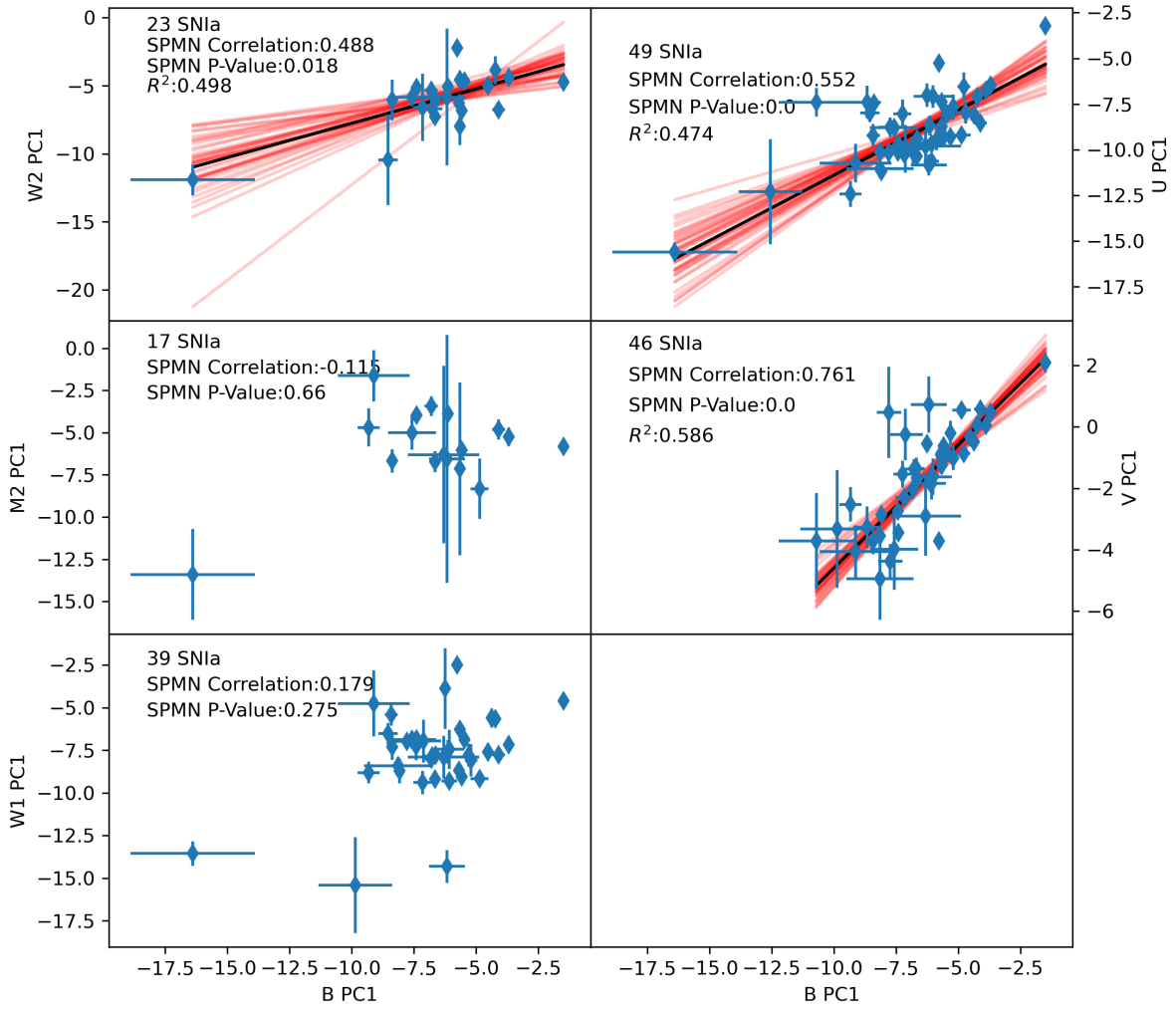

Figure A.1: The correlation between the B band and other Swift UVOT bands for the PC1 weights. Only the $UVW2$, U, and V bands have a statistically significant correlation based on the Spearman rank-order coefficient test. The red lines indicate the spread of the MCMC draws from Linmix, and the black line is the mean linear fit from which we calulate the r^2 value. The PC1 weights are most directly related to the decline rate of the light curves.

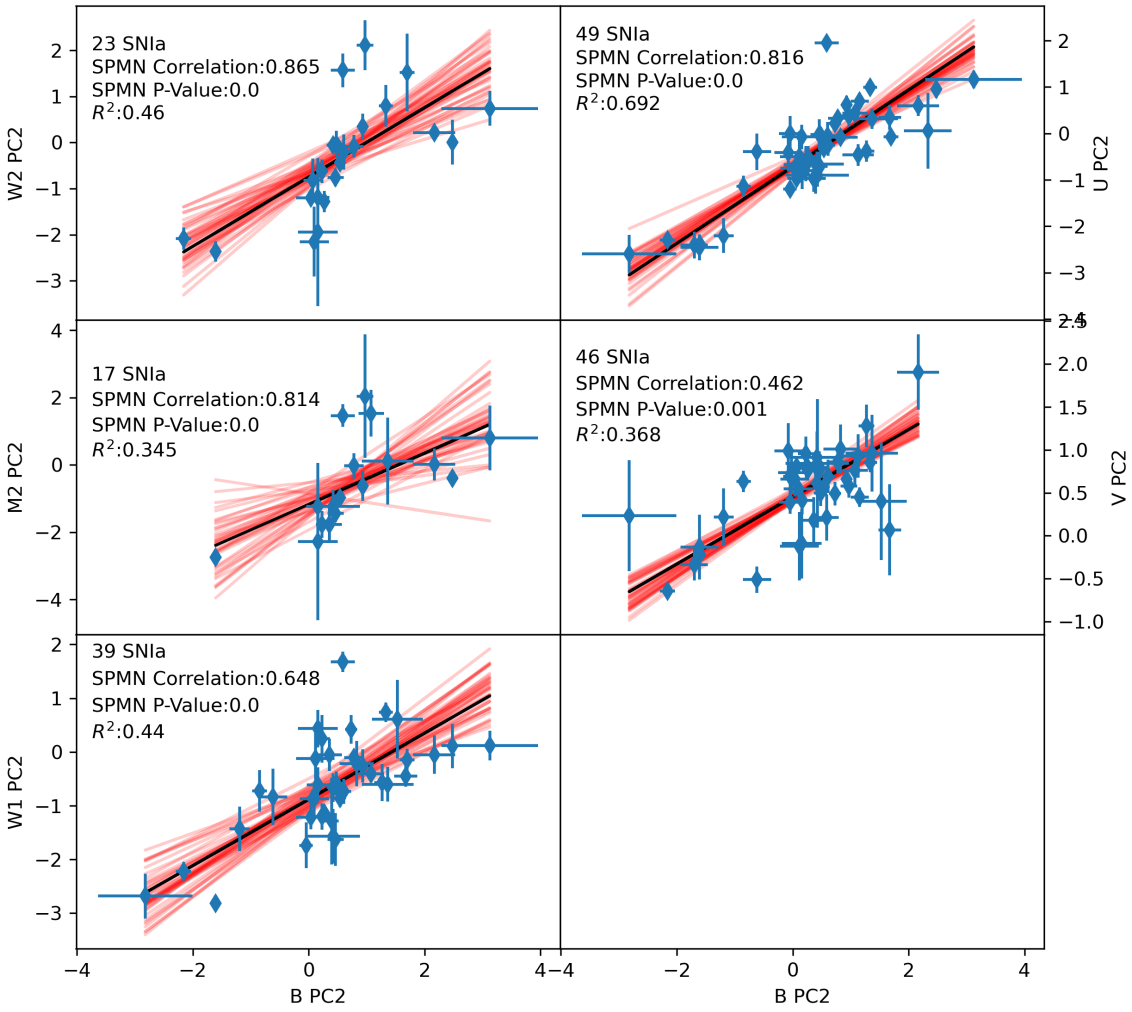

Figure A.2: The correlation between the B band and the other Swift UVOT bands for the PC2 weights. The statistical significance of the correlation is based on the Spearman rank-order coefficient test. The red lines indicate the spread of the MCMC draws from Linmix, and the black line is the mean linear fit from which we calulate the r^2 value. The PC2 weights are most directly related to the spread of the light curves.

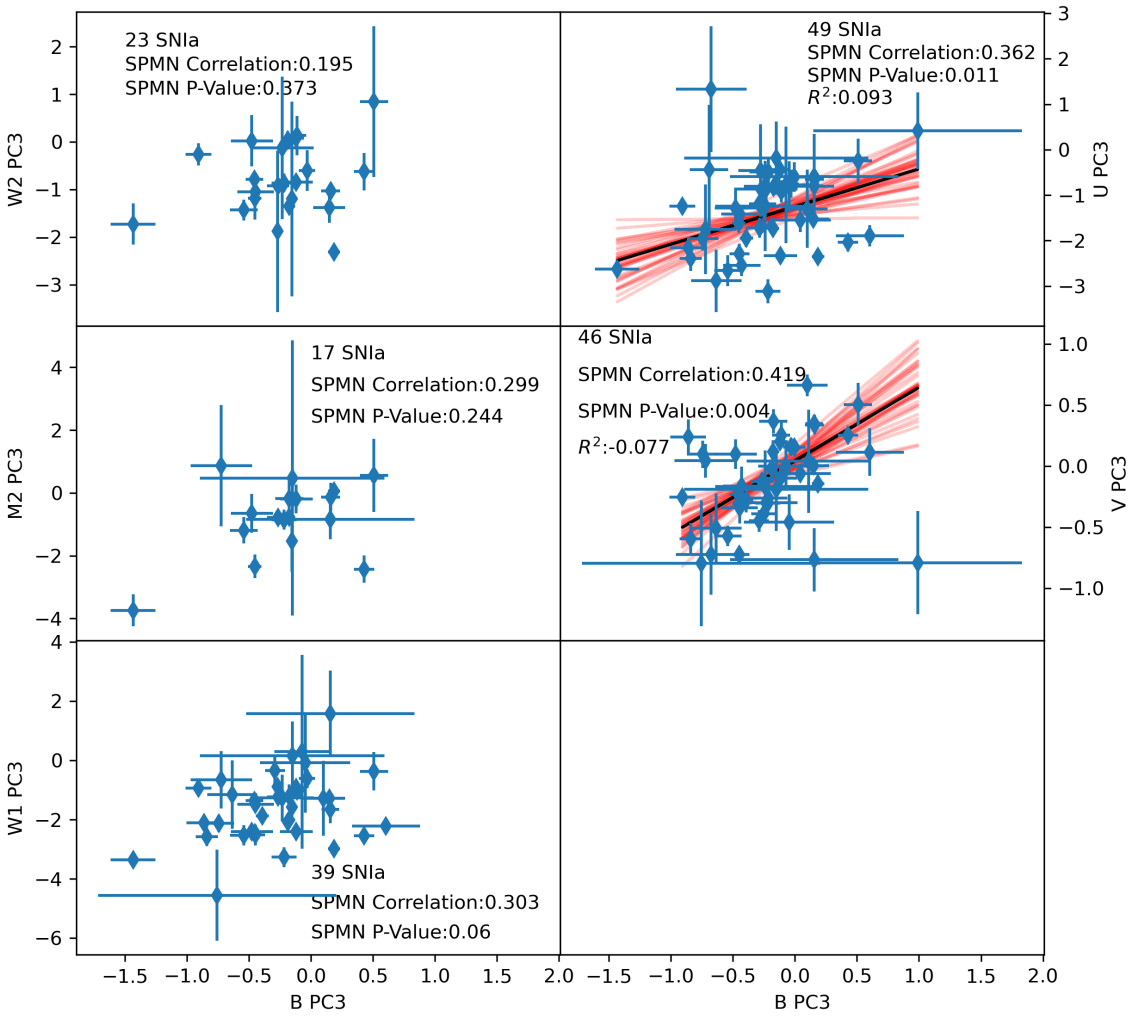

Figure A.3: The correlation between the B band and the other Swift UVOT bands for the PC3 weights. Only the U and V bands have a statistically significant correlation based on the Spearman rank-order coefficient test. The red lines indicate the spread of the MCMC draws from Linmix, and the black line is the mean linear fit from which we calulate the r^2 value. The PC3 weights are most directly related to the pre-peak rise in the light curve and late phase adjustments.

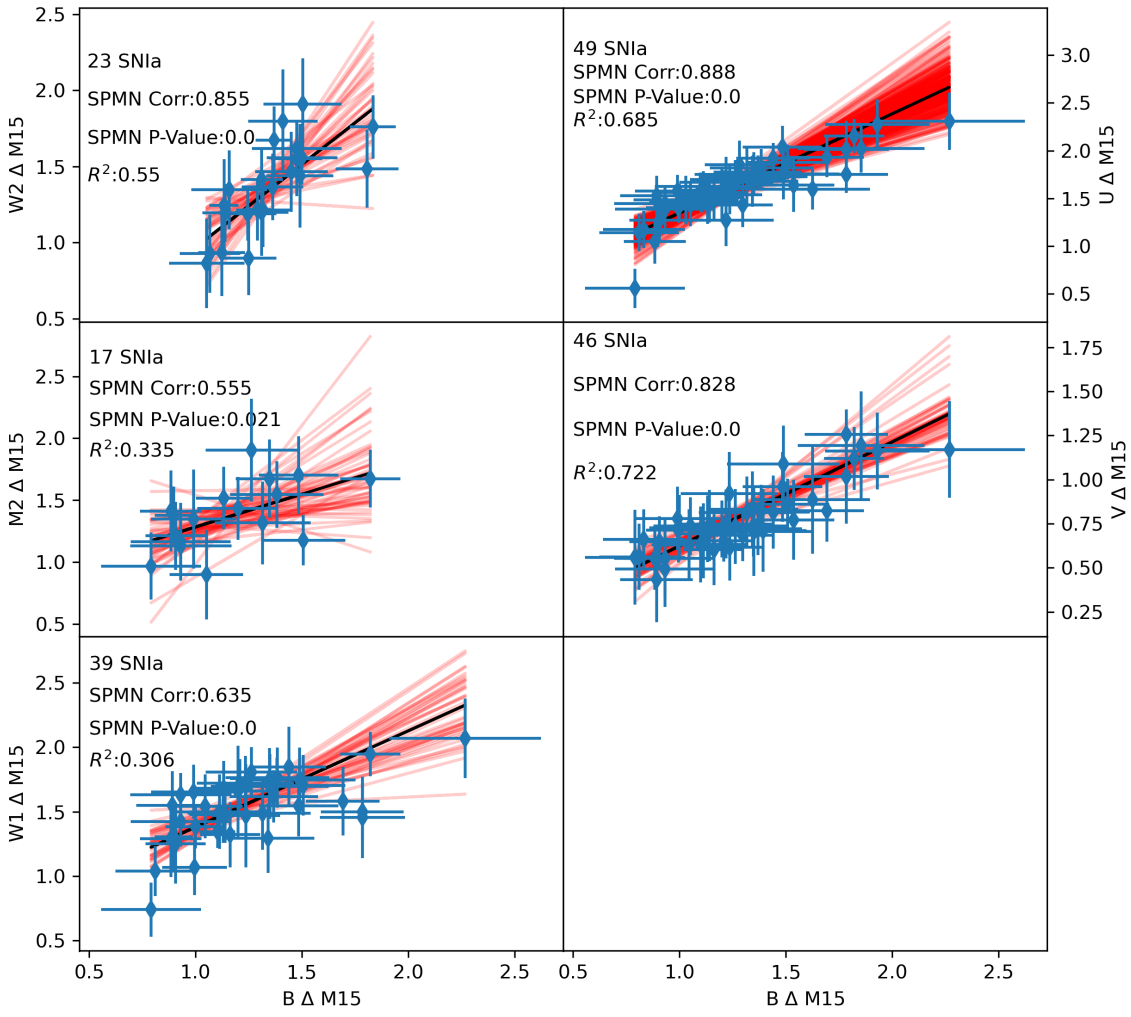

Figure A.4: The correlation between the B band and the other Swift UVOT bands for the 15 day decline rate post-peak. The red lines indicate the spread of the MCMC draws from Linmix, and the black line is the mean linear fit from which we calulate the r^2 value. The decline rate is calculated from the best fit FPCA model for each individual light curve.

APPENDIX B

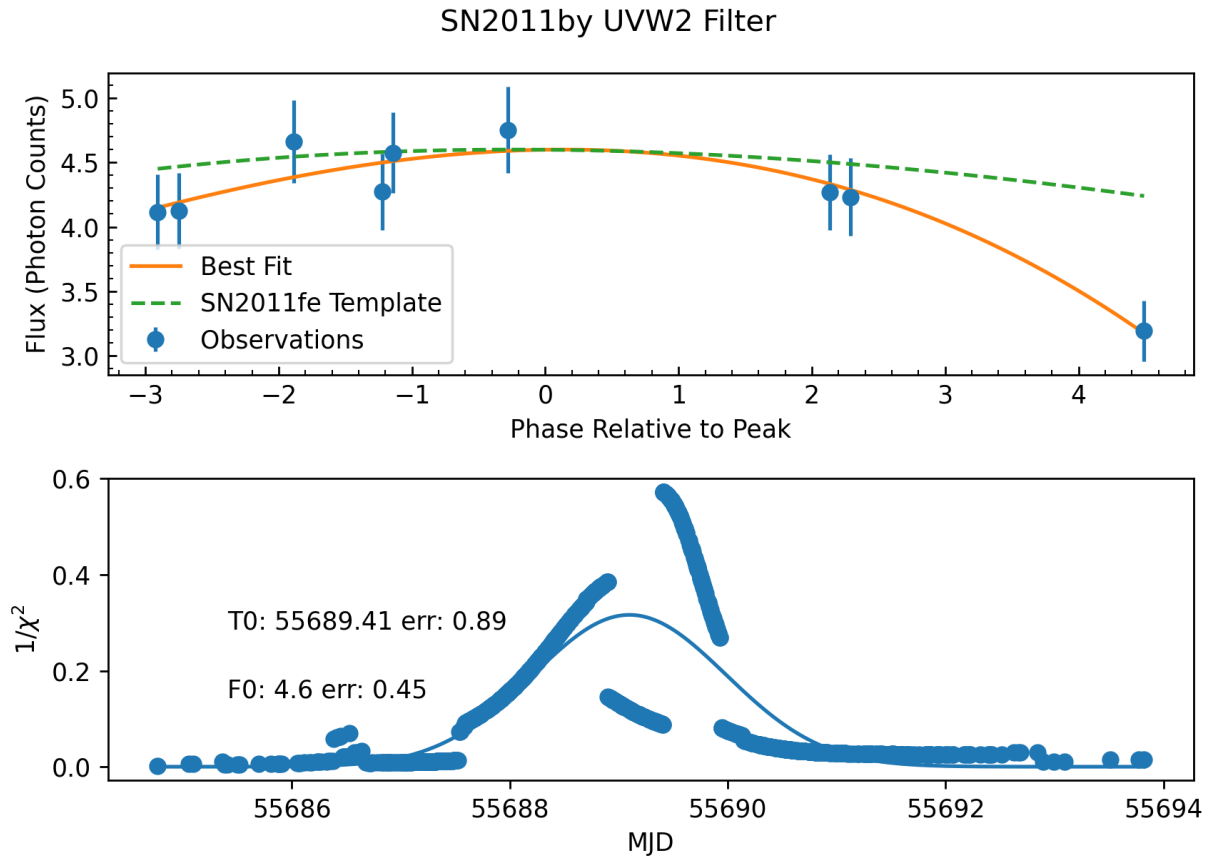

Figure B.1: An example of stretch-based fitting. Top: The $UVW2$ filter observations of SN2011by (blue points). The orange line shows the best fit for SN2011by, and the green line shows the unmodified SN2011fe light curve for comparison. Bottom: Blue points show the $1/\chi^2$ values from random draws of the peak phase estimate. The blue line shows the Gaussian fit to this distribution. The estimate for the peak phase (T0) and peak photon count (P0) with uncertainties are also shown.

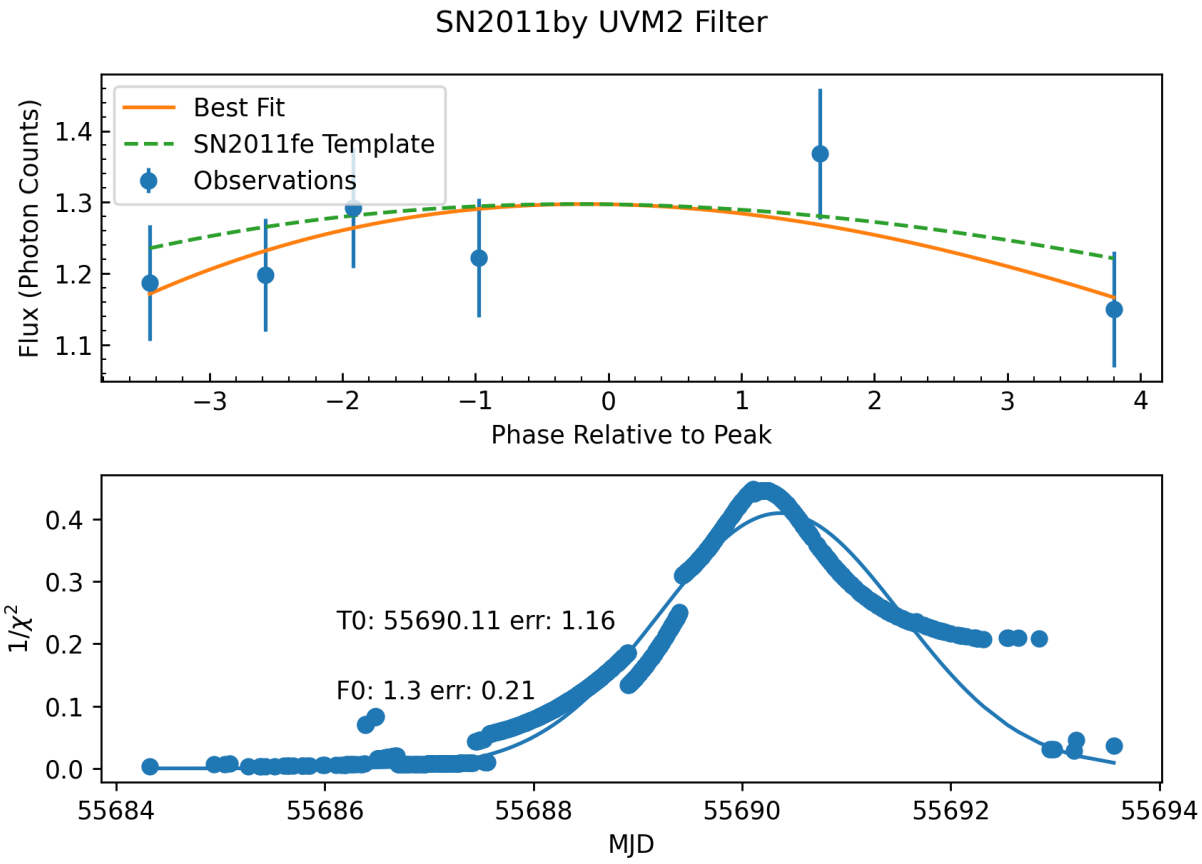

Figure B.2: As Figure B.1, but for $UVM2$ band observations of SN2011by.

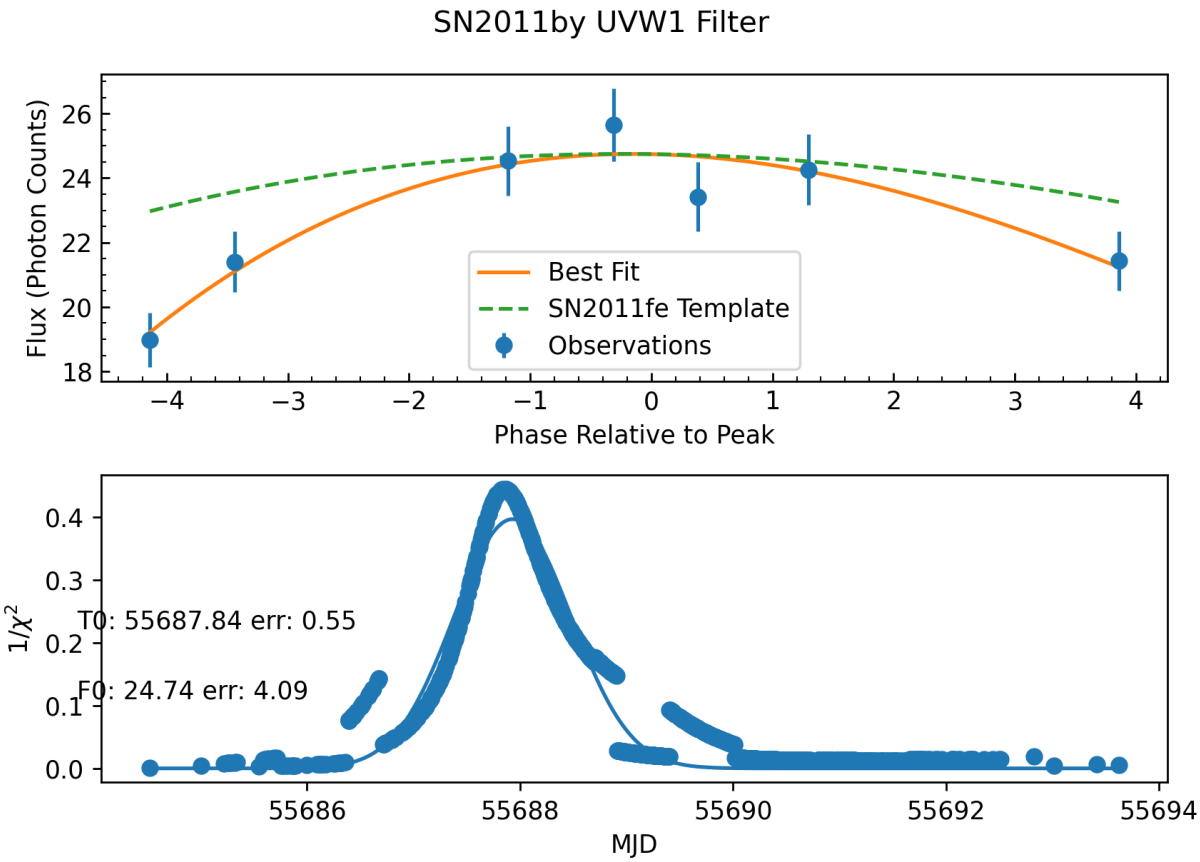

Figure B.3: As Figure B.1, but for $UVW1$ band observations of SN2011by.

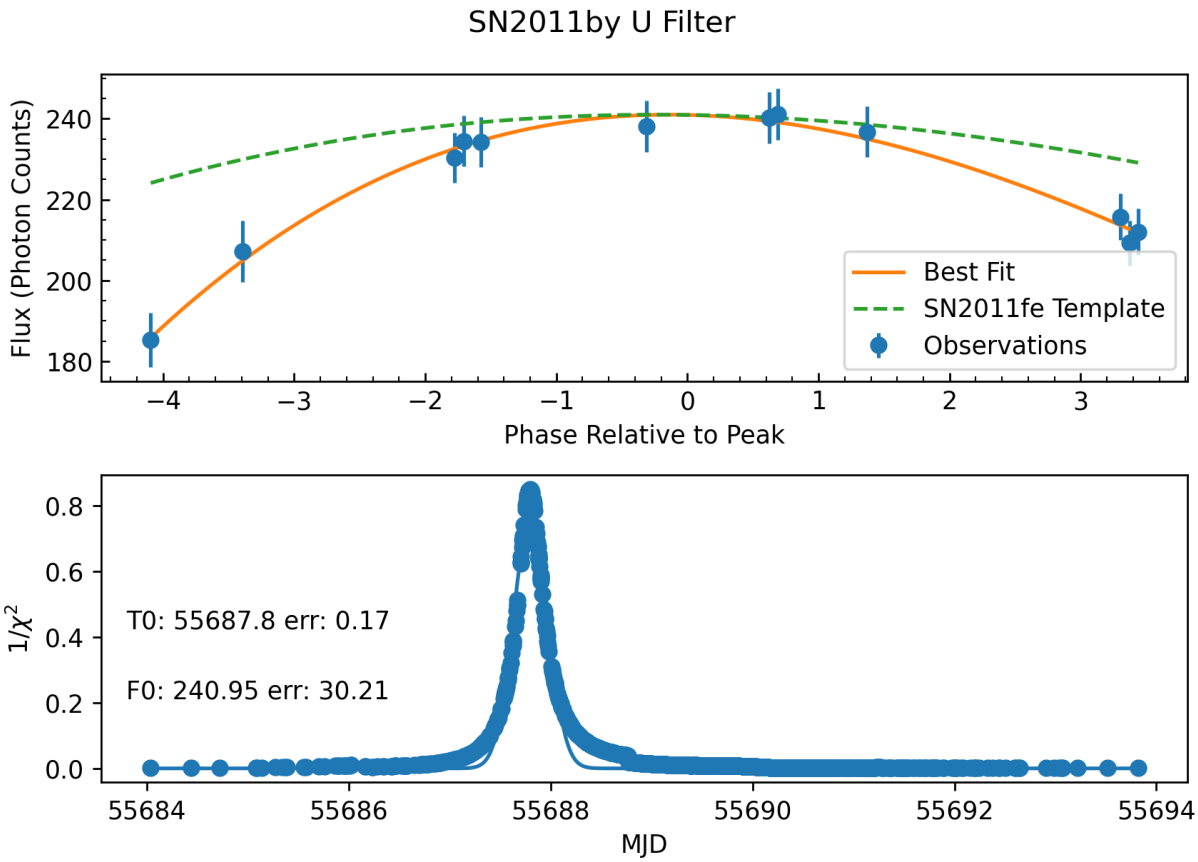

Figure B.4: As Figure B.1, but for U band observations of SN2011by.

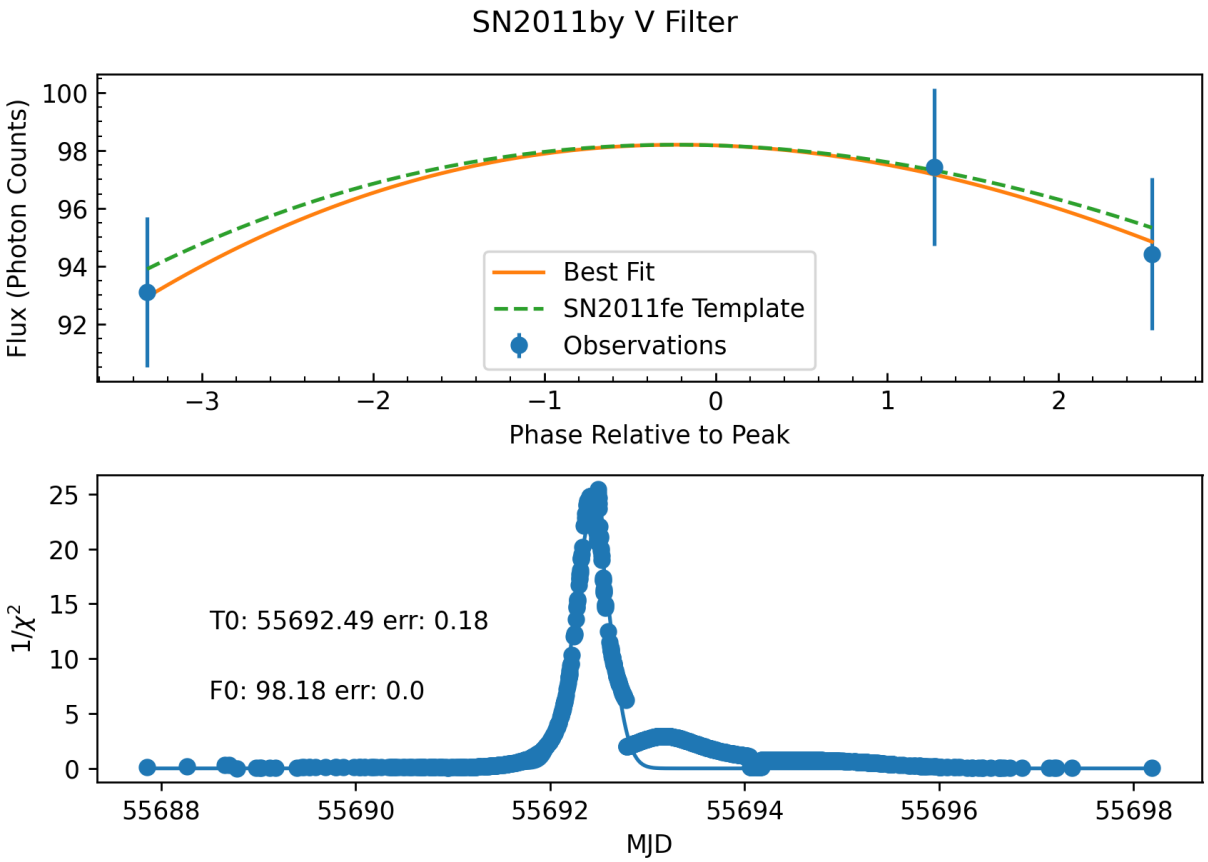

Figure B.5: As Figure B.1, but for V band observations of SN2011by.